DOT/FAA/CT-86/13

KRASH Analysis Correlation — — Transport Airplane Controlled Impact Demonstration Test

Gil Wittlin

Prepared by
Lockheed-California Company
Burbank, California

December 1986

Final Report

This document is available to the U.S. public through the National Technical Information Service, Springfield, Virginia 22161.

U.S. Department of Transportation

Federal Aviation Administration

Technical Center
Atlantic City Airport, N.J. 08405

NOTICE

This document is disseminated under the sponsorship of the Department of Transportation in the interest of information exchange. The United States Government assumes no liability for the contents or use thereof.

The United States Government does not endorse products or manufacturers. Trade or manufacturer's names appear herein solely because they are considered essential to the object of this report.

1. Report No.	2. Government Accession No.	3. Recipient's Catalog No.
DOT/FAA/CT-86-13		

4. Title and Subtitle	5. Report Date
KRASH ANALYSIS CORRELATION - TRANSPORT AIRPLANE CONTROLLED IMPACT DEMONSTRATION TEST	December 1986
	6. Performing Organization Code
7. Author(s): Gil Wittlin	8. Performing Organization Report No.: LR 30916
9. Performing Organization Name and Address: Lockheed-California Company, Burbank, CA 91520	10. Work Unit No.
	11. Contract or Grant No.: DTFA03-84-C-00004
12. Sponsoring Agency Name and Address: U.S. Dept. of Transportation, Federal Aviation Admin. Technical Center, Atlantic City International Airport, NJ 08405	13. Type of Report and Period Covered: Feb. 1985 - Aug. 1985
	14. Sponsoring Agency Code: ACT-330

15. Supplementary Notes

FAA Technical Monitors - C. Caiafa and L. Neri, ACT-330

16. Abstract

The analyses results of a transport airplane Controlled Impact Demonstration (CID) test using program KRASH are described. Pre-CID analyses, presented in FAA technical report DOT/FAA/CT-85/9, are provided in summary form. The KRASH post CID correlation consists of modeling two sequences; a symmetrical impact of the fuselage with the ground (after engine-loss at initial air-to-ground impact) and the unsymmetrical air-to-ground including initial engine ground contact and subsequent fuselage impact with the ground. The analyses and test results are compared with regard to floor acceleration responses, fuselage shear and bending moment distribution, wing and engine acceleration responses, wing bending moment distribution, structural failures, fuselage underside crush, and sequence of events.

17. Key Words (Suggested by Author(s))	18. Distribution Statement
Crashworthiness, Transport Aircraft, Crash Dynamics, Analysis, Math Model, Floor Pulse, Controlled Impact Demonstration, CID, full-scale crash test	Document is available to the U.S. public through the National Technical Information Service, Springfield, VA 22161

19. Security Classif. (of this report)	20. Security Classif. (of this page)	21. No. of Pages	22. Price*
Unclassified	Unclassified	121	

228:17,18

* For sale by the National Technical Information Service, Springfield, Virginia 22161

FOREWORD

This report was prepared by the Lockheed-California Company, under Contract DTFA03-84-C-00004, sponsored by the Federal Aviation Administration Technical Center. This report describes the analytical modeling effort performed from February 1985 through August 1985. The work was administered under the direction of L. Neri and C. Caiafa of the FAA.

The Lockheed-California Company effort was performed by Gil Wittlin. The Lockheed effort was performed within the Flutter and Dynamics Department.

TABLE OF CONTENTS

LIST OF FIGURES

LIST OF FIGURES (Continued)

LIST OF FIGURES (Continued)

LIST OF FIGURES (Continued)

LIST OF TABLES

LIST OF TABLES (Continued)

EXECUTIVE SUMMARY

The analyses results of a transport airplane Controlled Impact Demonstration (CID) test using program KRASH are presented. The pre-CID analysis results, which are reported in FAA technical report DOT/FAA/CT-85/9, are briefly summarized. The actual CID test impact conditions which deviated from the planned impact scenario are described. The post-CID analyses are performed for two sequences: a symmetrical impact of the fuselage with the ground (after engine-loss at initial air-to-ground impact) and the unsymmetrical air-to-ground impact including initial engine ground contact and subsequent fuselage impact with the ground. The symmetrical analysis is an abbreviated analysis which concentrates on floor pulse definitions as a result of a direct impact on the fuselage. The latter unsymmetrical analysis considers engine attachment failure, airplane motion and subsequent involvement of the fuselage impact sequence. An assessment of the analytical procedures and results indicates that:

- The analyses results compare favorably with the test results.
- The KRASH model results show overall agreement with fuselage responses including accelerations, underside crush and structural integrity for the complete unsymmetrical impact initiated on the No. 1 engine, as well as the fuselage-only impact phase.
- The KRASH modeling can accurately depict the sequence of events and respective failures for an unsymmetrical impact event.
- Anaytically determined wing and engine responses show agreement with test data with regard to spanwise moment distribution and indicate that the CID unsymmetrical impact conditions produce wing loads below the estimated structural integrity of the wing, which is supported by the test data.
- The KRASH models demonstrate the ability to analyze a range of impact conditions and thus can be applied in additional parameter studies.
- The results indicate several areas where improved model representations may be beneficial, i.e., wing/engine and engine/fuselage attachment.

SECTION 1

INTRODUCTION

On December 1, 1984, the FAA/NASA performed a Controlled Impact Demonstration (CID) impact test using a narrow-body transport airplane. This test is one milestone in a series of tasks in a joint FAA/NASA/industry program (references 1 and 2) to improve methodology for determining the dynamic response of transport category aircraft to crash related impacts. The purpose of developing improved methodology is to help ensure that a high level of occupant safety will be continued in future transport airplanes involved in impact survivable accidents. The program is multifaceted. The initial tasks to review past accident data and establish candidate survivable crash scenarios were completed. The results of these studies, performed by the major manufacturers (references 3, 4, and 5) are summarized in reference 6. The overall program approach is presented in references 7 and 8. Some of the key elements of the on-going joint effort are outlined in figure 1-1. Program KRASH, which has recently been updated (reference 9), has been used to analyze the anticipated response of the CID test specimen for the planned impact condition. The results of the pre-CID analyses including section and airplane drop tests comparisons are provided in reference 10. The test data obtained from supporting tests has been used in the modeling of the CID impact and will also be used in subsequent parameter variation studies. The CID test, post-CID KRASH analyses, and application of the analysis methodology are described in this study.

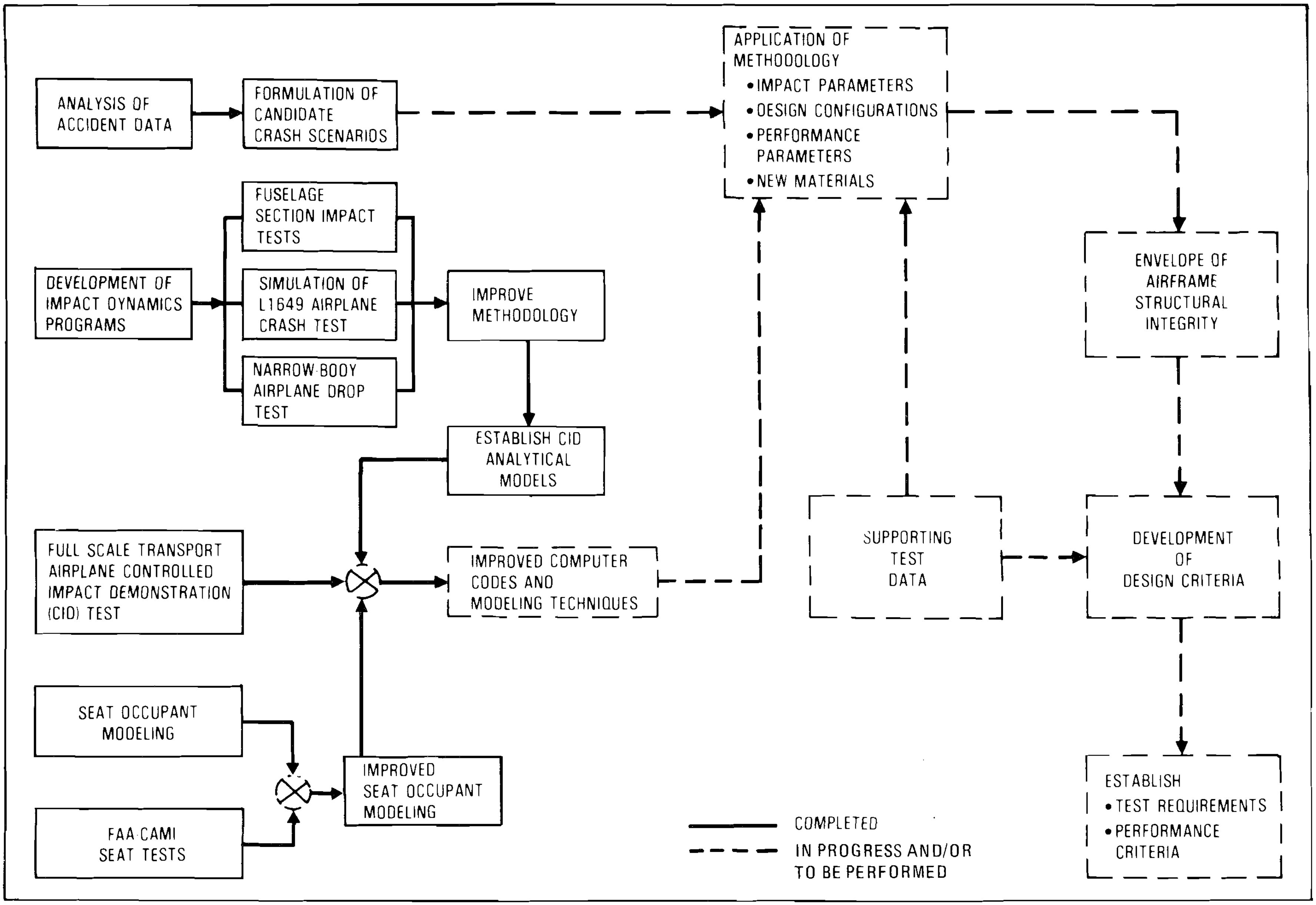

FIGURE 1-1. TRANSPORT AIRPLANE IMPACT DYNAMICS PROGRAM - MAJOR TASKS

SECTION 2
SUMMARY OF PRE-CID ANALYSES

2.1 KRASH MODELS

The CID pre-test analyses were performed using the following models; a stick model consisting of 17 masses and 16 beam elements (figure 2-1), and an expanded model consisting of 48 masses and 137 beam elements (figure 2-2). The underside crushing load-deflection characteristics as a function of location along the fuselage are shown in figures 2-3 and 2-4. The KRASH model fuselage stations (F.S.) and corresponding airplane body station (B.S.) locations are shown in figure 2-5.

The planned impact condition for the CID test was as follows:

- Symmetrical (0° yaw, 0° roll)
- 1° pitch attitude, nose-up
- 17 ft/sec sink speed
- 155 knots forward velocity

The stick and expanded models were run for variations of initial lift conditions to represent a range from no lift to an estimated balanced 1g aerodynamic loading for the planned attitude and impact velocities.

2.2 KRASH ANALYSES RESULTS

For each model the results were presented in reference 10 for the planned impact condition, with variations as noted above. The comparison of accelerations for the full range of conditions is shown in figure 2-6. The results for the condition that is considered closest to approximating the planned impact are presented in figure 2-7. A summary of a comparison for the stick and expanded model results for Load Interaction Curve (LIC) ratios, accelerations and crush distances are shown in figure 2-8. Figure 2-8 also shows the estimated crush distance measured as a result of a narrow-body

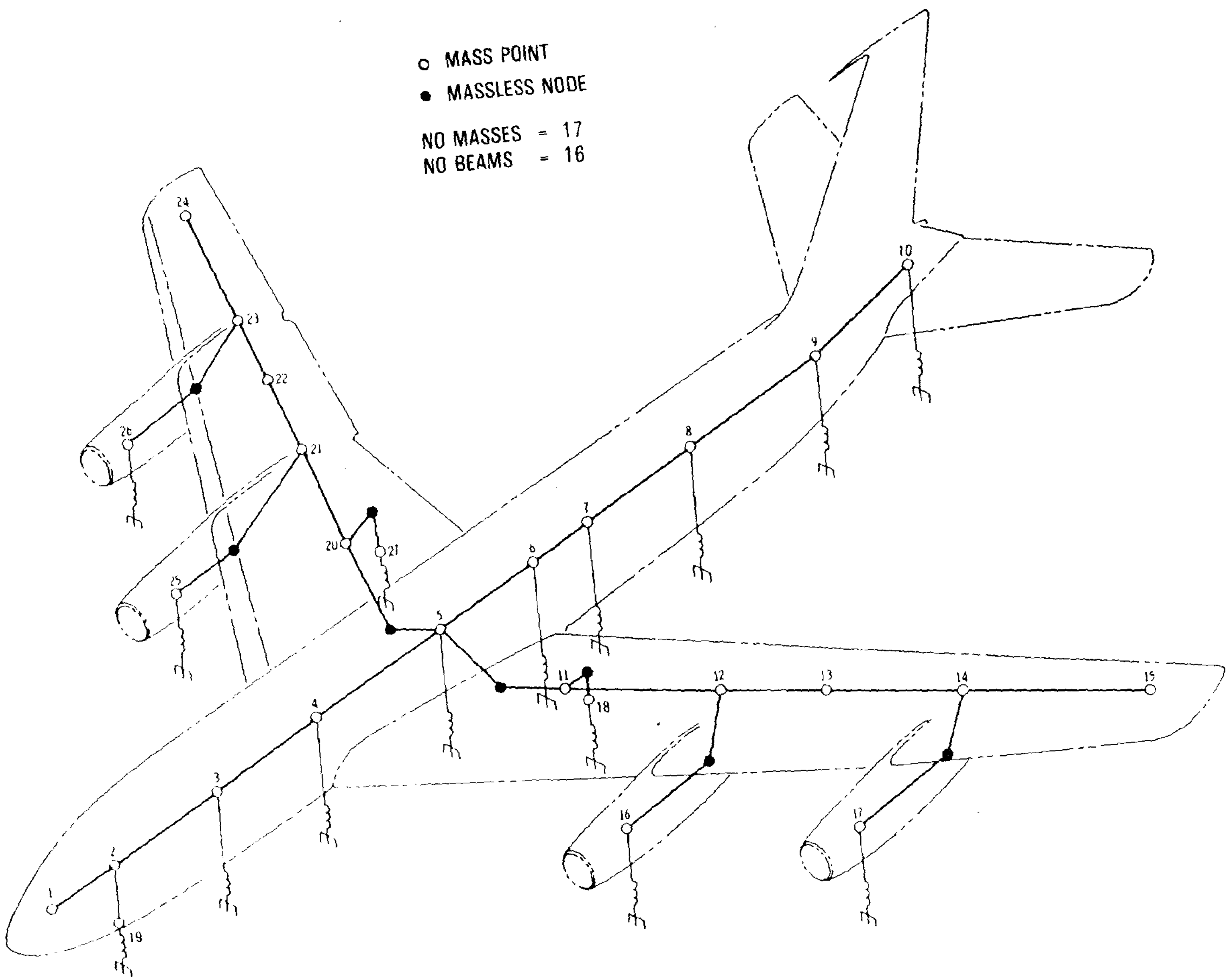

FIGURE 2-1. CID KRASH STICK MODEL

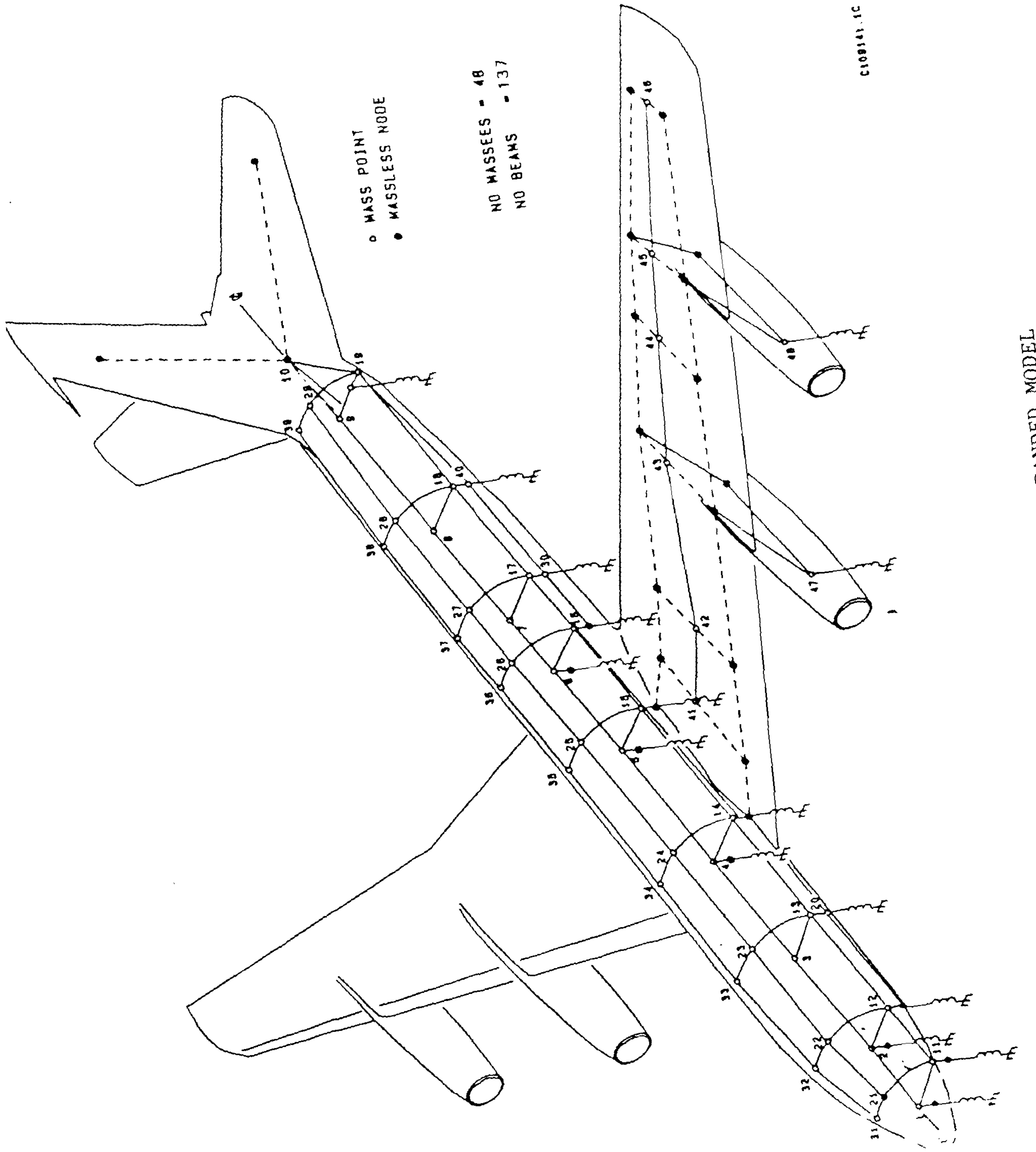

FIGURE 2-2. CID KRASH EXPANDED MODEL

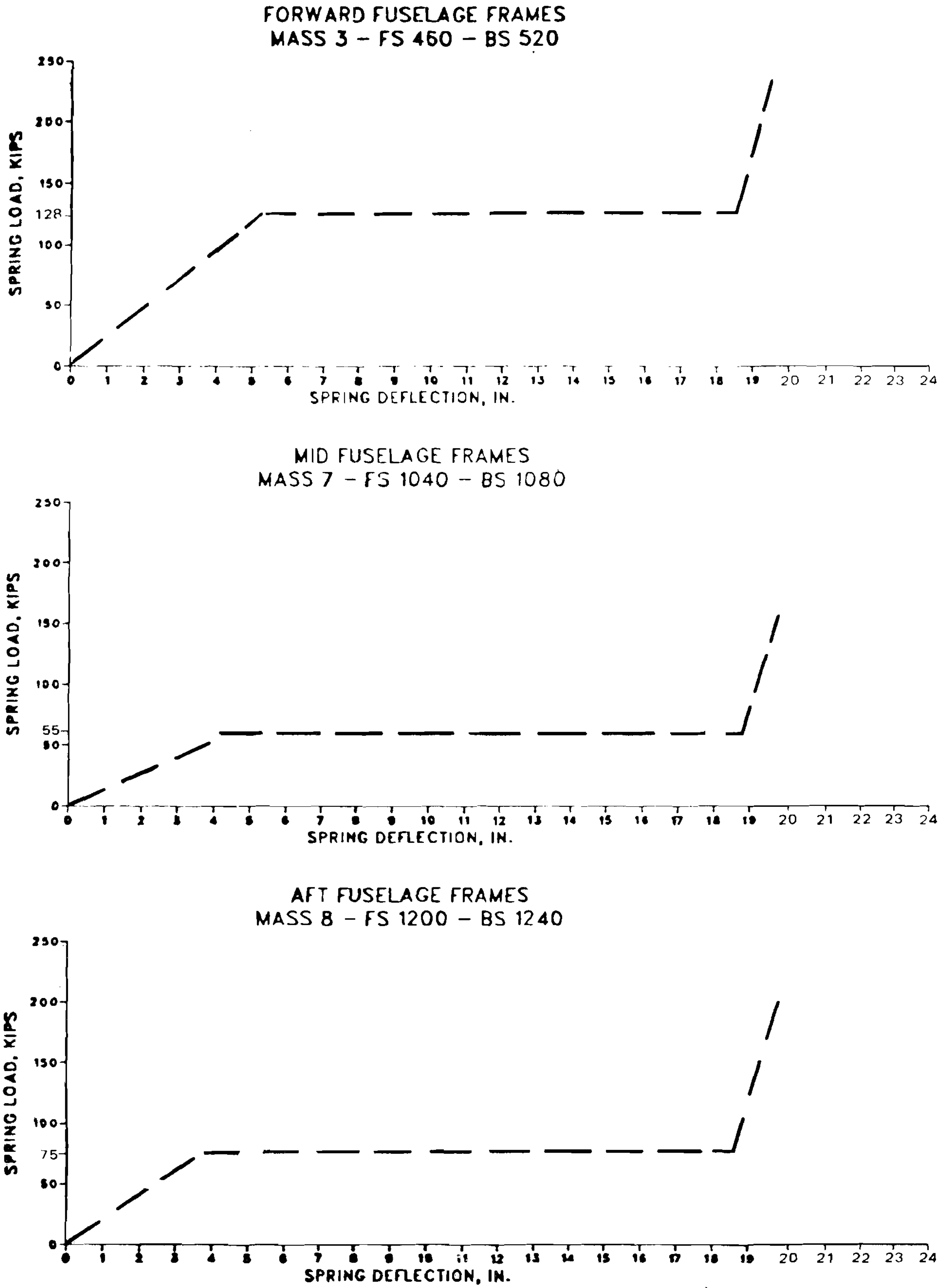

FIGURE 2-3. CID MODEL FRAME CRUSH SPRINGS

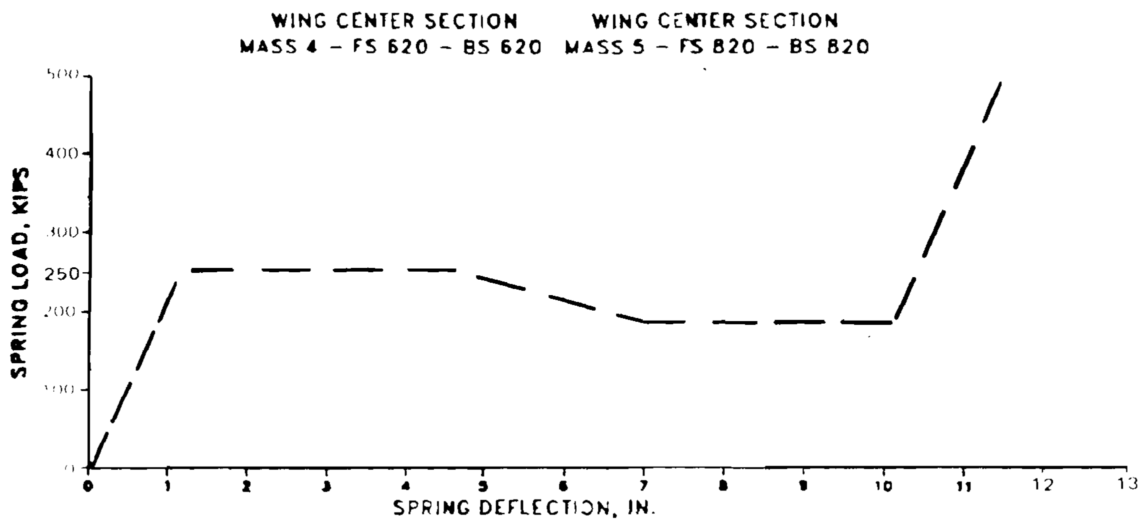

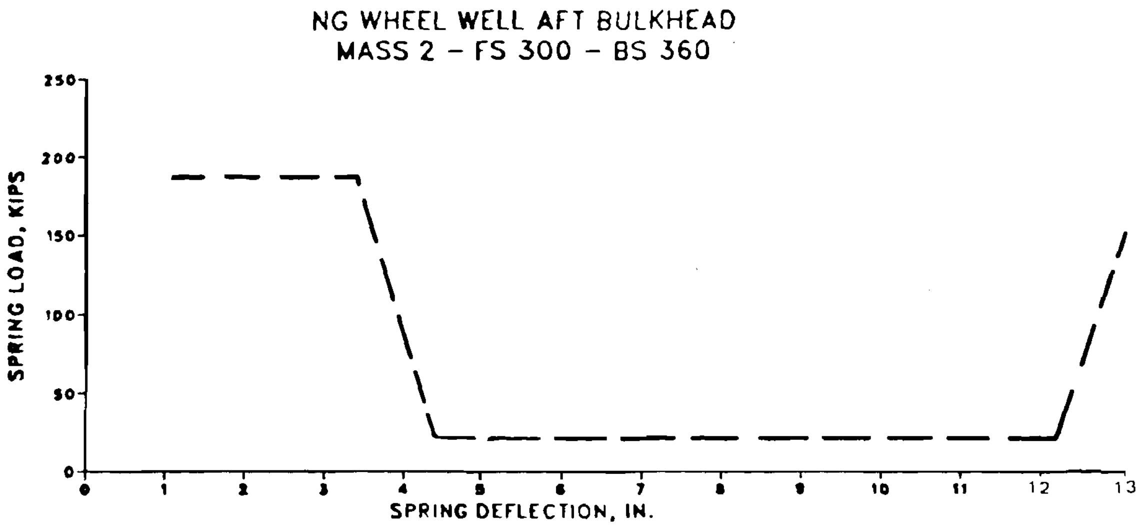

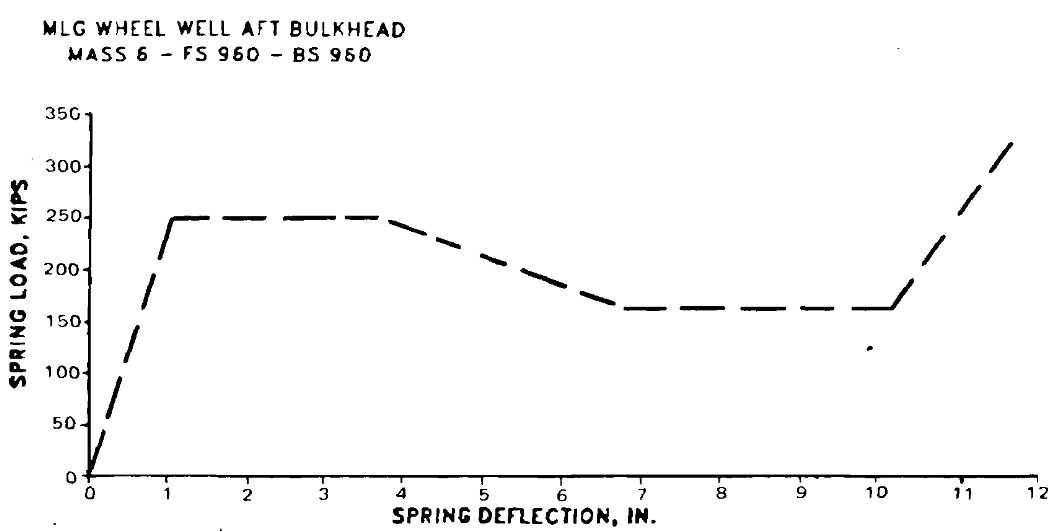

FIGURE 2-4. CID MODEL HARD POINT SPRINGS

MASS NO.	KRASH FUSELAGE STATION	AIRPLANE BODY STATION	LOCATION REPRESENTATION
1	199	259	Nose Gear Wheel Well, forward bulkhead
2	300	360	Nose Gear Wheel Well, rear bulkhead
3	460	520	Forward fuselage frames
4	620	620	Wing center section, forward
5	820	820	Wing center section, rear
6	960	960	Main landing gear rear bulkhead
7	1040	1080	Mid fuselage frames
8	1200	1240	Mid-aft fuselage frames
9	1400	1440	Aft pressure bulkhead
10	1570	1610	Empennage

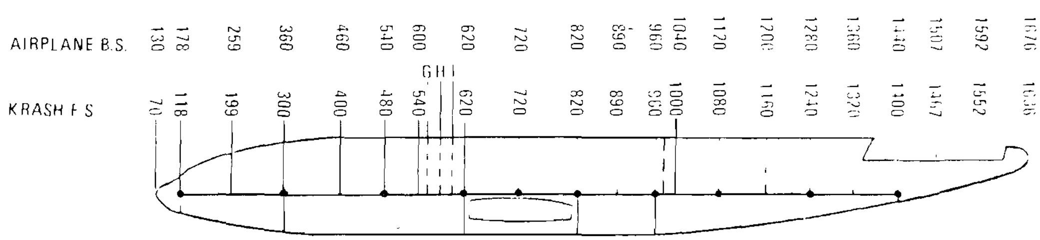

FIGURE 2-5. KRASH MODEL FUSELAGE MASS POINT LOCATIONS

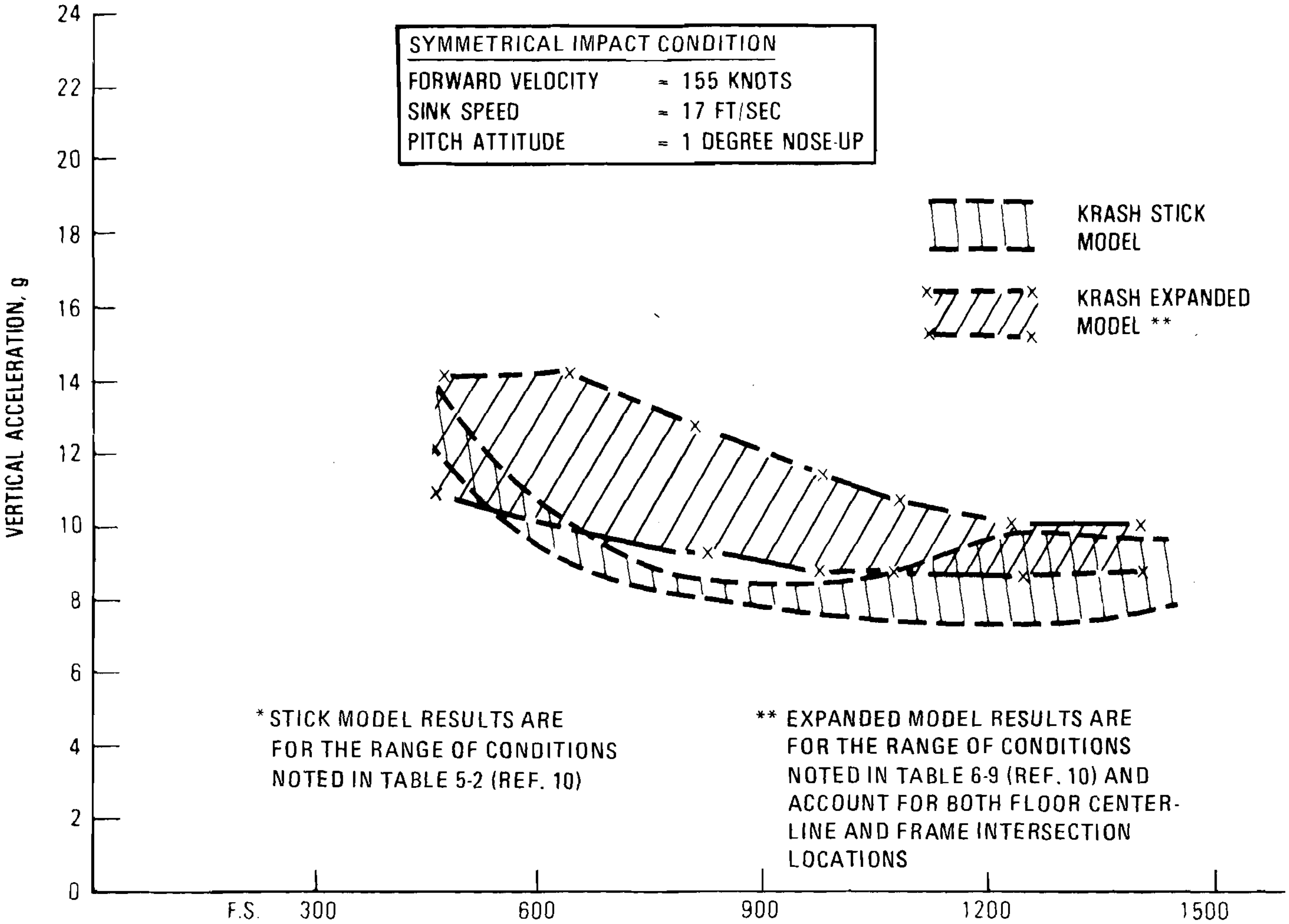

FIGURE 2-6. COMPARISON OF KRASH STICK MODEL ANALYSES VERSUS EXPANDED MODEL RESULTS FOR CID PLANNED SYMMETRICAL IMPACT CONDITION

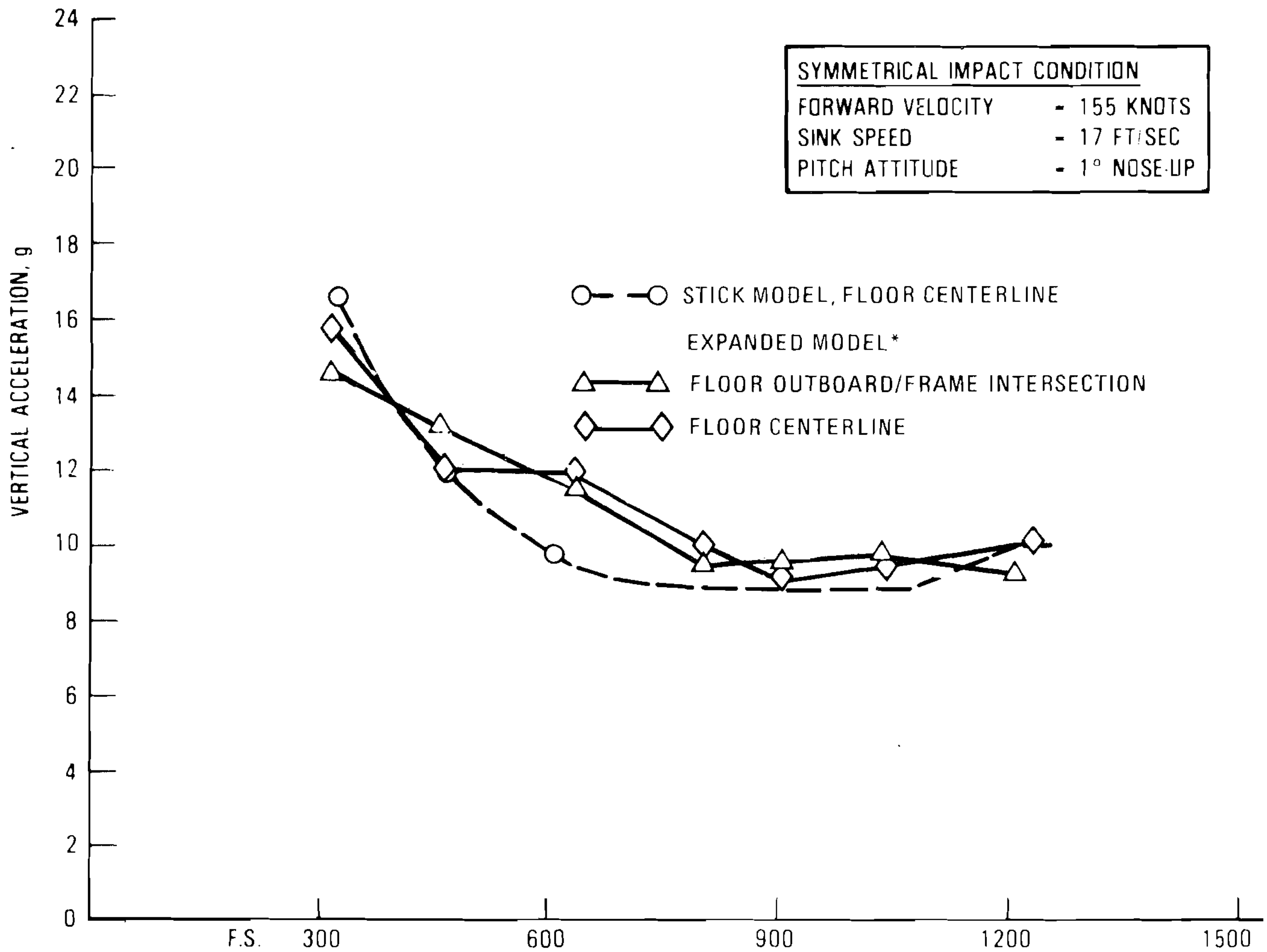

FIGURE 2-7. COMPARISON OF PRE-CID KRASH STICK AND EXPANDED MODELS ANALYSES RESULTS FOR PLANNED SYMMETRICAL IMPACT CONDITION

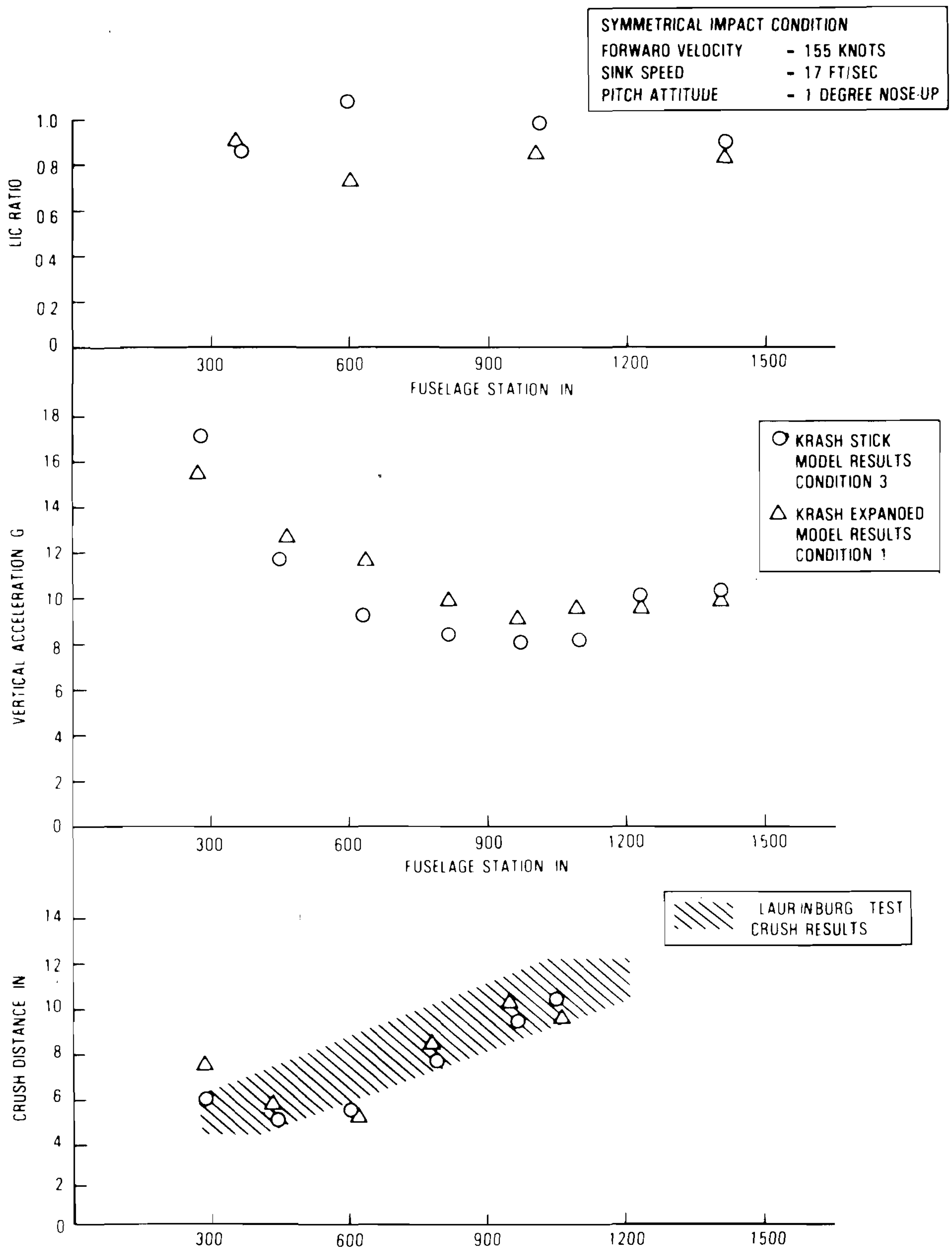

FIGURE 2-8. PRE-CID TESTS KRASH ANALYSIS RESULTS FOR PLANNED SYMMETRICAL IMPACT CONDITION

airplane drop test conducted at Laurinburg, North Carolina prior to the CID test, which produced a 17 ft/sec sink speed for a full airplane (195,000 lb.) at a 1° nose-up pitch attitude and with no forward velocity.

Pre-CID analyses acceleration peak responses are plotted in figure 2-9, along with a constant ΔV = 17 ft/sec curve. The data cluster about the constant ΔV curve. The stick model, due to its level of simplicity, tends to provide lower frequency acceleration responses than the expanded model. The higher peak accelerations are generally associated with shorter duration pulses than the lower peak values. The stick model results tend to be of lower amplitude and broader in response duration. As the expanded model results are filtered to a lower cutoff value, the responses shift to lower values and tend toward better agreement with the stick model results. An alternative to comparing peak values is to present an equivalent triangular pulse amplitude which can be obtained from a plot of impulse (g-sec) data, which is the acceleration integrated over time for the duration of interest. This provides an average value. The peak associated with a triangular pulse is twice the average value. This approach eliminates questions that could arise over the print interval or filter characteristics (i.e., cutoff frequency, decay rate). The data presented in figures 2-5, 2-6, and 2-7 represent peaks associated with triangular pulse shapes with a base duration (Δt) of between 0.10 sec and 0.15 sec. The response can contain higher peak but shorter duration pulses. The stick model, while it may provide floor pulse definitions, particularly if the aircraft responds in a lower frequency mode, does not generally contain sufficient detail to evaluate individual structural element behavior. The expanded model contains more detail and therefore can provide more element load and deflection data. For example, the summary of beam peak deflections obtained from the expanded model are shown in table 2-1. The accuracy of the deflection results depends on the ability to adequately represent complex structural designs with relatively simple elements.

The analysis results are particularly sensitive to the:

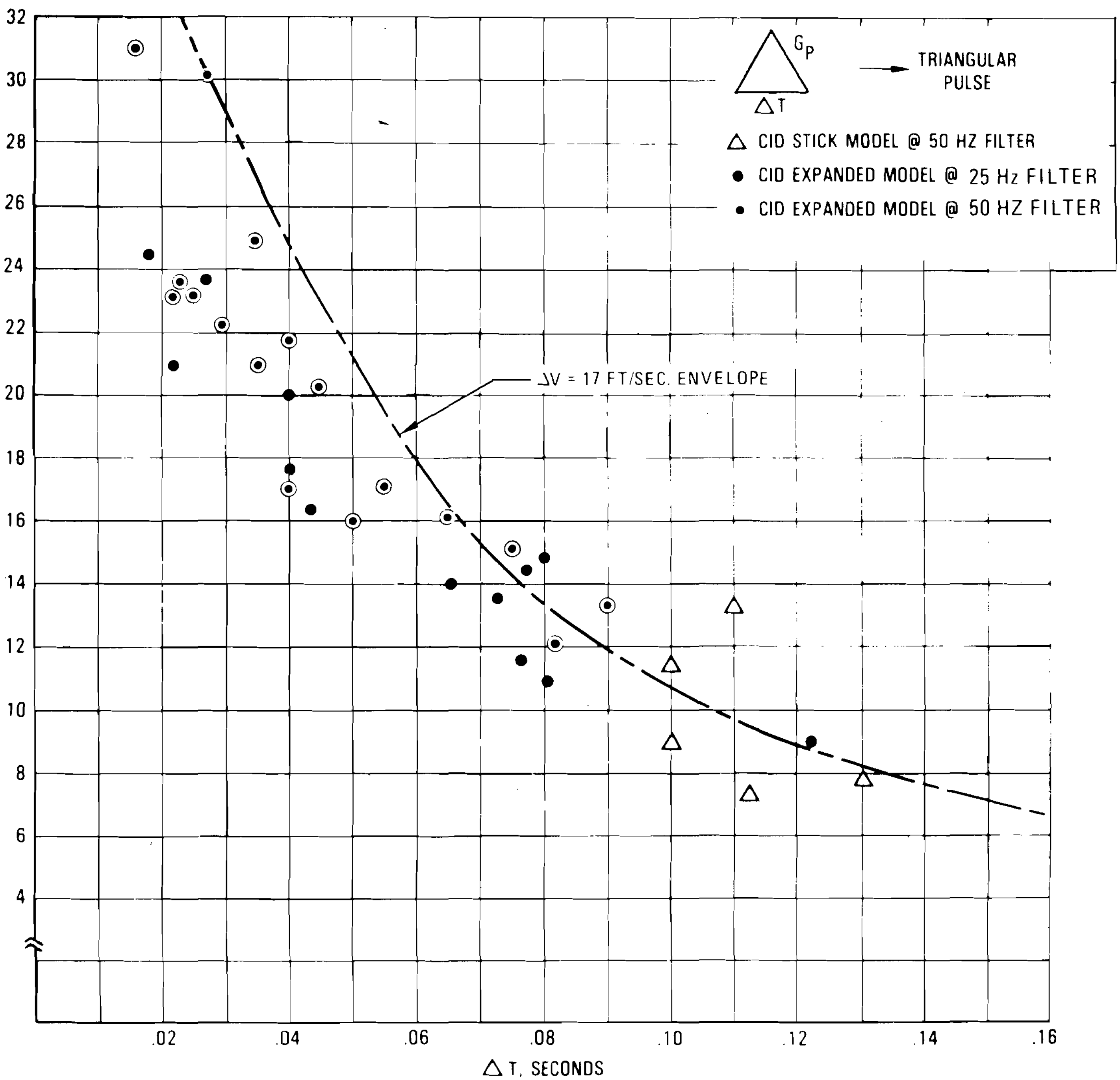

FIGURE 2-9. CID PRE-TEST ANALYSIS - VERTICAL ACCELERATION PULSE, 17 FT/SEC, +1° NOSE-UP

- Representation of the hard point load-deflection characteristics. Bottoming out loads could easily result in localized failures and subsequent disruption of structural integrity.

- Extent to which the structure yields or fails. This is difficult to evaluate because a large segment of structure, consisting of several frames and stringers, is defined by only a few beam elements.

TABLE 2-1. SUMMARY OF BEAM PEAK DEFLECTION RANGE FROM PRE-CID ANALYSIS USING THE CID EXPANDED MODEL

DESCRIPTION	LOCATION	DEFLECTION, inches
Upper Shell Lateral	station 960 WL 205-271	1.22 to 4.0
Upper Shell Lateral	station 960 WL 271-290	0.66 to 1.7
Transverse Floor Beams-Vertical	station 620 station 820 station 960	0.61 to 1.27 0.84 to 1.6 1.1 to 3.0
Upper Cabin Longeron Vertical	station 460-620 WL 205-271/WL 271-290	0.67 to 1.06/0.34 to 0.69
	station 620-820 WL 205/271/WL 271-290	0.64 to 2.87/0.76 to 1.090
	station 820-960 WL 205-271/WL 271-290	0.56 to 0.78/0.40 to 1.04
	station 960-1040 WL 205-271/WL 271-290	0.26 to 1.16/0.15 to 0.55
	station 1040-1200 WL 205-271/WL 271-290	1.02 to 2.7/0.36 to 1.69
Floor Vertical Inboard	station 460-620 station 620-820 station 820-960 station 960-1040 station 1040-1200	1.71 to 2.46 1.81 to 5.9 0.37 to 0.86 0.33 to 3.1 1.7 to 2.1
Outboard	station 460-620 station 620-820 station 820-960 station 960-1040	0.69 to 1.44 0.50 to 2.18 0.91 to 0.98 0.62 to 0.88

SECTION 3

POST-CID KRASH ANALYSES

3.1 CID TEST RESULTS

The CID test was performed on December 1, 1984, at the NASA Dryden Dry Lake Bed, Edwards Air Force Base, California. The actual impact conditions deviated from the planned conditions, as shown in table 3-1. Due to an initial roll and yaw, the aircraft impacted first on the left wing outboard engine (No. 1), rotated onto the No. 2 engine, and then subsequentally the forward fuselage made ground contact approximately 400 msec. after initial engine impact. Floor peak vertical responses were developed within 500 msec. after initial fuselage impact. The actual CID impact sequence is shown in figure 3-1 and includes wing cutter impact and subsequent initiation of post-crash fire. The measured response data included fuselage bending responses at six fuselage stations (figure 3-2), as well as numerous fuselage frame, floor, seat and occupant responses. In all, 352 channels of data were recorded. The acceleration response data was reduced for three time periods:

1. Initial engine and fuselage impacts (t = 0 to t = 1.0 second)
2. No. 3 engine - cutter impact (t = 1.5 seconds to t = 2.5 seconds)
3. BS860 crack and slideout (t = 4.0 seconds to t = 5.5 seconds)

For the purpose of the KRASH correlation the first time period is used because it represents the air-to-ground impact for which the KRASH model is to be validated. Typical floor normal pulses for this time period are provided in figures 3-3 through 3-11. The plot of peak vertical accelerations versus fuselage station, which is shown in figure 3-12, indicates the scatter in response levels that is measured along the fuselage. Additional CID test acceleration histories are presented in Appendix A. The relationship between airplane body station and KRASH program fuselage station locations is shown in figure 2-5.

TABLE 3-1. COMPARISON OF CID TEST PLANNED AND ACTUAL IMPACT CONDITIONS

	PLANNED	ACTUAL* WING	(FUSELAGE)
SINK RATE, FPS	17^{+3}_{-2}	17.3	(14.0)
GROSS WEIGHT, LB	175 – 195000	192,383	
GLIDE PATH, DEGREES	3.3 TO 4.0	3.5	
ATTITUDE, DEGREES	1 ± 1 (NOSE-UP)	0	(0 TO -2)
LONGITUDINAL VELOCITY, KNTS	150^{+5}_{-5}	151.5	(150)
ROLL, DEGREES	0 ± 1	13**	
YAW, DEGREES	0 ± 1	13***	

*INITIAL IMPACT ON LEFT WING OUTBOARD ENGINE, SUBSEQUENT CONTACT ON FUSELAGE (BS360-460 REGION) WAS AS NOTED FOR IMPACT VELOCITIES AND PITCH ATTITUDE.

**LEFT WING DOWN

***NOSE LEFT

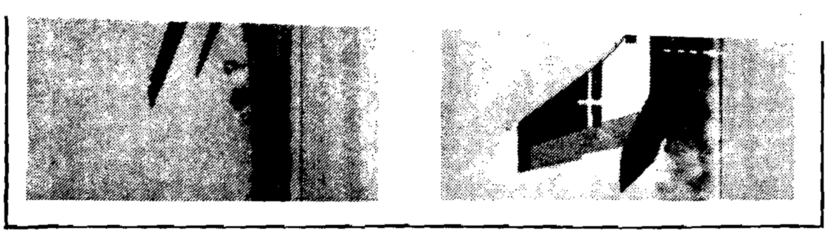

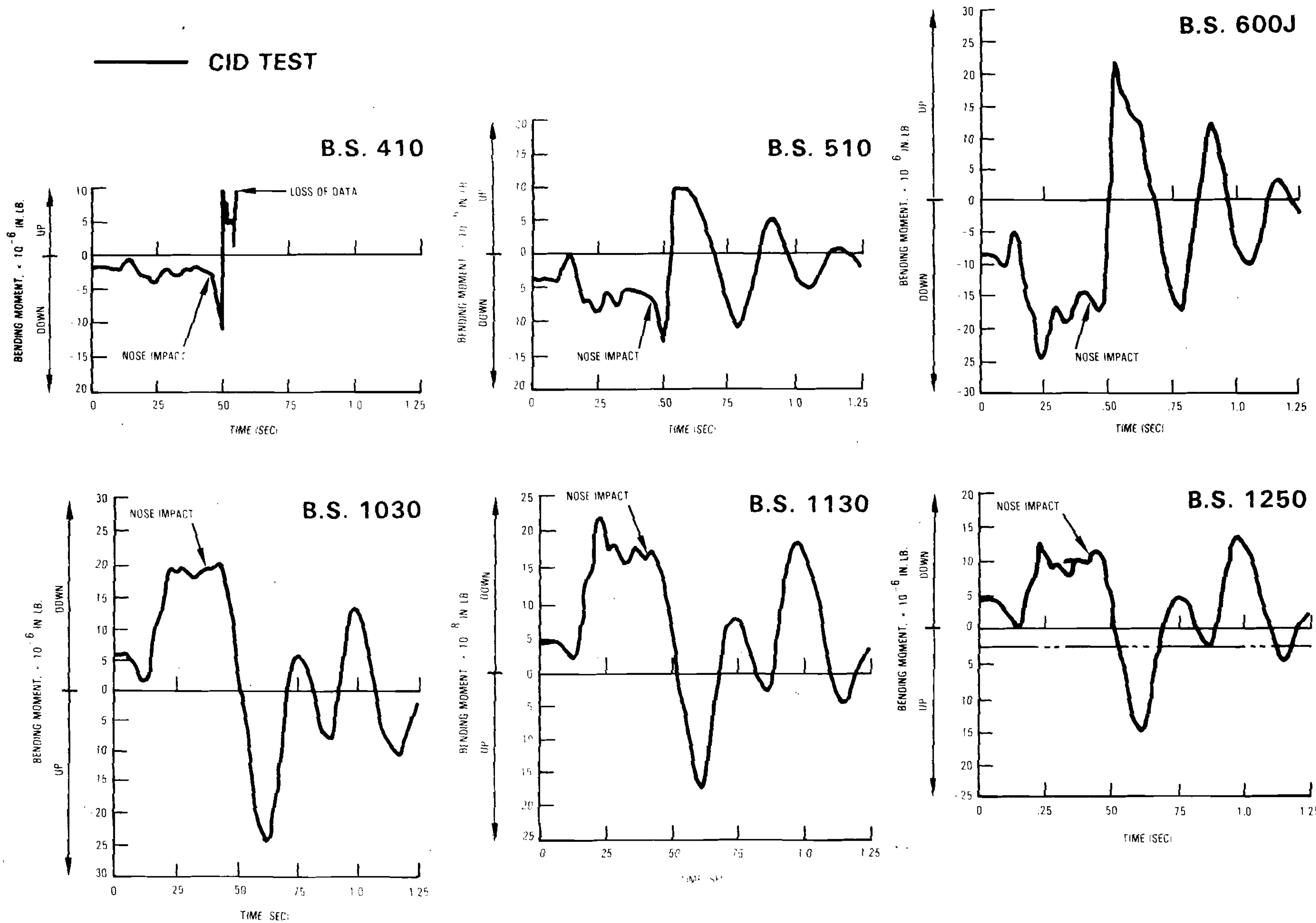

FIGURE 3-2. CID TEST RESULTS, MOMENT RESPONSES

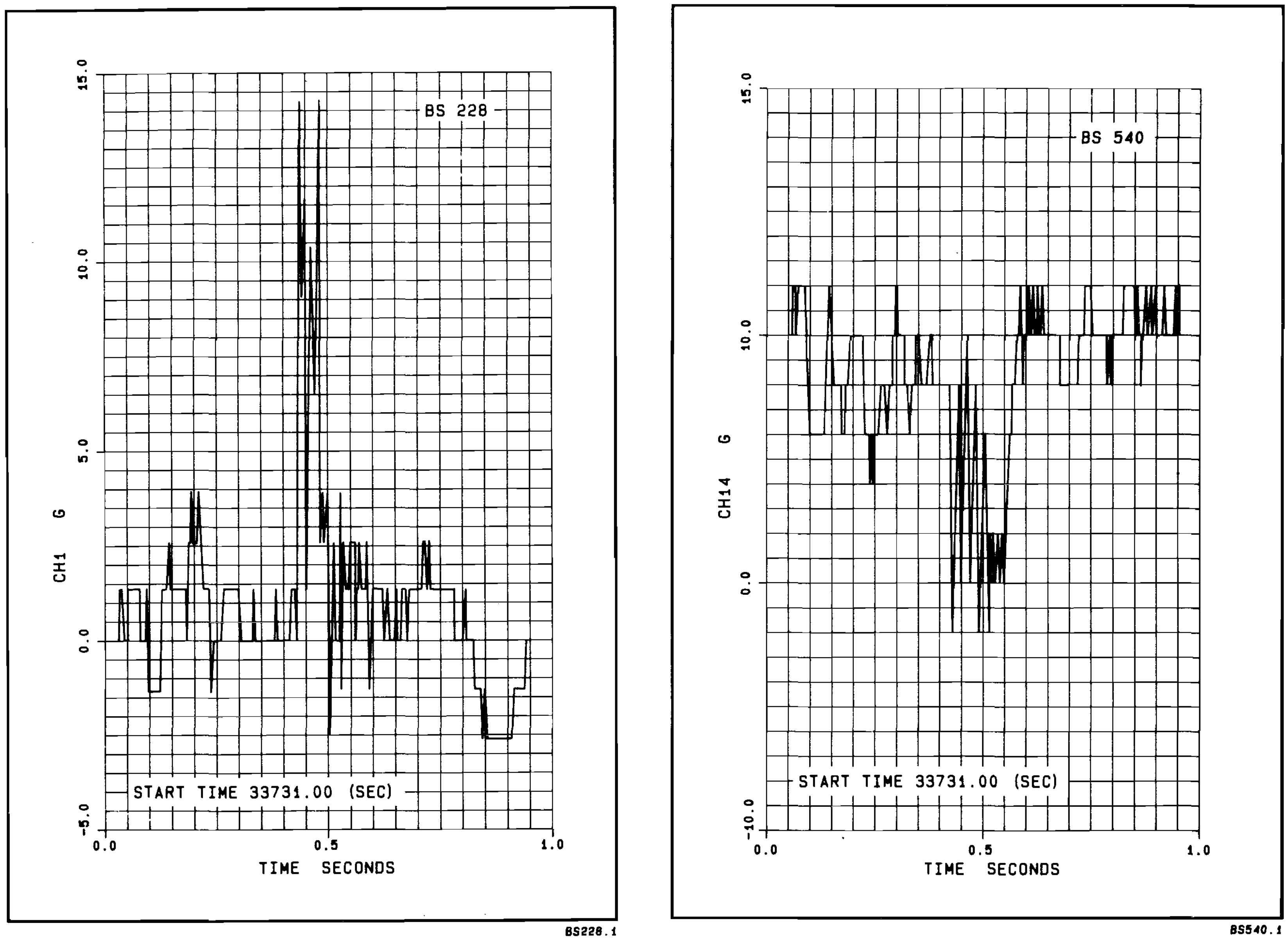

FIGURE 3-3. CID TEST NORMAL (VERTICAL) DIRECTION FLOOR ACCELERATIONS - BS228 - BS540

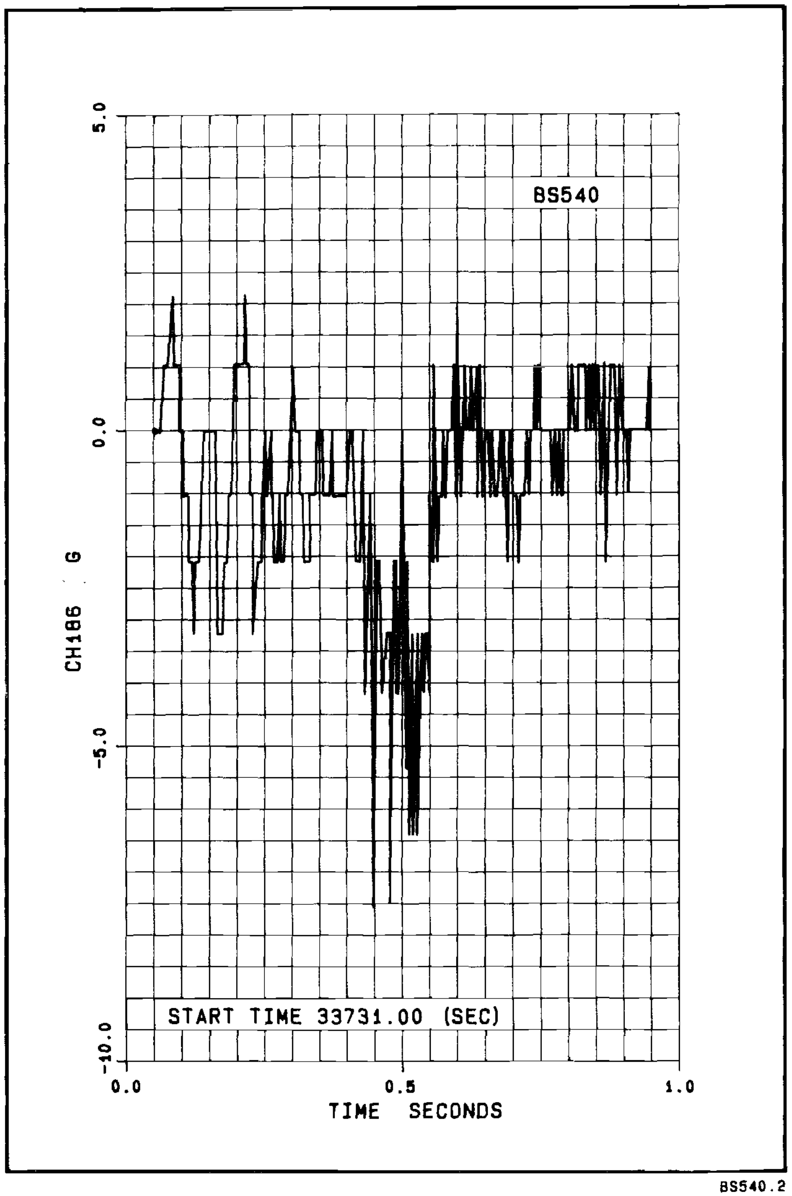

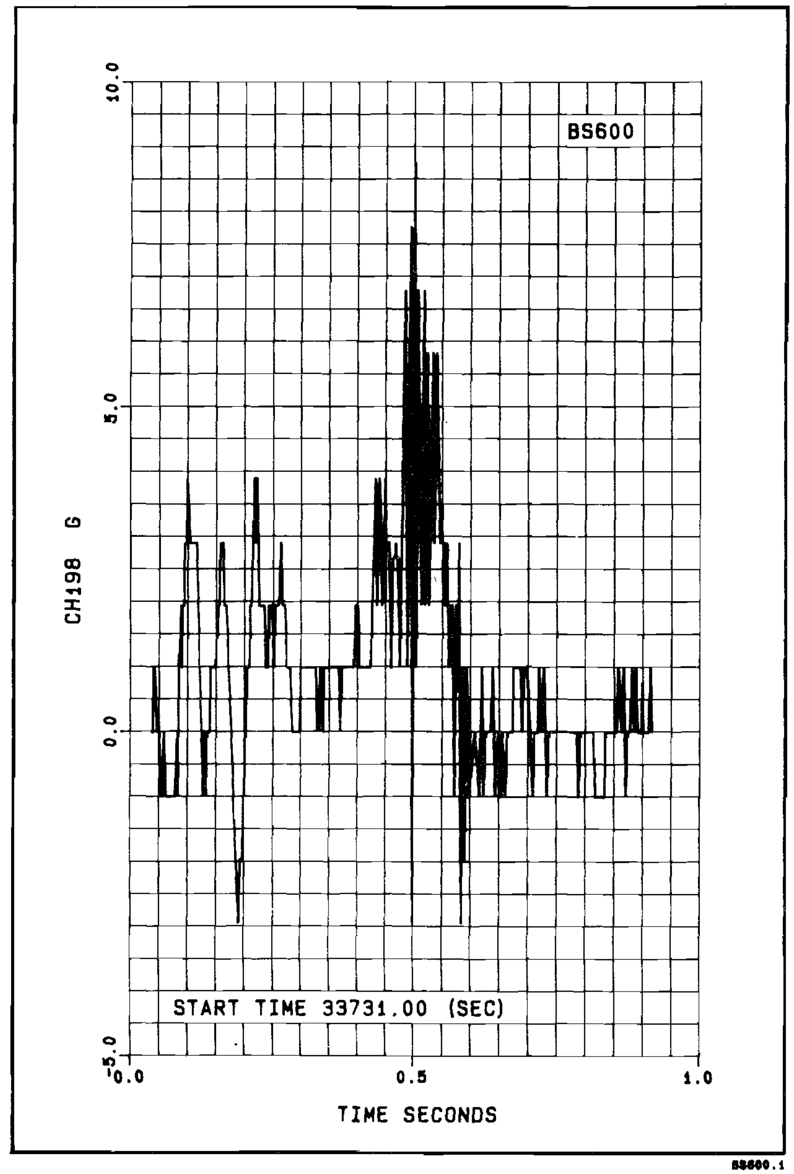

FIGURE 3-4. CID TEST NORMAL (VERTICAL) DIRECTION FLOOR ACCELERATIONS - BS540 - BS600

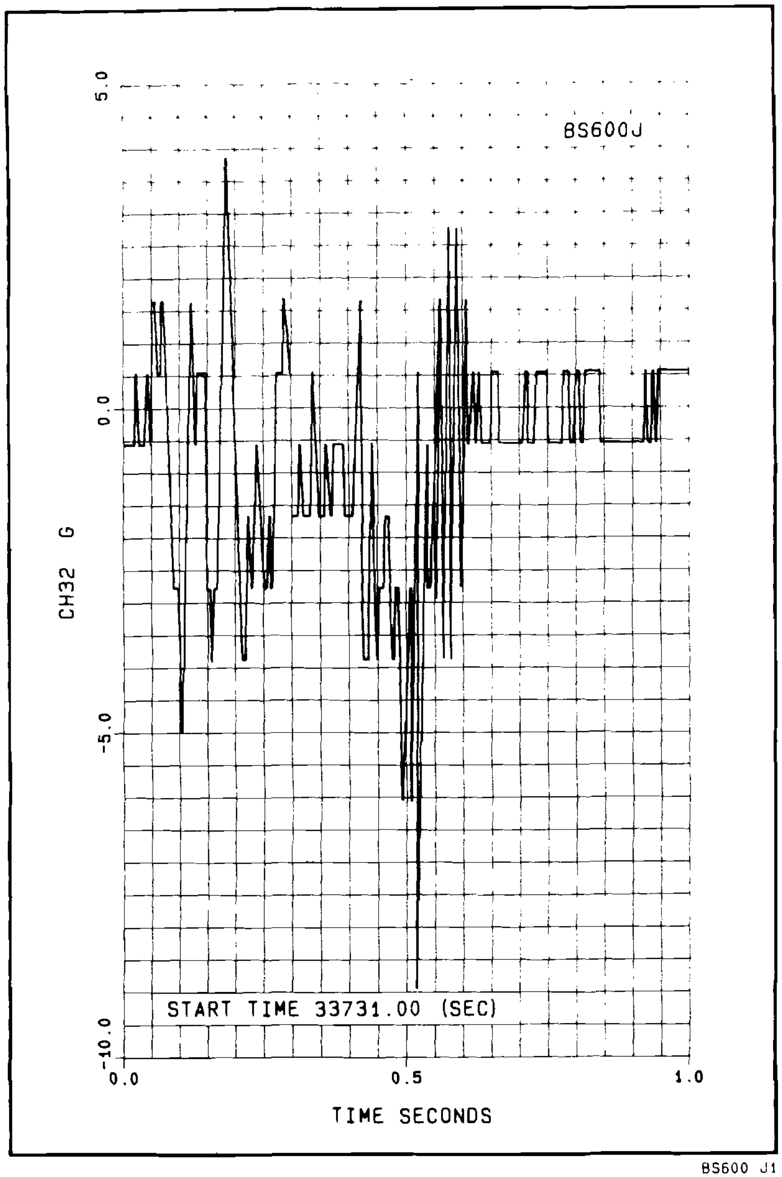

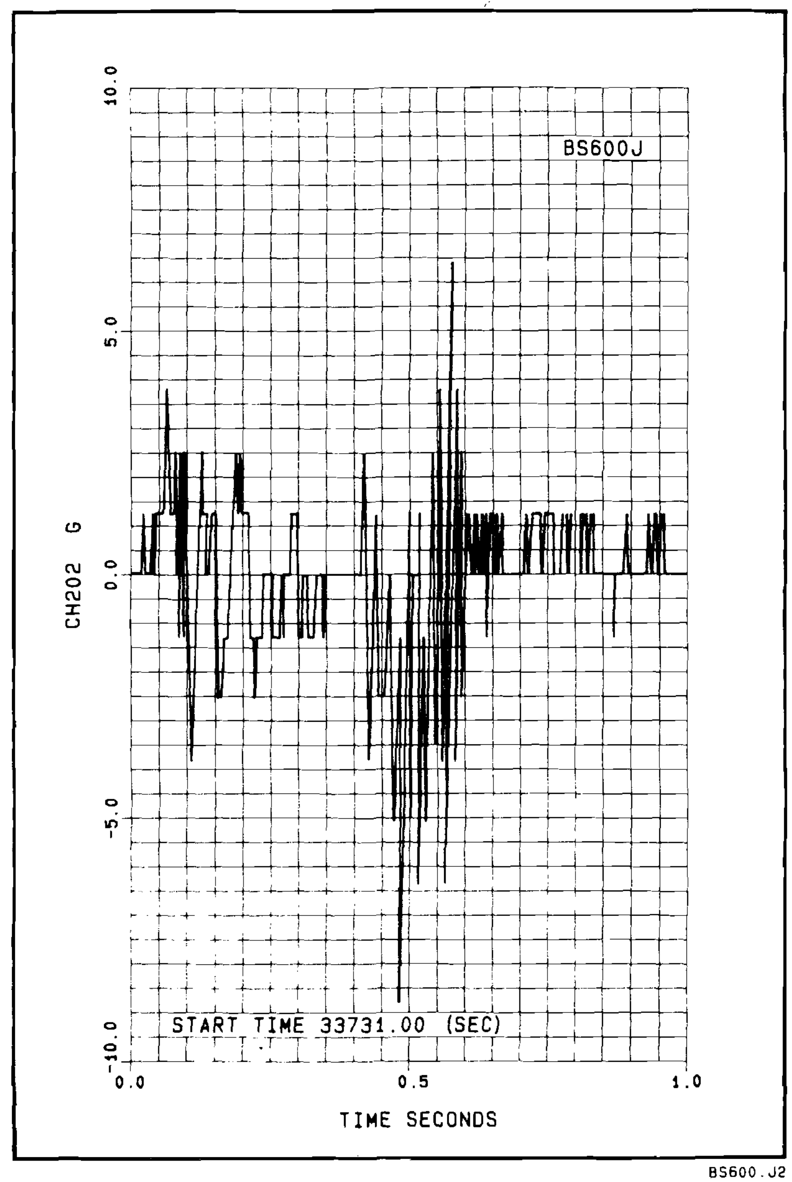

FIGURE 3-5. CID TEST NORMAL (VERTICAL) DIRECTION FLOOR ACCELERATIONS - BS600J

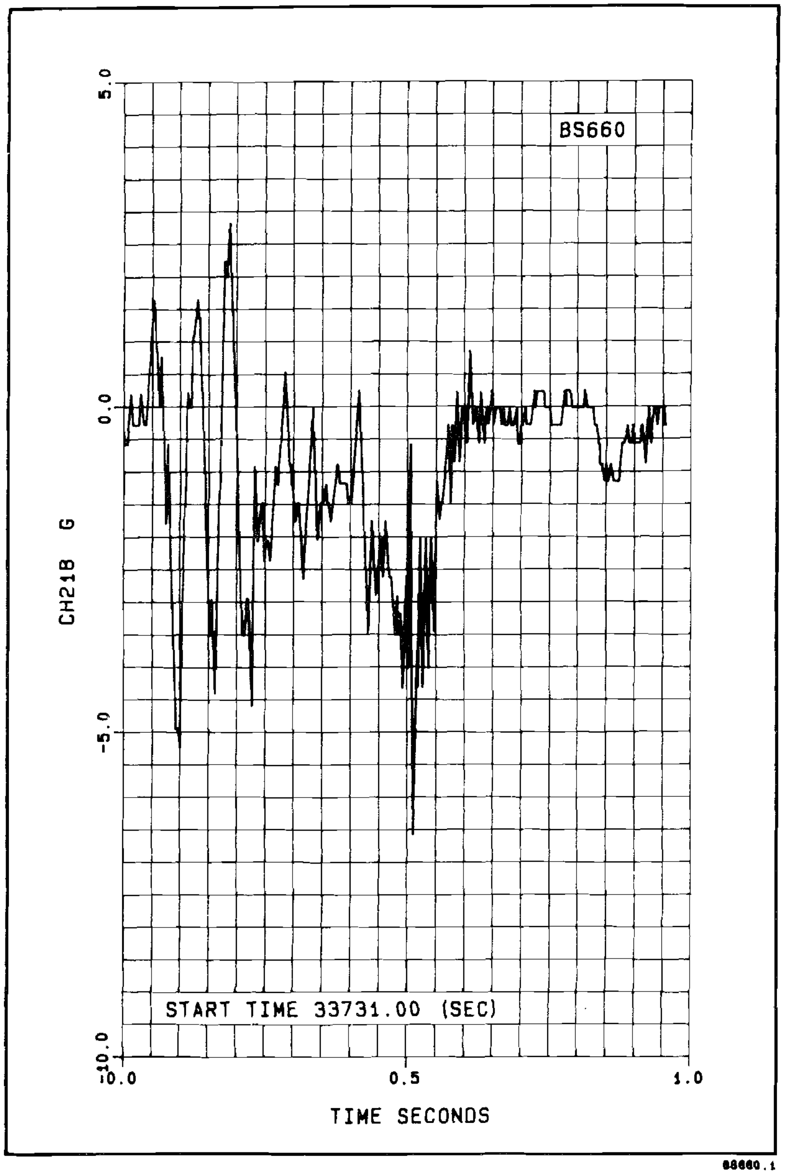

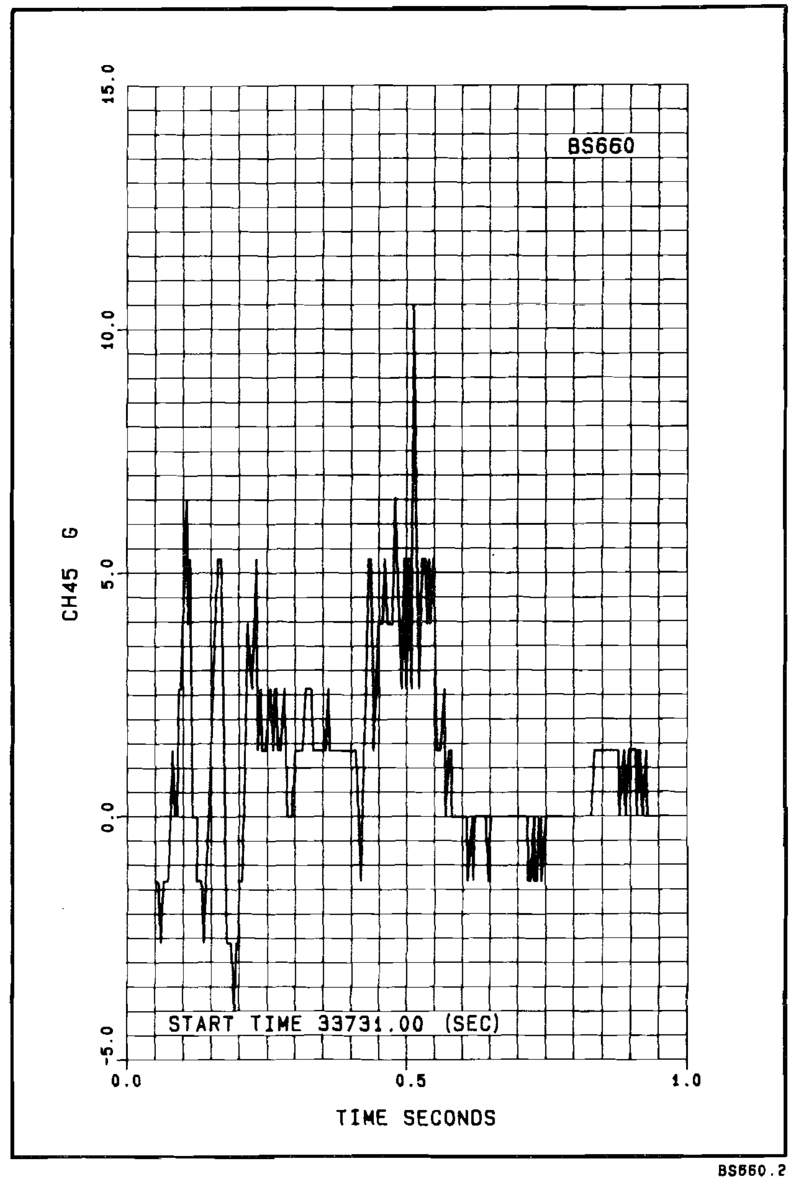

FIGURE 3-6. CID TEST NORMAL (VERTICAL) DIRECTION FLOOR ACCELERATIONS - BS660

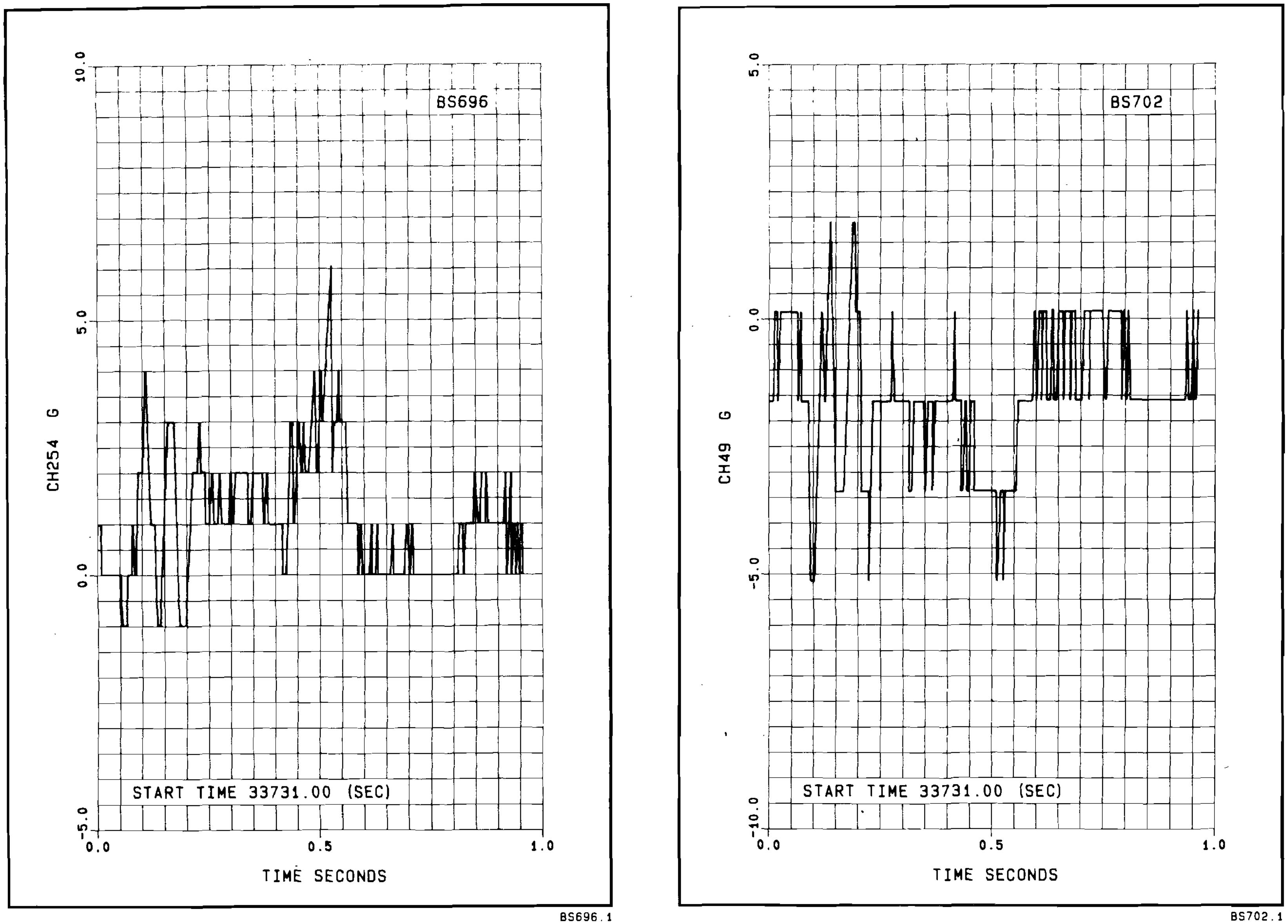

FIGURE 3-7. CID TEST NORMAL (VERTICAL) DIRECTION FLOOR ACCELERATIONS - BS969 - BS702

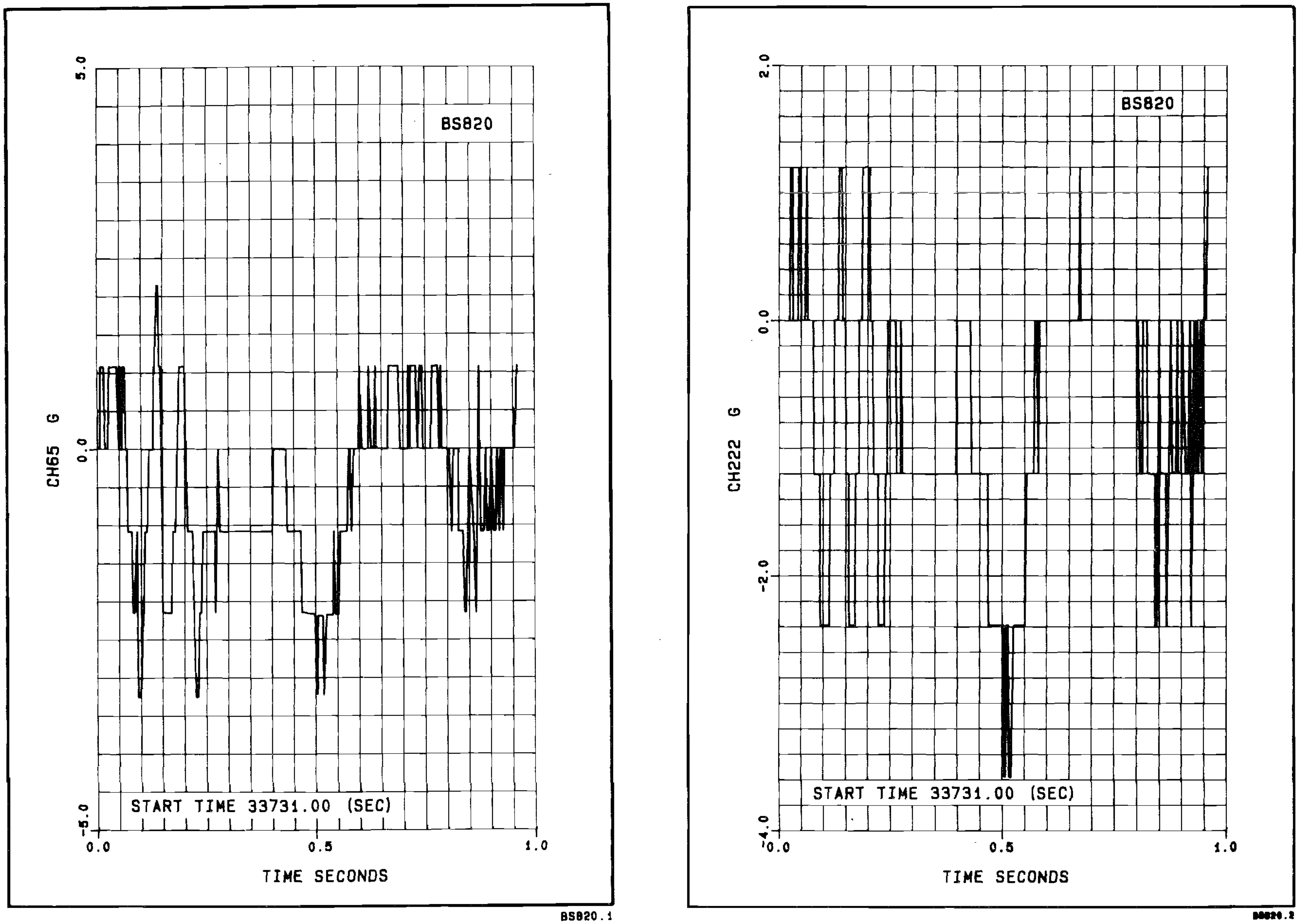

FIGURE 3-8. CID TEST NORMAL (VERTICAL) DIRECTION FLOOR ACCELERATIONS - BS820

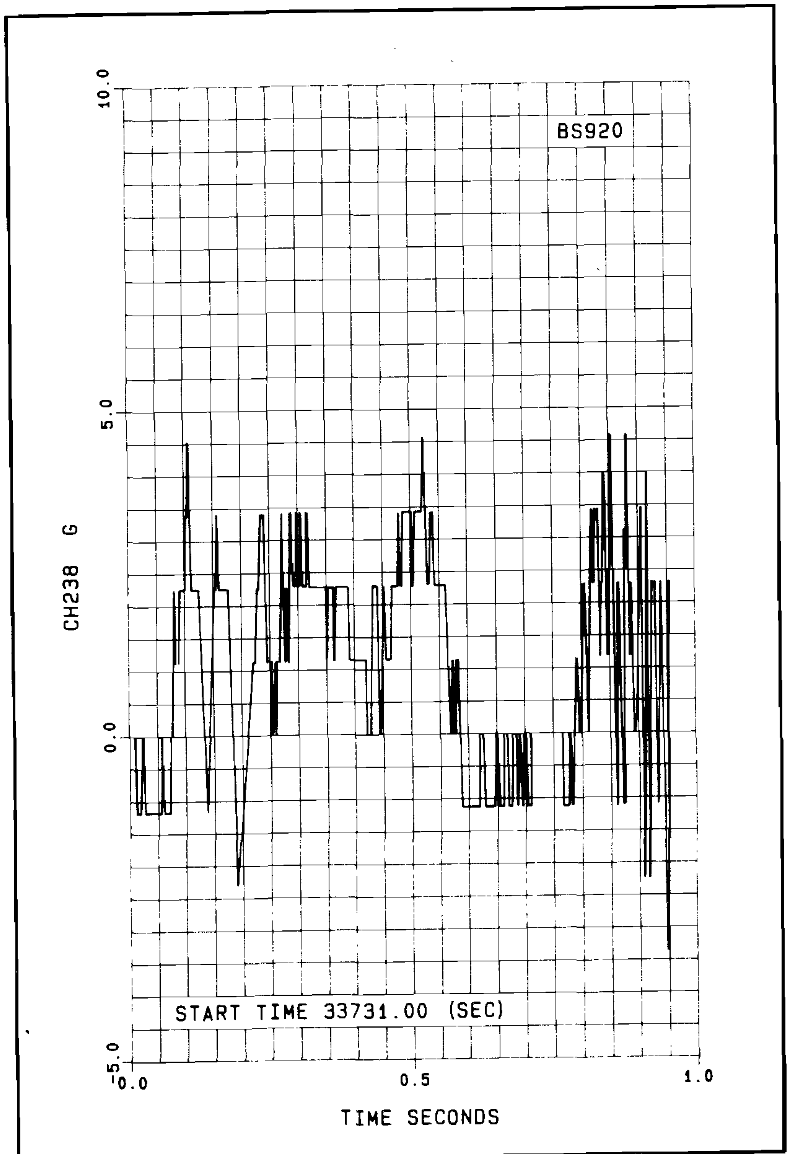

BS920.1

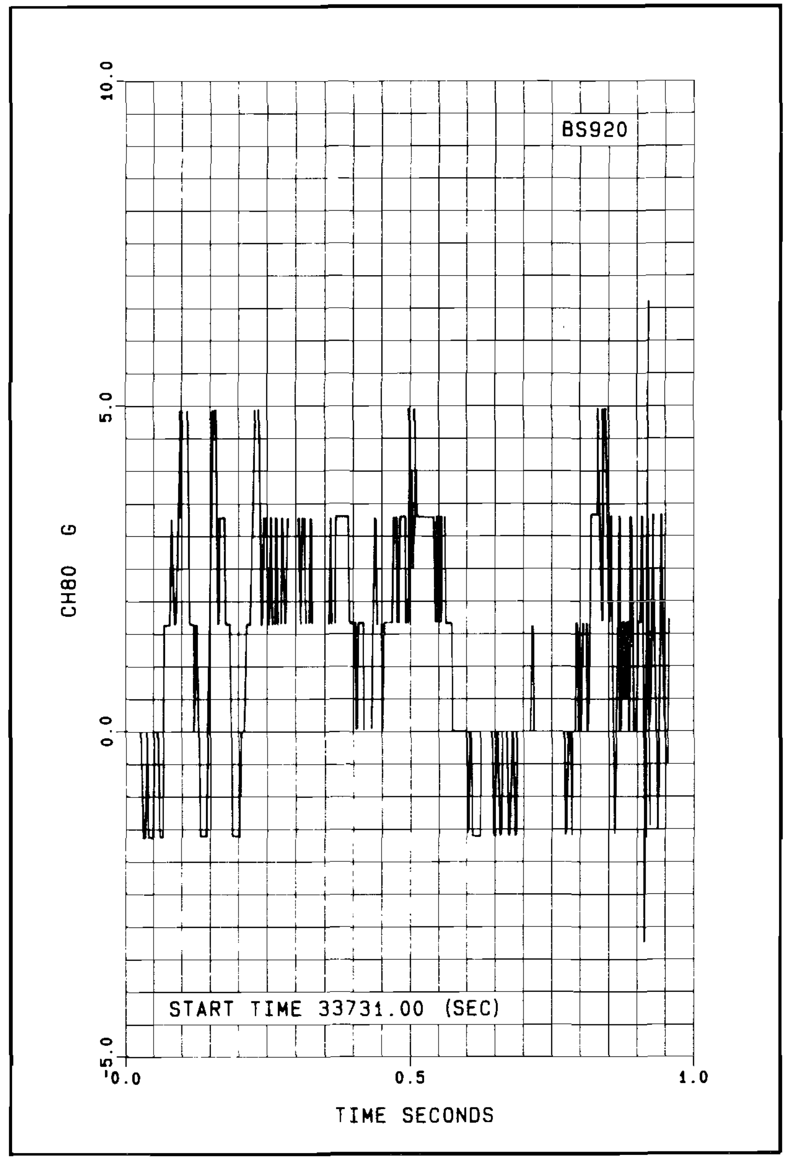

BS920.2

FIGURE 3-9. CID TEST NORMAL (VERTICAL) DIRECTION FLOOR ACCELERATIONS - BS920

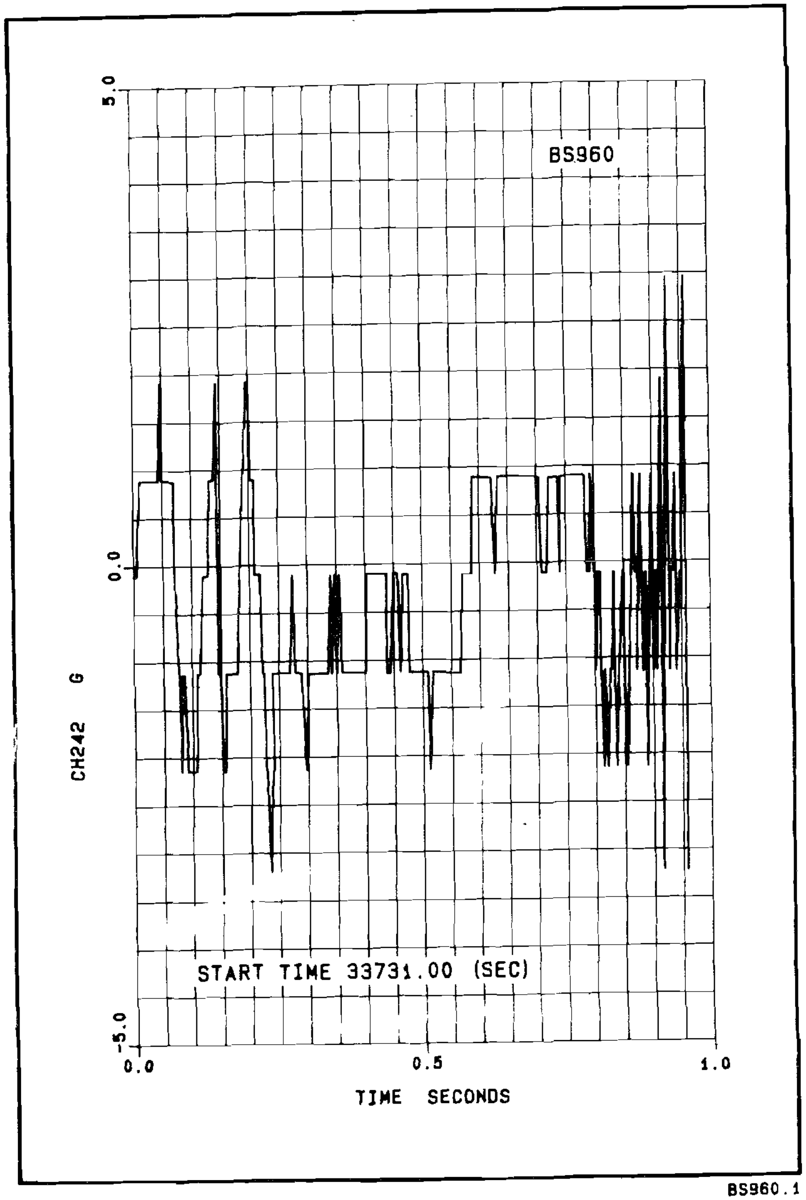

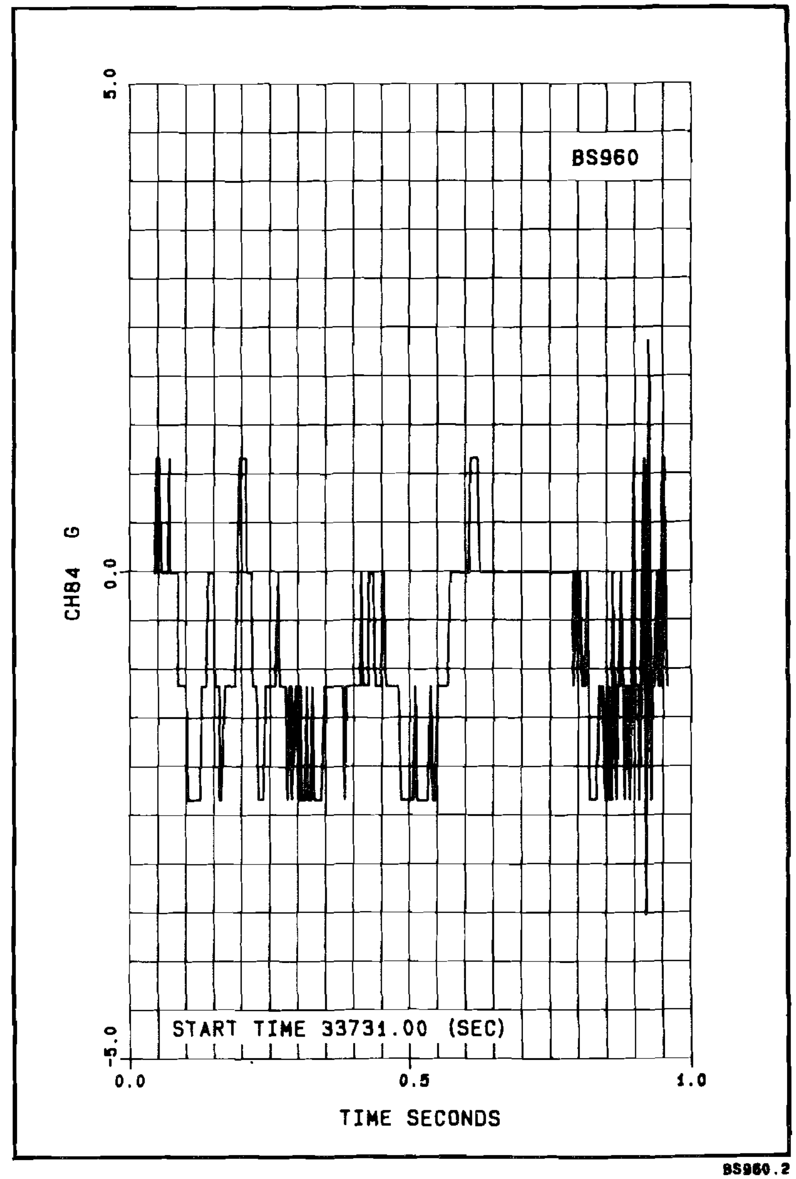

FIGURE 3-10. CID TEST NORMAL (VERTICAL) DIRECTION FLOOR ACCELERATIONS - BS960

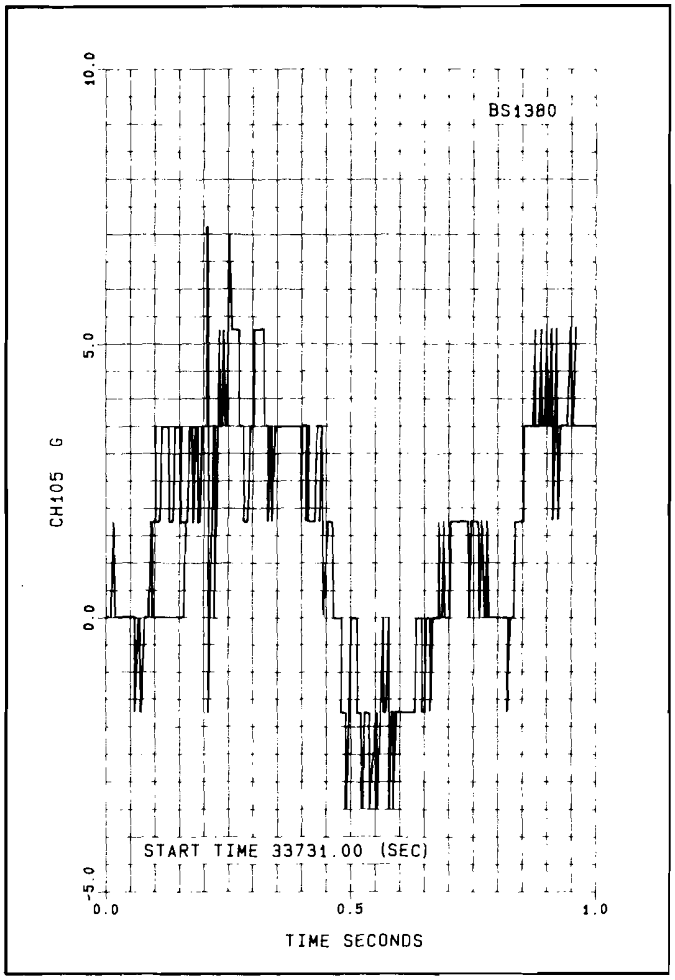

FIGURE 3-11. CID TEST NORMAL (VERTICAL) DIRECTION FLOOR ACCELERATIONS - BS1380

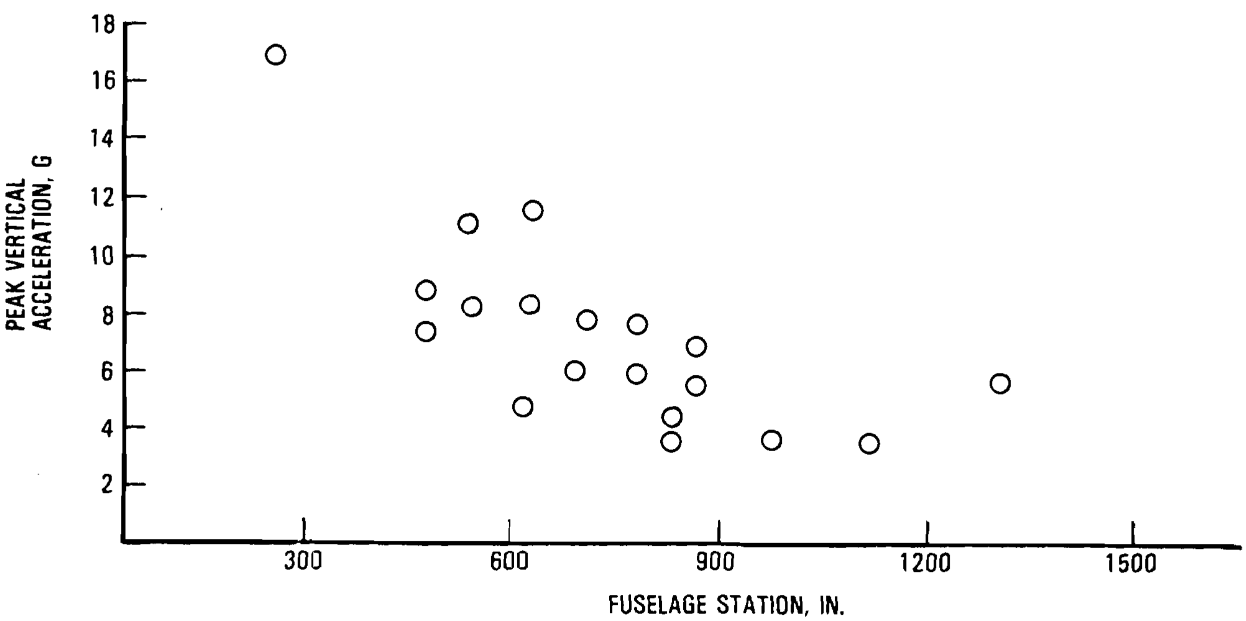

FIGURE 3-12. TEST DATA PEAK NORMAL ACCELERATION DISTRIBUTION

3.2 KRASH CORRELATION

3.2.1 Symmetrical Impact on Forward Fuselage

The comparison of analysis with test data was performed in two stages. The emphasis on the analysis was to determine floor responses so as to ascertain the potential effect on seat dynamic testing requirements. The initial impact on the left wing outboard engine (engine No. 1) did not produce the most significant floor pulses. The impact onto the forward fuselage resulted in higher floor responses than the engine impacts. Thus, as a first priority the analysis was performed for the initial fuselage impact. For simplification, this portion of the impact was considered to be symmetrical. The KRASH stick model was used in the initial comparisons.

The moment response data (figure 3-2) indicates that the airplane upon impact on the forward fuselage responds in a fuselage fundamental frequency mode of approximately 3 to 3.5 Hz and that structural damping is around seven percent of critical. The KRASH stick model frequency and damping characteristics are approximately 3 Hz and eight percent of critical, respectively. To ascertain these values the KRASH model was simulated in "free-fall" (no ground contact spring) and subjected to an acceleration pulse triangular in shape at FS300 (BS360). The results of the response are depicted in figure 3-13. The comparison of frequency and critical damping values indicates that the KRASH model contains stiffness mass and damping properties in agreement with the test article.

The fuselage impact was simulated for flat (0°) and nose-down attitudes (-1°, -2°), based on the findings presented in the post-CID briefing (reference 11) and the review of motion-picture/video coverage of the event. The sink speed is 14 ft/sec for all the fuselage symmetrical impact analyses. The affects of initial lift due to prior engine impact is included by applying upward external forces acting on the engine masses and allowing KRASH85 to balance the vehicle using the NASTRAN IC subroutine. This external load is

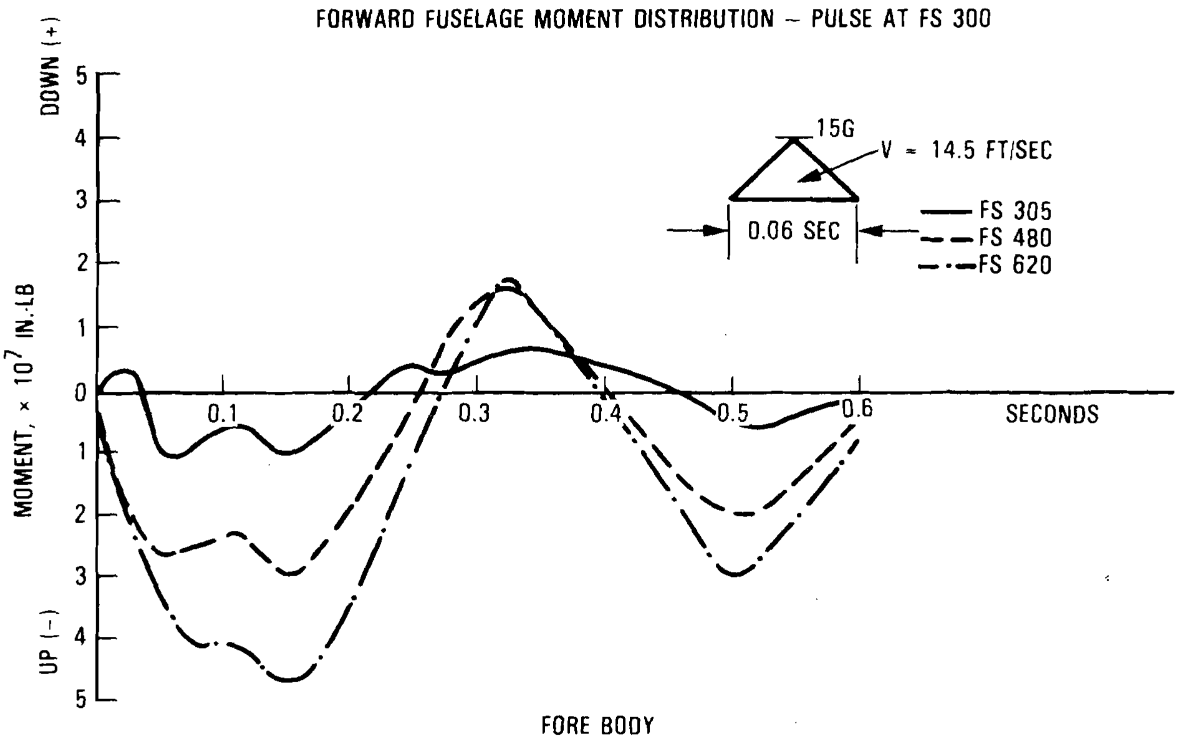

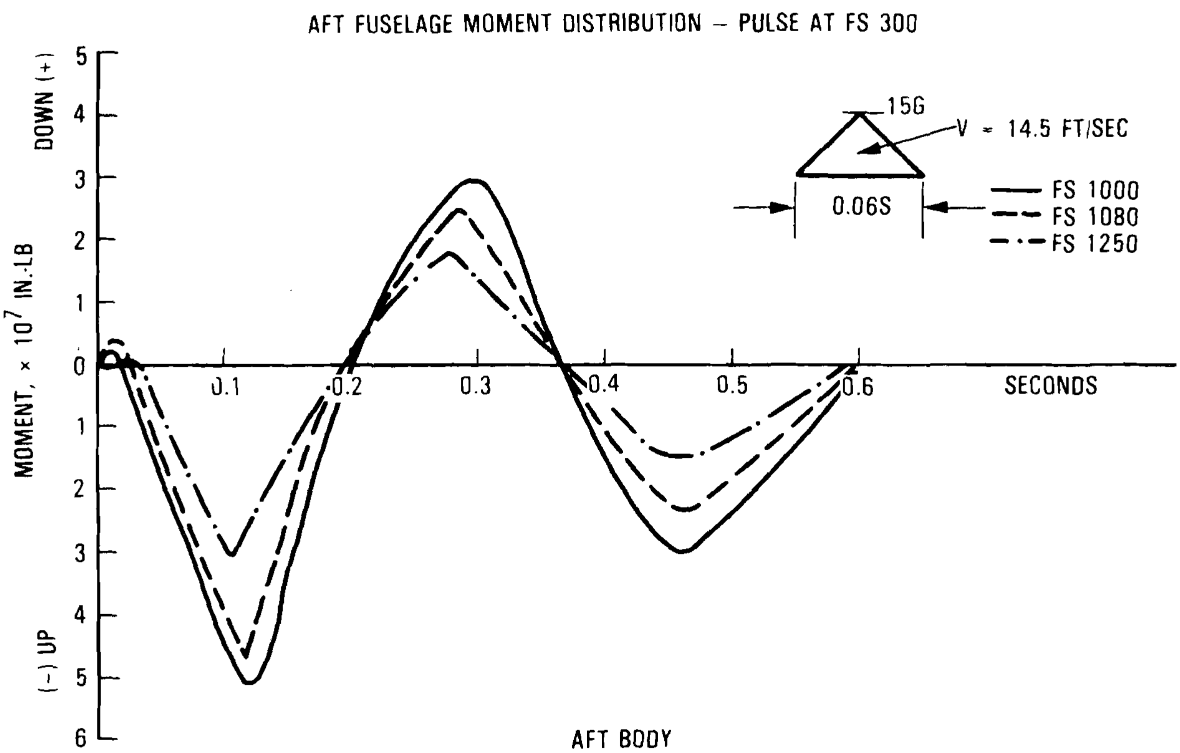

FIGURE 3-13. MOMENT RESPONSE DUE TO PULSE AT FS300 - CID KRASH STICK MODEL

applied at impact and relieved shortly thereafter. The moment distribution to account for the initial engine impact is obtained from the moment response data shown in figure 3-2 at the time noted "nose impact."

Comparisons between the KRASH stick model results for three attitudes (0°, -1°, -2°) for moment response, fuselage underside crush and airframe acceleration with post-test recorded results, were made. Figures 3-14 through 3-16 show the moment comparisons. Tables 3-2, 3-3 and 3-4 show comparisons of the crush and LIC, and vertical acceleration results, respectively. Figure 3-17 is a plot of LIC, peak vertical acceleration and crush distances for all three attitudes along with an indication of the corresponding estimated levels. The CID acceleration test results are faired to show an approximate level. The test data does show scatter as can be observed in figure 3-12. The LIC values are shown at FS350, 480, 600, 990, 1090 and 1210, which are close to the location of the moment bridges. The nose-down attitudes (-1°, -2°) tend to show better overall agreement with the test results.

Samplings of the time history responses for the stick model symmetrical impact onto the forward fuselage are shown in figures 3-18 through 3-23. The analytically determined responses at several fuselage stations are compared to the test data at corresponding locations. The test envelope was approximated for the time of interest as noted in the respective figures. As can be observed in the comparisons there is a general agreement in the pulses.

The correlation of the analysis with test results, as might be expected, does not agree with all aspects of the test results. For example, the aftbody down bending moments (figures 3-14 through 3-16) are much higher than those measured. The crushing from the MLG aft is probably more than experienced at impact. The more extensive aft fuselage crush occurs toward the end of the ground impact, while the aircraft is settling to a final position and does not influence the peak responses. Furthermore, the acceleration response comparisons (figures 3-18 through 3-23) reflect differences with regard to phasing and amplitude. These differences, however, are no greater than can be noted in the scatter of test measured responses at reasonably close fuselage locations (figure 3-12).

It is of interest to note is that the pretest CID model (mass, stiffness, damping, crush characteristics), was not altered. The correlation effort concentrated on assessing the affect of varying fuselage initial impact attitude within the range associated with the CID test would have on the responses. A difficulty in matching all the test results, other than the fact that a math model can only approximate complex nonlinear behavior, is that there are many variables that are not known. The modeling described is a "symmetrical representation" of an unsymmetrical impact. Initial conditions, such as rotational velocity, rotational acceleration and time varying external loading, along with the sequence and magnitude of the fuselage underside crush influence the phasing of the responses.

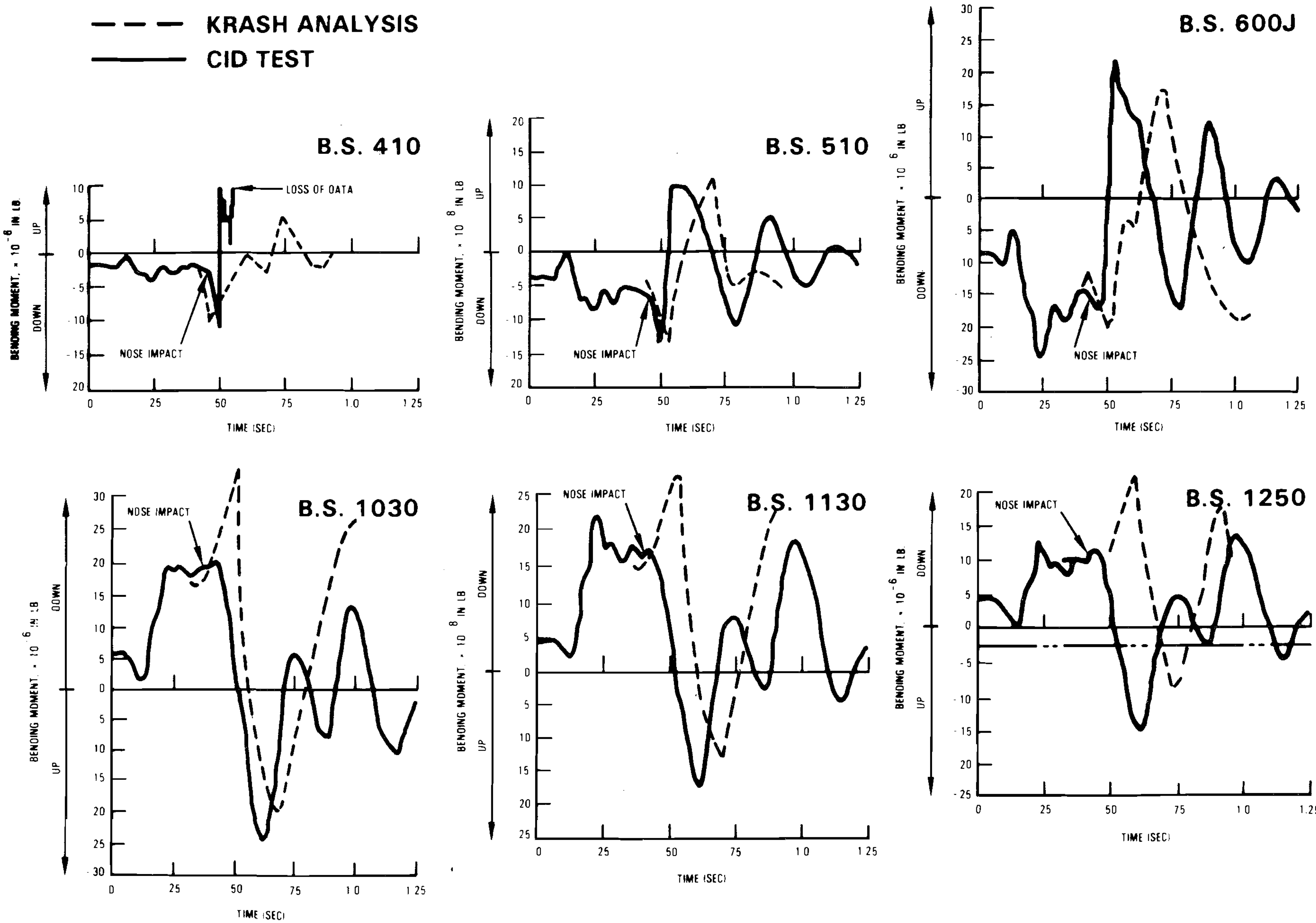

FIGURE 3-14. COMPARISON OF KRASH VERSUS TEST RESULTS, 0 DEGREE PITCH ATTITUDE, 14 FT/SEC SINK SPEED

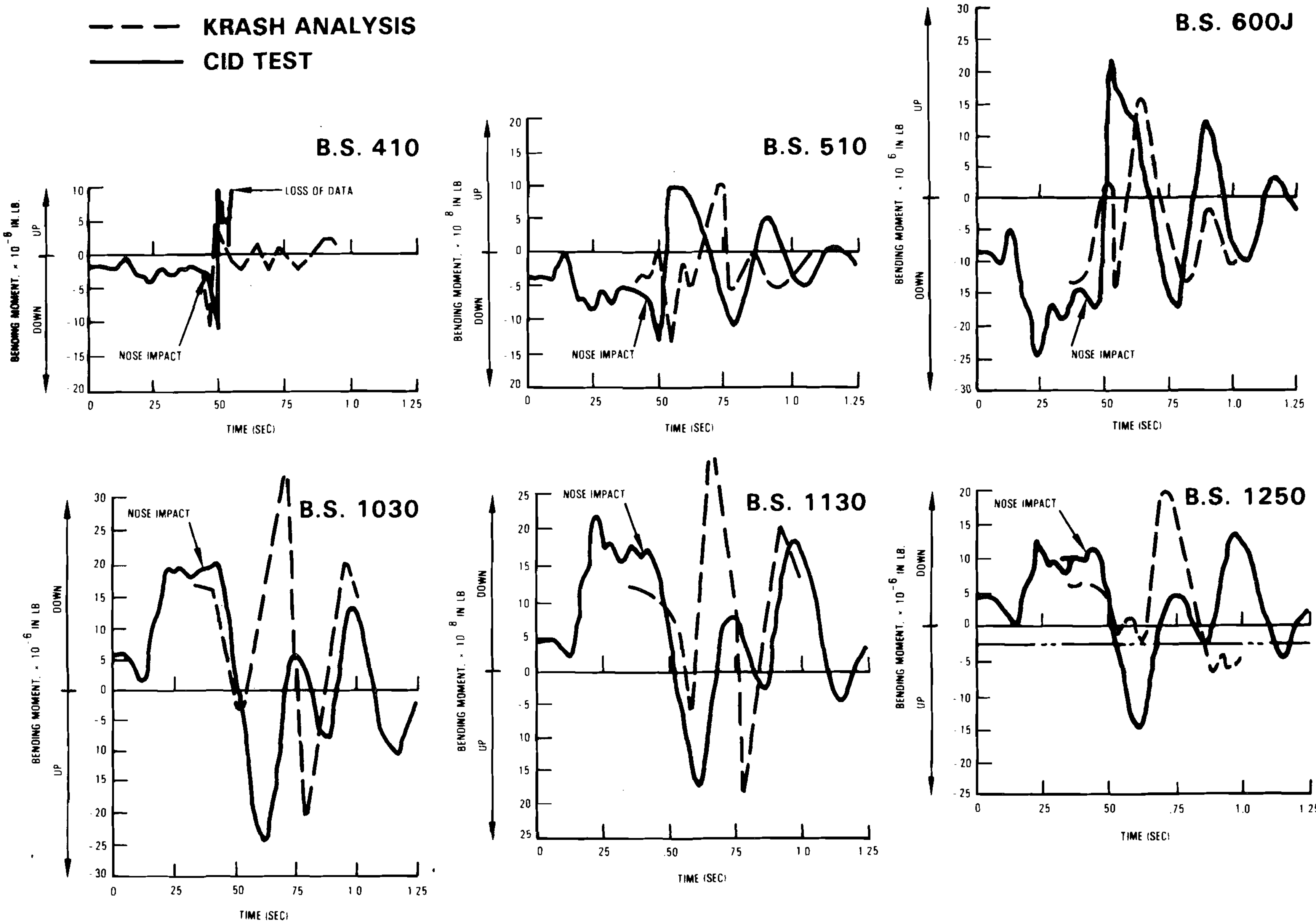

FIGURE 3-15. COMPARISON OF KRASH VERSUS TEST RESULTS, 1 DEGREE NOSE DOWN ATTITUDE, 14 FT/SEC. SINK SPEED

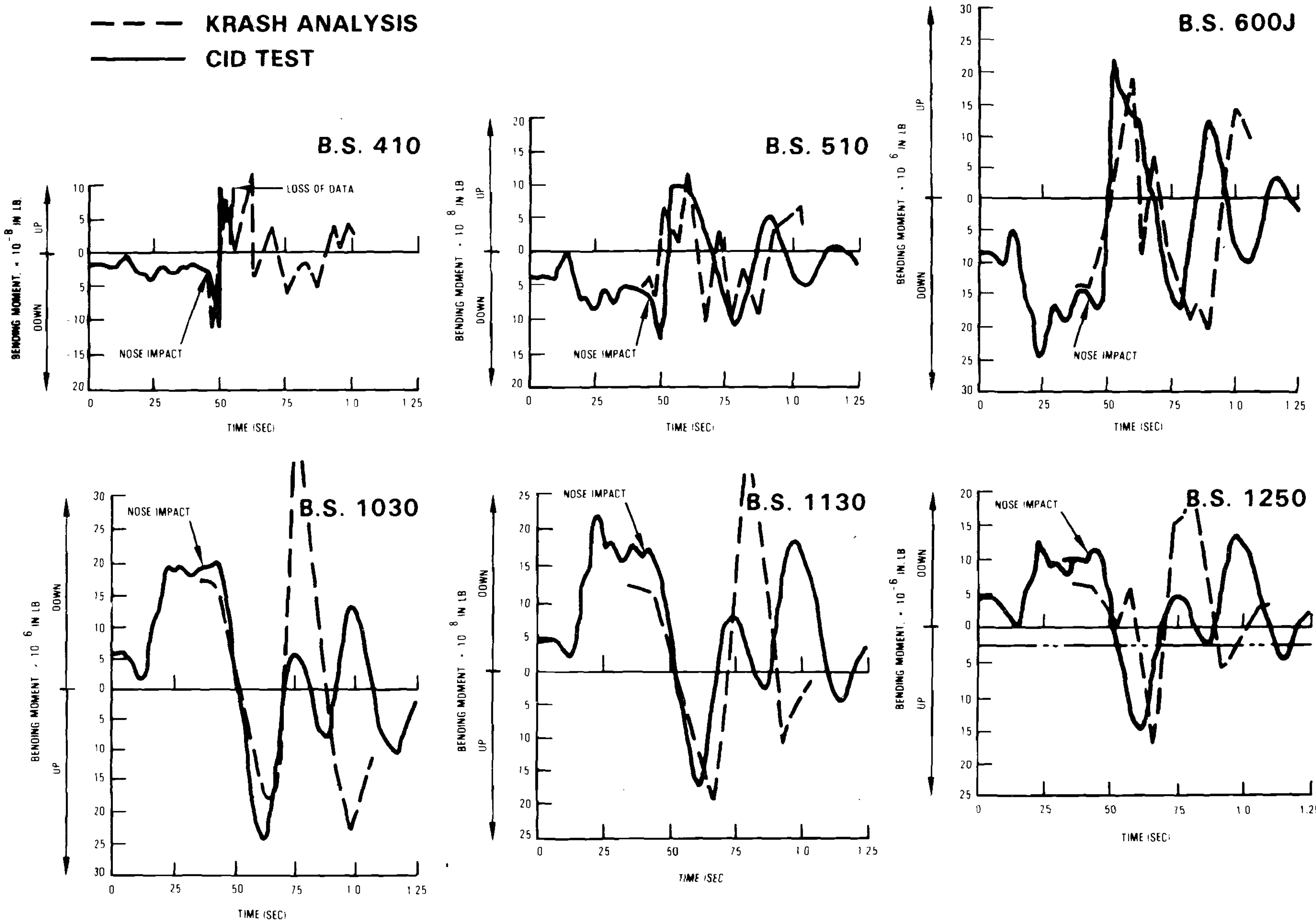

FIGURE 3-16. COMPARISON OF KRASH VERSUS TEST RESULTS, 2 DEGREE NOSE DOWN ATTITUDE, 14 FT/SEC. SINK SPEED

TABLE 3-2. COMPARISON OF FUSELAGE CRUSH OBTAINED FROM KRASH ANALYSIS AND POST-TEST MEASUREMENTS, STICK MODEL

LOCATION	MEASUREMENT, IN.	DEFLECTION (IN.) FROM KRASH ANALYSIS		
BS (FS)	POST–TEST MEASUREMENT, IN.	0^{o} PITCH	-1^{o} PITCH	-2^{o} PITCH
360 (300)	6.5	5.9	6.3	7.6
520 (460)	9.1 (1)	3.9	4.2	4.6
960 (960)	5.6	4.1 – 6.7 (2)	2.2 – 4.0 (2)	4.6 – 5.9 (2)
1120 (1080)	15.0 (1)	3.4 – 7.3 (2)	1.0 – 3.5 (2)	5.0 – 8.0 (2)
1220 (1180)	13.5 (1)	–	–	2.3 (2)

(1) APPEARS TOO HIGH FOR INITIAL IMPACT. MOST LIKELY INCREASED DEFLECTION OCCURRED AFTER KEEL BEAM SEPARATED DUE TO CUTTER IMPACT AND CONTRIBUTION FROM POST–CRASH FIRE.

(2) OCCURRED AFTER INITIAL IMPACT AS AIRCRAFT SETTLES AFT OF C.G. DOES NOT INFLUENCE PEAK RESPONSE.

TABLE 3-3. COMPARISON OF FUSELAGE LIC RATIOS OBTAINED FROM ANALYSIS AND TEST DATA, STICK MODEL

LOCATION BS (FS)	ESTIMATED TEST RESULTS	LIC RATIO FROM KRASH ANALYSIS		
		0^{o} PITCH	-1^{o} PITCH	-2^{o} PITCH
360 (300)	.33	.58	.48	.49
510 (450)	.40	.57	.38	.50
600 (600)	.40	.56	.33	.46
1030 (990)	.33	.77	.82	.59
1130 (1090)	.33	.78	.83	.63
1250 (1210)	.37	.72	.78	.46

TABLE 3-4. COMPARISON OF VERTICAL ACCELERATION RESPONSES FOR FUSELAGE IMPACT AT 14 FT/SEC., STICK MODEL

LOCATION (F.S.)	ACCELERATION RESPONSE(1)			
	ANALYSES (2)			ESTIMATED TEST RESULTS (PEAK G AND LOCATION)
	0 DEGREE	-1 DEGREE	-2 DEGREE	
199	13.2 (11.2, .120)	-13.2 (15.4, .050)	13.0 (16, .05)	14.4 (FS162)
300	11.1 (10.8, .120)	9.4 (10, .050)	9.2 (12.4, .05)	N.A.
460	10.6 (11.2, .100)	7.3 {7.6, .100} {6.8, .160}	7.3 {7.8, .054} {6.0, .150}	6-7.2 (FS480)
620	11.0 (12, .090)	6.8 (6.6, .160)	5.4 {4.7, .084} {4.6, .150}	3.5-10 (FS540) 5-6 (FS700)
820	11.7 (12, .090)	5.7 (6.1, .160)	5 (4.3, .130)	3.5-5.0 (FS820-FS860)
960	9.9 (11.5, .090	7.5 (6.2, .160)	5.3 (4.6, .120)	3.0-6.0 (FS920-FS960)
1000	8.6 (11.2, .090)	8.3 (6.2, .150)	5.5 (6, .100)	N.A.
1200	7.8 (9, .102)	9.3 {5.4, .150} {9.2, .070}	4.9 (5.6, .150)	4-5.2 (F1280)
1400	5.8 (6.7, .200)	6.7 (6.5, .140)	4.2 (5.6, .14)	N.A

(1) EQUIVALENT TRIANGULAR PULSE BASED ON IMPULSE DATA

(2) A(B, C); A = PEAK G 50 HZ FILTER
B = PEAK G TRIANGULAR PULSE BASED ON IMPULSE DATA
C = BASE DURATION ASSOCIATED WITH TRIANGULAR PULSE, SECONDS

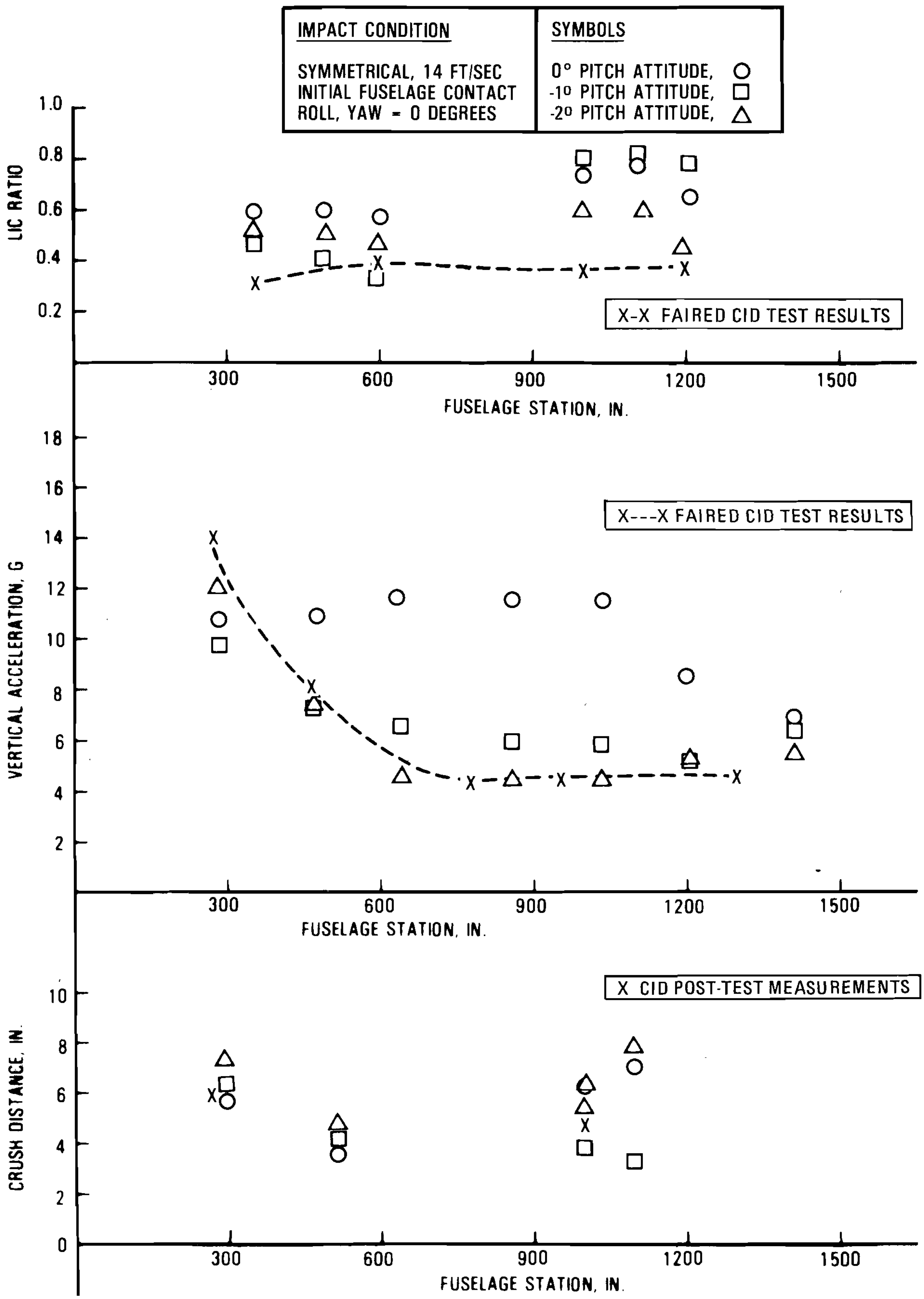

FIGURE 3-17. KRASH STICK MODEL RESULTS FOR SYMMETRICAL IMPACT ON FUSELAGE AT 14 FT/SEC.

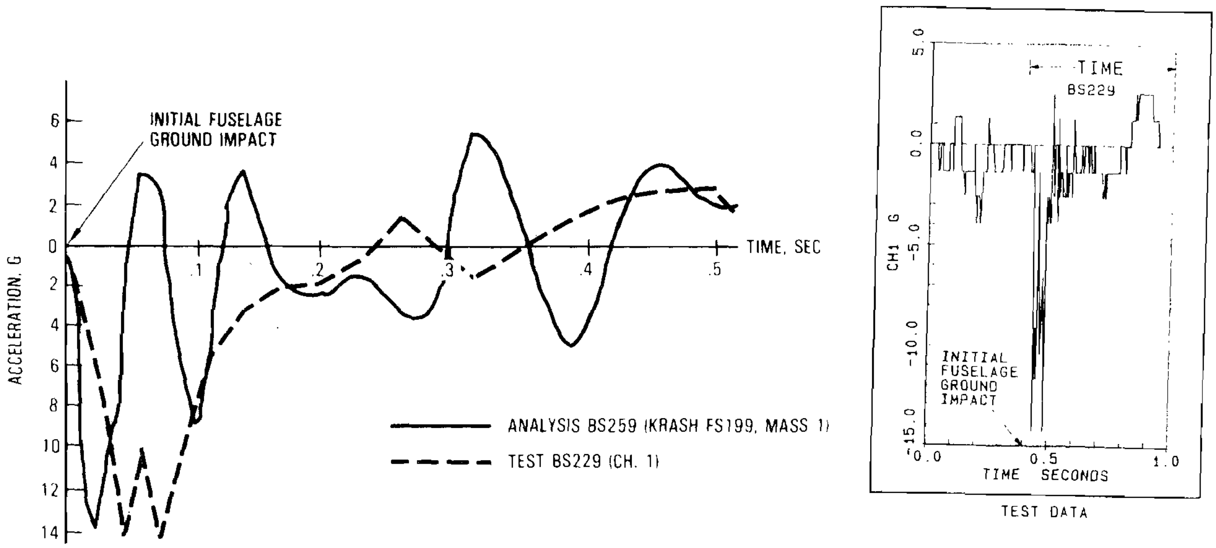

FIGURE 3-18. ACCELERATION RESPONSE, KRASH ANALYSIS VERSUS CID TEST DATA, BS229, STICK MODEL

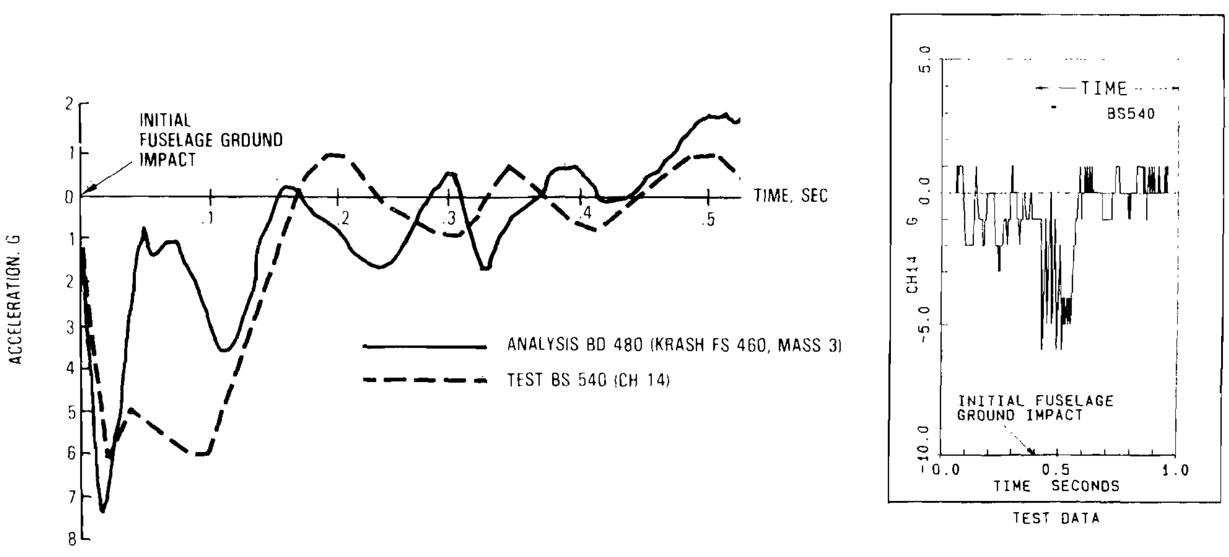

FIGURE 3-19. ACCELERATION RESPONSE, KRASH ANALYSIS VERSUS CID TEST DATA, BS540, STICK MODEL

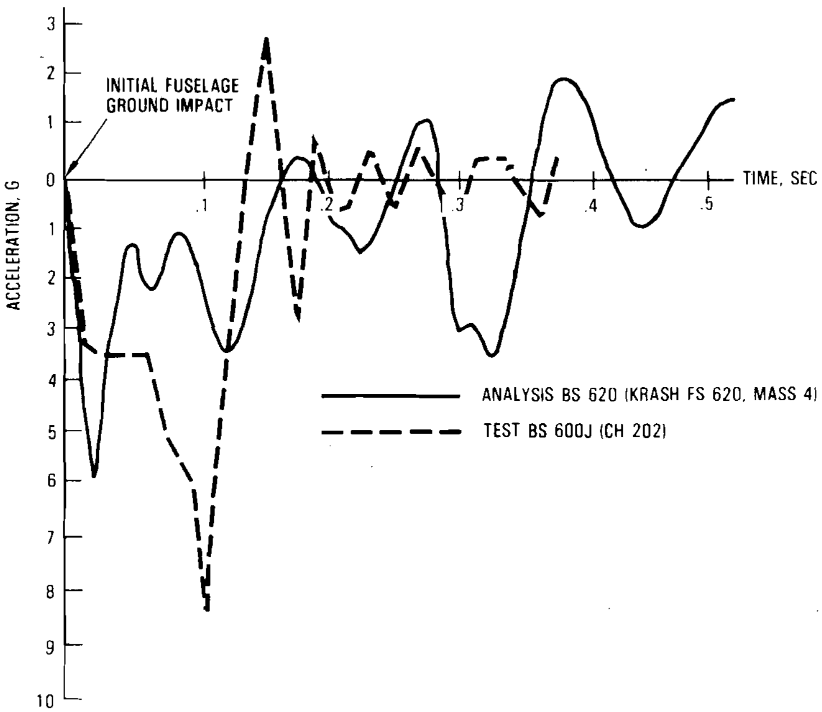

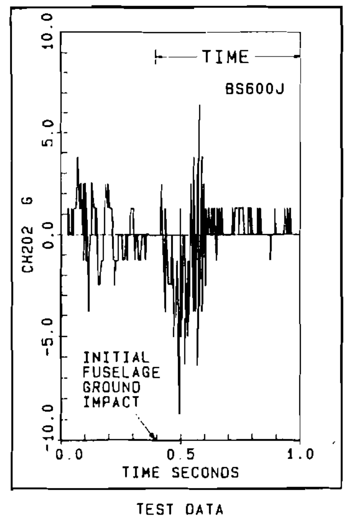

FIGURE 3-20. ACCELERATION RESPONSE, KRASH ANALYSIS VERSUS CID TEST DATA, BS600J, STICK MODEL

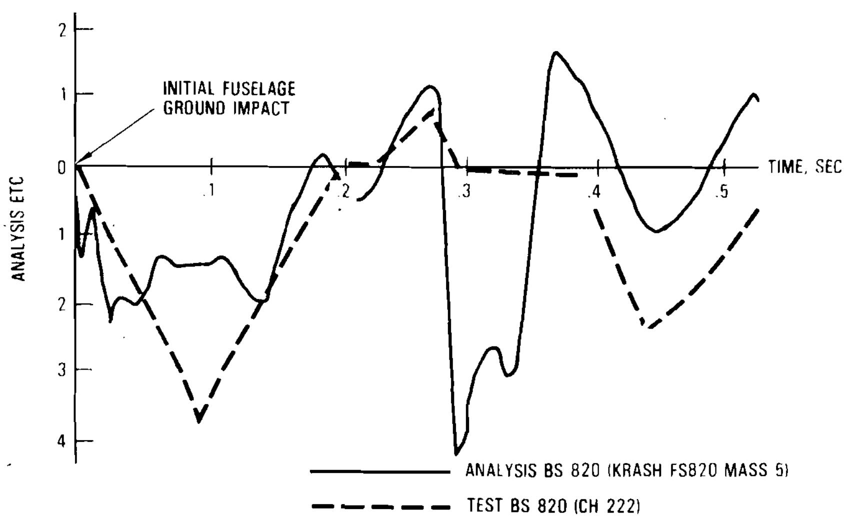

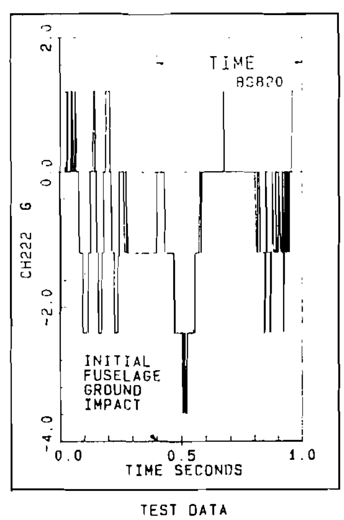

FIGURE 3-21. ACCELERATION RESPONSE, KRASH ANALYSIS VERSUS CID TEST DATA, BS820, STICK MODEL

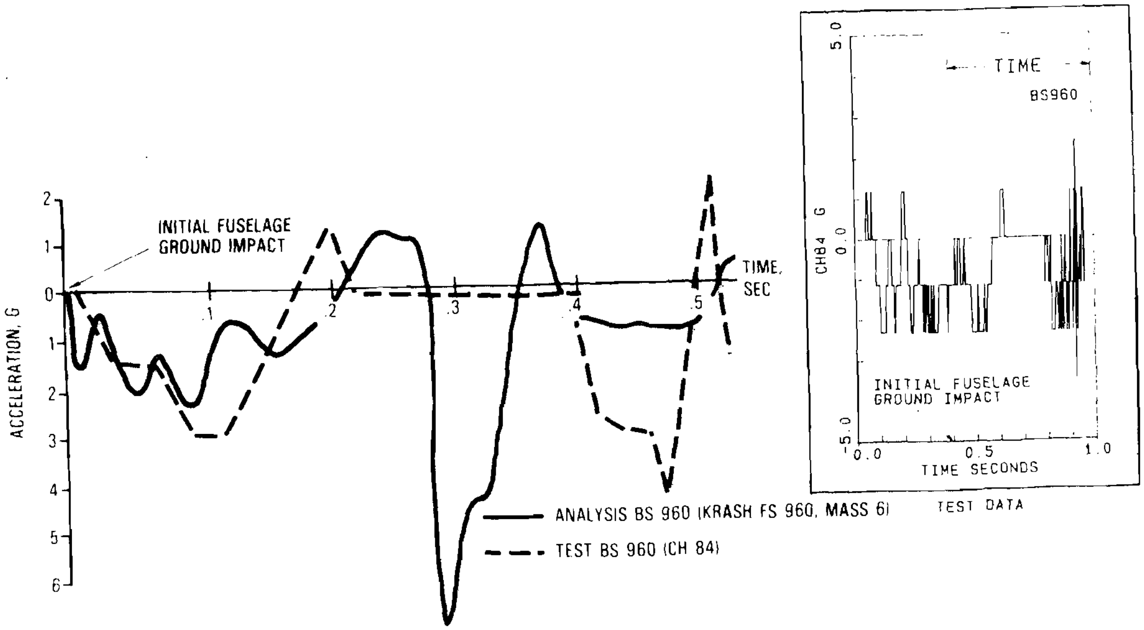

FIGURE 3-22. ACCELERATION RESPONSE, KRASH ANALYSIS VERSUS CID TEST DATA, BS960, STICK MODEL

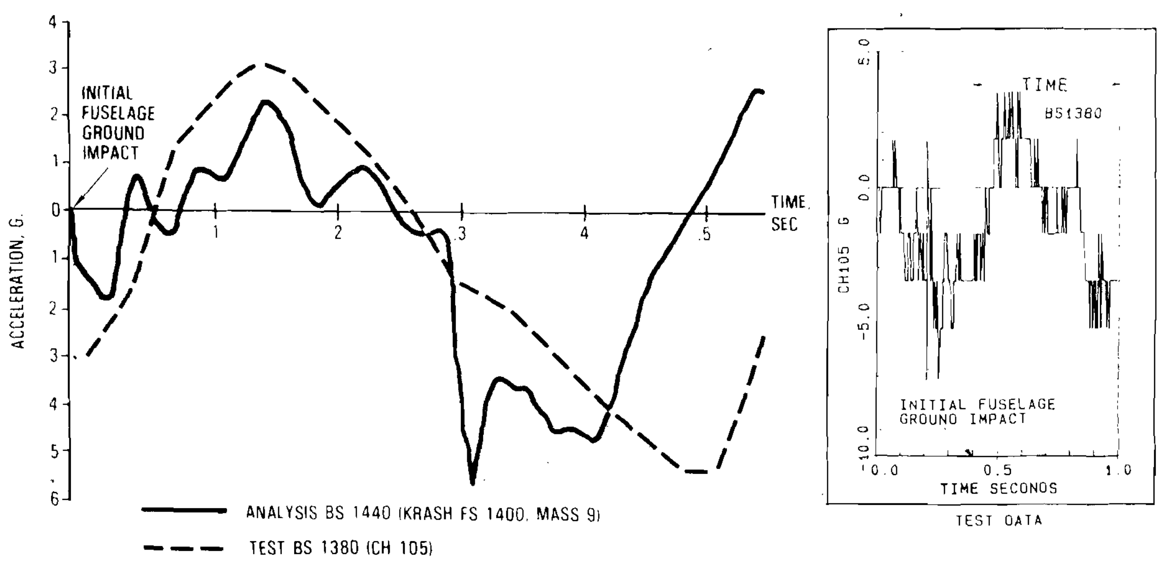

FIGURE 3-23. ACCELERATION RESPONSE, KRASH ANALYSIS VERSUS CID TEST DATA, BS1380, STICK MODEL

3.2.2 Unsymmetrical Impact on Engine No. 1

Subsequent to the fuselage symmetrical impact analysis, the KRASH stick model was used to simulate the complete unsymmetrical impact sequence from initial left outboard engine (No. 1) ground contact through fuselage impact. The initial condition investigated for this unsymmetrical impact was:

Sink Speed	=	17.3 ft/sec
Forward Velocity	=	150 knots
Roll Angle	=	13 degrees (left wing down)
Yaw Angle	=	13 degrees (nose left)
Pitch Angle	=	+1, 0, -1/2, -1 degrees

The initial runs, using the pre-CID input data for engine load-deflection curves, resulted in engine separation (rupture of engine wing attachment beam). This occurred early in the run and, thus, the engine failure was associated with little energy being absorbed and, consequently, at initial fuselage contact the airplane cg velocity was significantly higher than the 14 ft/sec (168 in/sec) noted at the FAA/NASA post-CID debriefings. The engine load-deflection curve was modified, as noted in figure 3-24, and the failure loads were increased to allow the engine to remain attached to the pylon longer. The beam attaching the engine to the wing in the KRASH model is not allowed to rupture until the engine restiffens. A ruptured beam in KRASH provides no load path. In addition, the initial aerodynamic loading was treated as acting unsymmetrical (higher lift on the right wing versus the left wing). The original analysis considered lift to act symmetrically, which results in a more rapid rotation onto the right side and subsequent right side outboard engine contact with the ground. Such an event did not occur during the CID test. In subsequent analyses the right wing was considered to have more initial lift than the left wing and it was maintained longer. With the revised model, the unsymmetrical impact condition, noted above, was run for a pitch attitude between 1 degree nose-down and 1 degree nose-up. Tables 3-5, 3-6 and 3-7 show the tabulated results for the unsymmetrical runs. When considering engine No. 2 contact, location of fuselage impact, fuselage impact velocity, and time at which fuselage contact is made, the flatter (0°, -1/2°

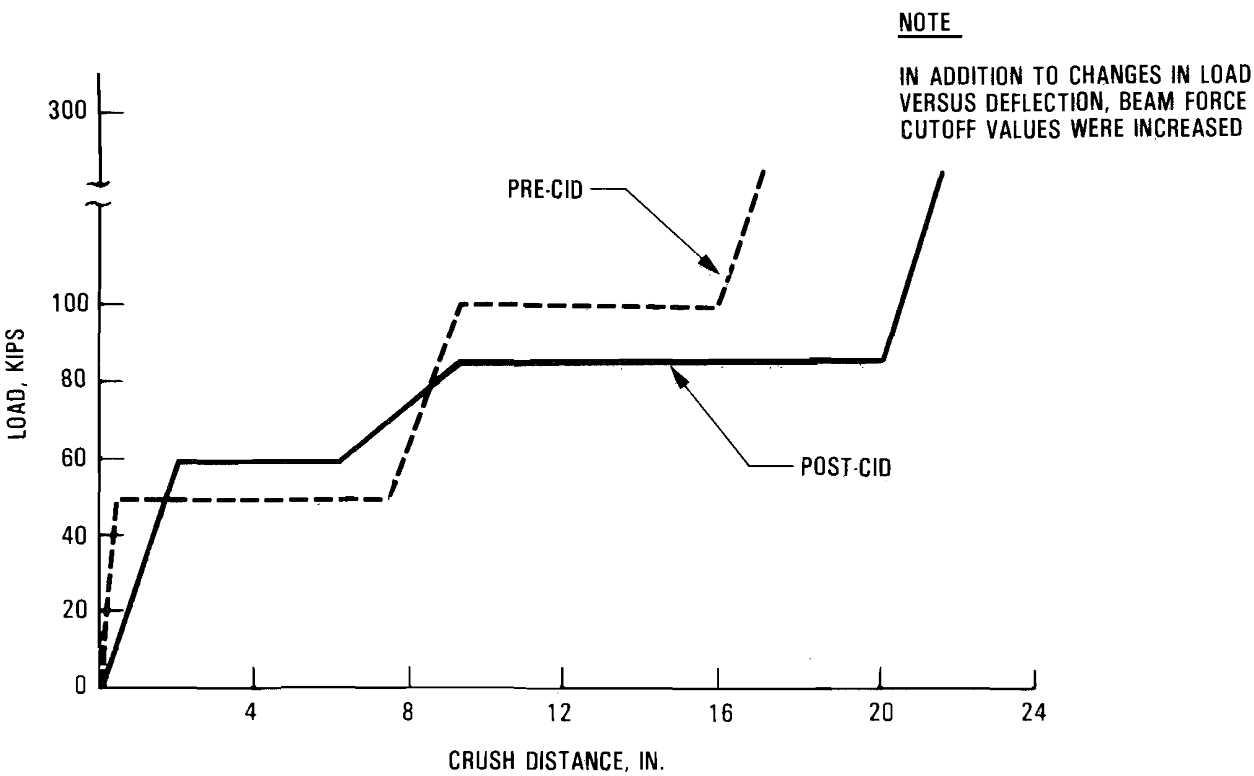

FIGURE 3-24. ENGINE CRUSH CHARACTERISTICS PRE- AND POST-CID ANALYSES

TABLE 3-5. COMPARISON OF UNSYMMETRICAL IMPACT SEQUENCE, ANALYSES VERSUS TEST, STICK MODEL

	KRASH ANALYSIS PITCH ATTITUDE				TEST DATA
	+1	0	-1/2	-1	
INITIAL FUSELAGE CONTACT					
MASS NO. (FIGURE 2-1)	7	6 (2)	6 (1)	2	2–3
TIME (SEC) (3)	.382	.400	.404	.377	.400
MASS IMPACT VELOCITY, IN./SEC	183	191	191	147	168
CG VELOCITY, IN./SEC	157	158	158	161	
ENGINE NO. 2 CONTACT					
TIME (SEC) (3)	.092	.078	.071	.064	.080

(1) MASS NO. 2 HITS 5 MSEC. LATER

(2) MASS NO. 2 HITS 39 MSEC. LATER

(3) AFTER ENGINE NO. 1 INITIAL GROUND CONTACT

TABLE 3-6. COMPARISON OF ANALYSES VERSUS TEST LIC, CRUSH AND VERTICAL ACCELERATION RESULTS FOR THE UNSYMMETRICAL IMPACT, STICK MODEL

LOCATION	KRASH ANALYSES PITCH ATTITUDE (DEGREES) +1	0	-1/2	-1	ESTIMATED TEST DATA RANGE
	LIC RATIO				
FS 350	.27–.49	.22–.49	.13–.52	.15–.59	.27–.33 (3)(4)
FS 600–620	.8–.82	.52–.61	.47–.51	.42–.48	.35–.40
FS 960–990	.73–18.3	.56–.81	.61–.73	.62–.73	.26–.33
FS 1210	.75	.60	.68	.80	.3–.37
	ACCELERATION PEAK VERTICAL G TRIANGULAR PULSE(1)				
199	23.0 (.090)	16.0 (.120)	11.6 (.140)	11.8 (.090)	14.4
300	14.0 (.120)	12.4 (.120)	9.6 (.150)	7.0 (.140)	NA (5)
460	7.2 (.170)	10.0 (.120)	8.2 (.140)	7.5 (.160)	6–9.0
620	7.0 (.160)	9.2 (.120)	8.2 (.140)	8.2 (.140)	6.5–10.0
820	7.0 (.140)	9.2 (.120)	9.6 (.120)	9.8 (.120)	3.5–5.5
960	8.0 (.140)	9.2 (.120)	9.4 (.120)	10.0 (.110)	3.5–6.5
1040	7.8 (.150)	9.2 (.120)	9.2 (.120)	10.0 (.110)	NA (5)
1200	7.4 (.190)	9.0 (.130)	8.1 (.130)	7.6 (.120)	4–5.5 (FS 1280)
1400	9.6 (.190)	7.6 (.180)	6.7 (.200)	7.8 (.180)	
	CRUSH DISTANCE, INCHES				
FS 300	2.2	4.3	5.2	6.3	6-7 (FS 320)
FS 460	2.2	3.9	4.6	5.2	6-7 (FS 480)
FS 620	3.5	4.6	5.1	5.2	NA (5)
FS 820	6.1	6.0	5.7	5.1	NA (5)
FS 960	9.2	7.4	6.2	5.0	5–7 (FS 920)
FS 1040	10.0	7.1	5.5	3.7	11 (FS 1180)(2)
FS 1200	2.5	–	–	–	

(1) G (Δt); PEAK G = $\frac{\text{IMPULSE X 2}}{\Delta t}$, (Δt) = BASE DURATION FOR TRIANGULAR PULSE, SEC.

(2) INCLUDES POST-FIRE CRUSH AFTER LOSS OF KEEL BEAM

(3) DATA TRACE LOST

(4) BASED ON ALLOWABLE MOMENT USED IN KRASH MODEL

(5) NA – NOT AVAILABLE

TABLE 3-7. COMPARISON OF ANALYSIS VERSUS TEST LONGITUDINAL AND LATERAL ACCELERATIONS RESULTS FOR THE UNSYMMETRICAL IMPACT, STICK MODEL

LOCATION (F.S.)	ACCELERATION PULSE, TRIANGULAR(1)				
	KRASH ANALYSES PITCH ATTITUDE (DEGREES) (2)				ESTIMATED TEST DATA RANGE
	+1	0	-1/2	-1	
	LONGITUDINAL				
199	3.6 (.140)	3.3 (.140)	3.7 (.140)	3 (.160)	4.9–6.5 (FS 162)
300	3.4 (.150)	3.6 (.130)	3.7 (.130)	3.1 (.130)	2.5–4.0 (FS 340)
460	3.6 (.140)	3.6 (.130)	3.5 (.130)	2.8 (.160)	3.0–3.2 (FS 480)
620	3.6 (.140)	3.4 (.130)	3.4 (.130)	2.8 (.160)	2.5–3.1 (FS 540–600)
820	3.6 (.140)	3.4 (.130)	3.4 (.130)	2.9 (.156)	2.0–3.5 (FS 702–820)
960	3.6 (.140)	3.4 (.130)	3.4 (.130)	3. (.150)	2.2–4.2 (FS 960)
1200	3.4 (.140)	3.2 (.130)	3.4 (.130)	2.9 (.150)	2.0–4.0 (FS 1120)
1400	2.9 (.140)	4. (.080)	3.4 (.130)	4.0 (.100)	1.0–3.5 (FS 1380)
	LATERAL				
199	2.3 (.160)	4. (.050)	3. (.090)	2.9 (.100)	4.0–5.0 (FS 162)
300	1.6 (.150)	2. (.080)	2.1 (.100)	2.0 (.100)	3.0–4.0 (FS 340)
460	1. (.150)	1.4 (.100)	1. (.100)	1.4 (.100)	2.8 (FS 480)
620	1. (.150)	1.2 (.100)	1. (.100)	1.0 (.100)	4.0–7.0 (FS 540)
820	1. (100)	1.0 (.100)	1. (.100)	1.0 (.100)	1.5 (FS 702–820)
960	1. (.100)	1.5 (.100)	1. (.100)	1.0 (.100)	1.0 (FS 960)
1200	1.3 (.100)	1.5 (.120)	1.(.100)	1.0 (.100)	1.5 (FS 1120)
1400	1.8 (.200)	1.7 (.140)	1. (.200)	2.0 (.120)	1.5–2.5 (FS 1380)

(1) $G(\Delta t)$; PEAK G $\approx \frac{\text{IMPULSE X 2}}{\Delta t}$; (Δt) = BASE DURATION FOR A TRIANGULAR PULSE, SEC

(2) POSITIVE PITCH ATTITUDE IS NOSE-UP

pitch attitudes tend to be more consistent with the test data. From table 3-6 a comparison of LIC ratios, acceleration levels and crushing distance seems to support the flat to nose-down attitudes. This range is consistent with the FAA/NASA post-CID debriefing data and observation of the high-speed film and video tapes of the crash sequence. The results for the 0°, -1/2°, -1° cases are shown in figure 3-25. Figure 3-25 compares three parameters; the Load Interaction Curve (LIC) ratio at several locations, the vertical acceleration triangular pulse accelerations, and crush along the fuselage. The equivalent vertical acceleration triangular pulse is obtained by taking the plotted mass impulse (g-sec), which is the acceleration pulse integrated over time, in the region of peak response. This yields an average acceleration. For a triangular pulse, the peak value is two times the average. This appears to present a more consistent interpretation of the response. If only the peaks are used, then the question of plot interval arises as to whether or not the peak value is plotted. The appropriate filter characteristics such as cut-off frequency and decay slope also enter into the interpretation of results. The acceleration data presented in figure 3-25 represents a triangular pulse with a base duration (Δt) of 100 to 150 milliseconds. For comparison, estimates of the range wherein the test data falls are also shown in figure 3-25. The test peak acceleration points, obtained from the tape of the digitized data, indicate some degree of scatter, either from different measurements at nearby locations, or in the interpretation of the representative peak. Thus, a faired test result curve is presented along with data points. Generally, the analytical data shows higher responses than the corresponding test results. The estimate of test LICs is probably low because it is based on measured versus allowable moments only. The analysis results are based on combined moment-shear and, thus, the allowable may be lower. The crush data are difficult to compare because the measured crush at the forward fuselage (FS350) and aft of the main landing gear bulkhead (FS960), reflects loss of keel beam from the wing rupture posts and/or the effects of post-crash fire. The measured crush in the wing center section (FS620-820), which was not as severely burned, is more realistic and the comparison between it and analysis appears reasonable.

The vertical, lateral and longitudinal acceleration responses, obtained from the KRASH unsymmetrical analyses for the 0° to -1° range of pitch attitude are shown in figure 3-26, along with the test data range from the CID test. The dashed line in figure 3-26 represents the -1/2° pitch attitude analytical condition. As noted earlier the vertical accelerations are at the upper bound of the test data range. The lateral acceleration distribution trend is in agreement with the test data, however, with a tendency to be lower throughout the fuselage. The longitudinal acceleration generated from analysis is between 3.5 and 4.0g throughout the fuselage. The test data indicates a maximum of 4 to 6g at the cockpit. Aft of the cockpit the longitudinal acceleration is generally in the 2g to 3g range.

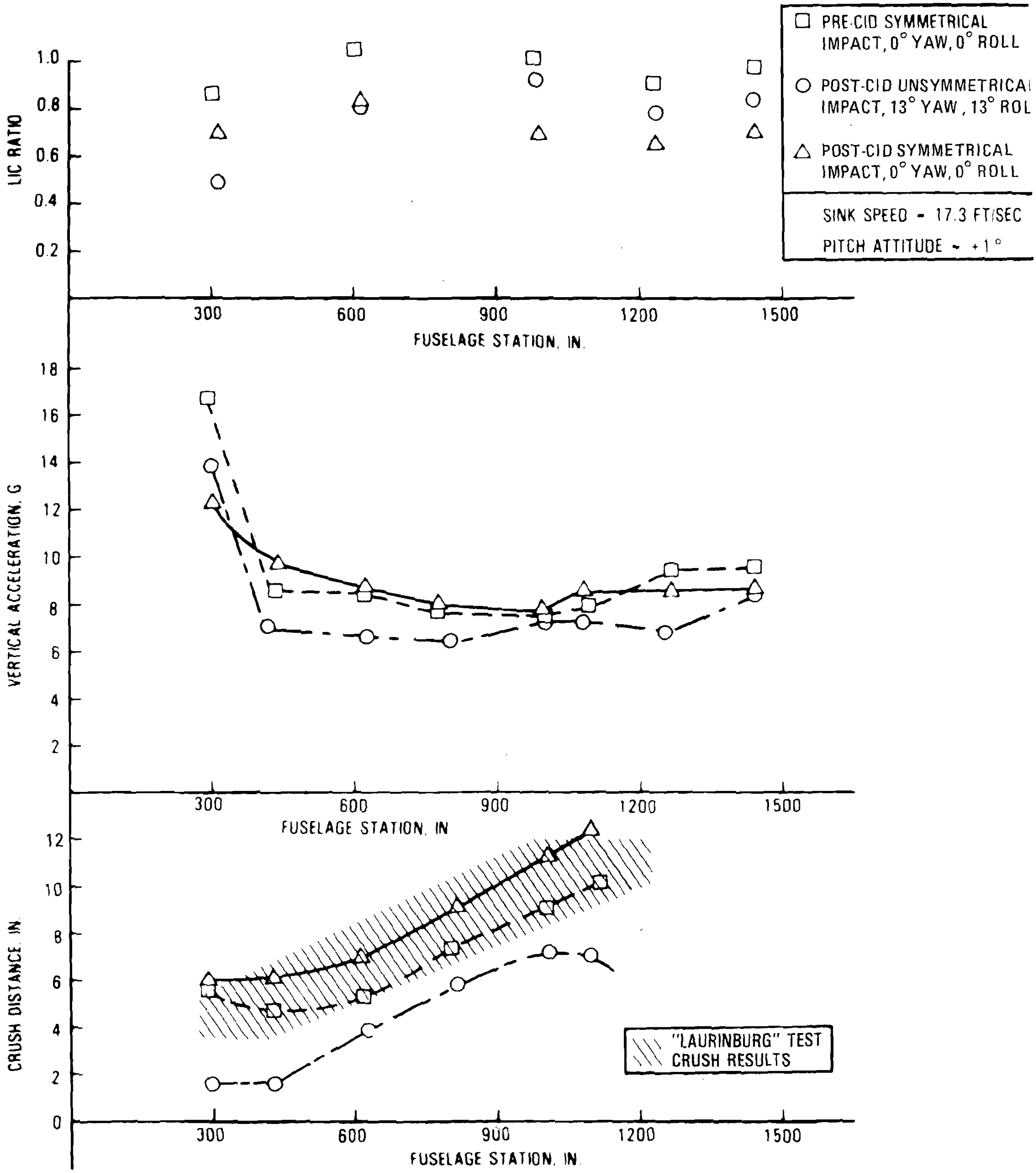

FIGURE 3-25. UNSYMMETRICAL IMPACT CONDITION COMPARISONS, INITIAL CONTACT ON ENGINE NO. 1

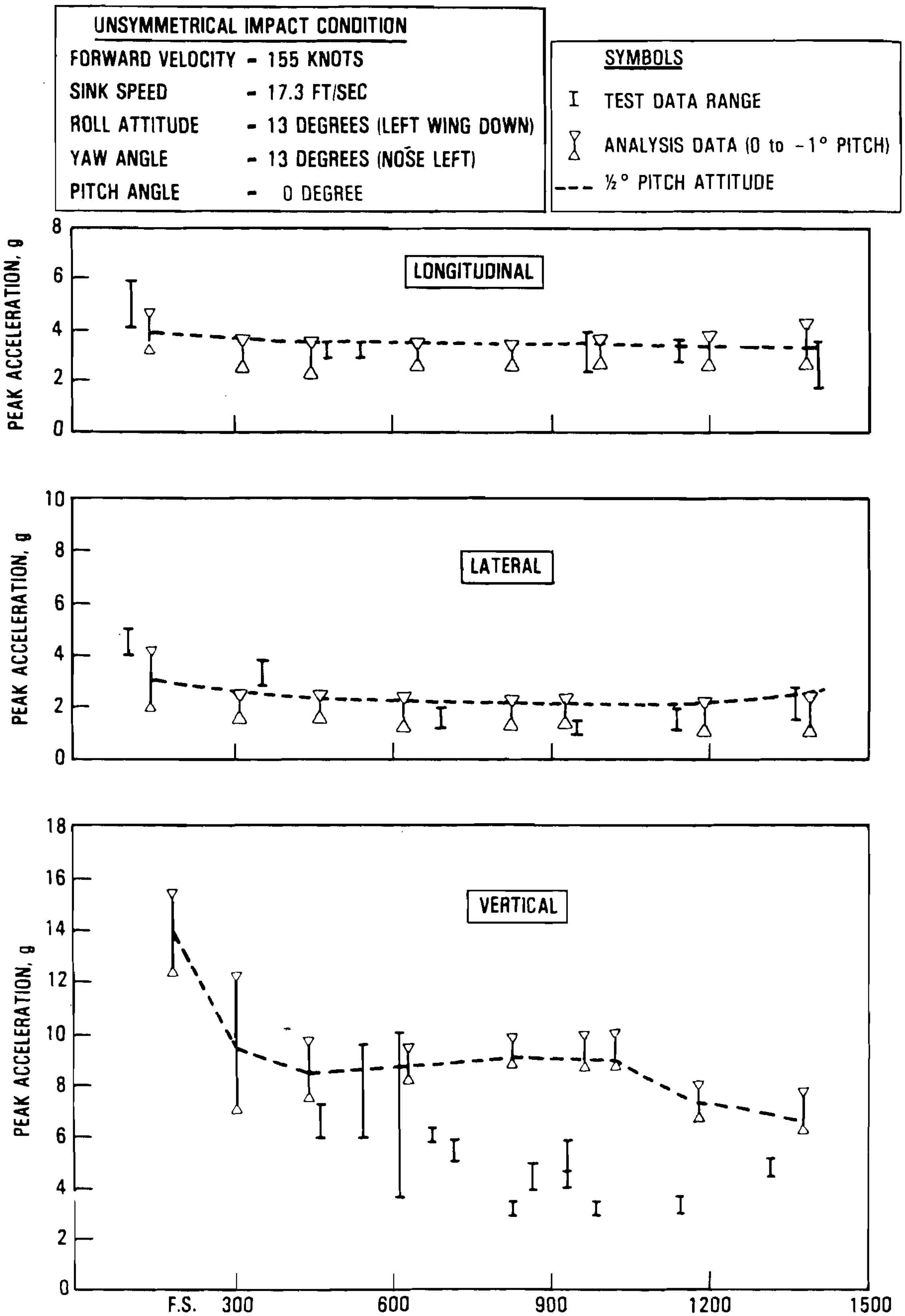

FIGURE 3-26. COMPARISON OF TEST VERSUS ANALYSIS STICK MODEL RESULTS - UNSYMMETRICAL IMPACT, STICK MODEL

All of the preceding analysis results for the unsymmetrical impact were performed assuming no initial rotational velocities. Subsequent to these analyses a KRASH stick model run was also performed for the 0° pitch attitude condition, but with assumed initial roll and pitch rates equal to 0.04 rad/sec. The wing engine No. 1 vertical impact velocity, which consists of both translational and rotational velocity components, was maintained at 17.3 ft/sec. The results from this analysis are shown in tables 3-8 and 3-9 and figure 3-27. From the table 3-8 it can be noted that the overall sequence is consistent with the observed test results. In some respects it is slightly better than the previous results without an initial rotational velocity, although fuselage contact is made 32 milliseconds later than the test data indicates. The peak triangular pulse acceleration levels and distribution appears to be closer to the test data (figure 3-27), although still higher than measured from FS600 through to the aft pressure bulkhead. The LIC ratios fall within the range of previous analyses results. The crush is more pronounced in the forward fuselage region and is less along the fuselage span. Although the crush at FS620 to FS1040 appears low compared to noted FAA/NASA post-test measurements, it must be remembered that the latter measurements are taken after the keel beam was dislodged when the No. 3 engine and subsequentially the fuselage was penetrated by the "Tomahawk." A nose-down attitude impact would be expected to have a crush distribution as noted in the latter analysis which includes initial rotational velocities. The acceleration data from tables 3-9 and 3-10 for the 0 degree pitch condition with the initial roll and pitch rotational velocities are plotted in figure 3-28. For comparison purposes the test data range is also shown.

3.2.3 Comparison of Fuselage versus Engine Impact Results

In Sections 3.2.1 and 3.2.2 the results from two KRASH model analyses are presented for the following conditions.

1. Initial impact on engine No. 1 through to impact onto the fuselage-unsymmetrical attitude, 17.3 ft/sec sink rate, 1/2 degree nose-down, 13 degree yaw (nose left), 13 degree roll (left wing down) - complete

2. Initial impact on fuselage-symmetrical attitude, 14 ft/sec, 1 degree nose-down abbreviated impact.

TABLE 3-8. COMPARISON OF ANALYSIS VERSUS TEST RESULTS FOR THE UNSYMMETRICAL IMPACT SEQUENCE - EFFECT OF INITIAL ROTATIONAL VELOCITY, STICK MODEL

	KRASH ANALYSIS PITCH ATTITUDE, DEGREES (4)				
	INITIAL ROLL/YAW RATES	NO INITIAL ROLL/YAW RATES			
	0	0	-1/2	-1	TEST DATA
INITIAL FUSELAGE CONTACT					
MASS NO. (FIGURE 2-1)	2	6(2)	6(1)	2	2–3
TIME (SEC) (3)	.432	.400	.404	.377	.400
FUSELAGE CONTACT VELOCITY IN./SEC	165	191	191	147	168
ENGINE NO. 2 CONTACT					
TIME (SEC) (3)	.083	.078	.071	.064	.080

(1) MASS NO. 2 HITS 5 MSEC. LATER
(2) MASS NO. 2 HITS 39 MSEC. LATER
(3) AFTER ENGINE NO. 1 INITIAL GROUND CONTACT
(4) INITIAL ROLL/PITCH RATES = .04 RAD/SEC, INITIAL ENGINE CONTACT VELOCITY = 17.3 ST/SEC

The former condition (No. 1) was run for 0.750 seconds and includes a sequence of impacts including engine No. 1, engine No. 2, forward fuselage, mid-fuselage and aft-fuselage. The latter condition (No. 2) starts with an initial loading developed from the previous engine impacts, but considers the forward fuselage contact at a reduced velocity (14 ft/sec) as the first significant impact. The resultant responses, from both models, should be in agreement if the reproduction of all force sequencing and phasing can be faithfully reproduced. Figure 3-29 compares the results obtained from both analyses. The unsymmetrical analysis also considers initial rotational velocity.

A comparison of the resultant LIC ratios indicates reasonably close agreement except at the fuselage aft end. A comparison of the acceleration distribution indicates that the symmetrical impact tends to provide lower acceleration levels than the faired test data curve, but not too much different than the lower bound of the test data envelope. The unsymmetrical analysis acceleration responses are higher than the test data from the mid

TABLE 3-9. COMPARISON OF ANALYSIS VERSUS TEST LIC RATIOS, CRUSH DISTANCES AND VERTICAL ACCELERATIONS RESULTS, UNSYMMETRICAL IMPACT - EFFECT OF INITIAL ROTATIONAL VELOCITY, STICK MODEL

LOCATION	KRASH ANALYSES PITCH ATTITUDE (DEGREES) INITIAL ROLL/YAW RATES 0	NO INITIAL ROLL/YAW RATES 0	NO INITIAL ROLL/YAW RATES -1/2	NO INITIAL ROLL/YAW RATES -1	ESTIMATED TEST DATA RANGE
	LIC RATIO				
FS 350	.15–.56	.22–.49	.13–.52	.15–.59	.27–.33 (3)(4)
FS 600–620	.43–.55	.52–.61	.47–.51	.42–.48	.35–.40
FS 960–990	.62–.78	.56–.81	.61–.73	.62–.73	.26–.33
FS 1210	.75	.60	.68	.80	.3–.37
	ACCELERATION PEAK VERTICAL G, TRIANGULAR PULSE(1)				
199	17.0 (.090)	16.0 (.120)	11.6 (.140)	11.8 (.090)	14.4
300	10.0 (.100)	12.4 (.120)	9.6 (.150)	7.0 (.140)	NA (5)
460	7.5 (.160)	10.0 (.120)	8.2 (.140)	7.5 (.160)	6–9.0
620	8.4 (.130)	9.2 (.120)	8.2 (.140)	8.2 (.140)	6.5–10.0
820	8.0 (.130)	9.2 (.120)	9.6 (.120)	9.8 (.120)	3.5–5.5
960	8.0 (.130)	9.2 (.120)	9.4 (.120)	10.0 (.110)	3.5–6.5
1040	8.3 (.120)	9.2 (.120)	9.2 (.120)	10.0 (.110)	NA (5)
1200	6.6 (.130)	9.0 (.130)	8.1 (.130)	7.6 (.120)	4–5.5 (FS 1280)
1400	6.4 (.170)	7.6 (.180)	6.7 (.200)	7.8 (.180)	
	CRUSH DISTANCE, IN.				
FS 300	7.8	4.3	5.2	6.3	6-7 (FS 320)
FS 460	5.5	3.9	4.6	5.2	6-7 (FS 480)
FS 620	4.5	4.6	5.1	5.2	NA (5)
FS 820	3.4	6.0	5.7	5.1	NA (5)
FS 960	3.0	7.4	6.2	5.0	5–7 (FS 920)
FS 1040	2.0	7.1	5.5	3.7	11 (FS 1180)(2)
FS 1200	–	–	–	–	

(1) G(Δt); PEAK G = $\frac{\text{IMPULSE X 2}}{\Delta t}$, ($\Delta$t) = BASE DURATION FOR TRIANGULAR PULSE, Sec.

(2) INCLUDES POST-FIRE CRUSH AFTER LOSS OF KEEL BEAM

(3) DATA TRACE LOST

(4) BASED ON ALLOWABLE MOMENT USED IN KRASH MODEL

(5) NA = NOT AVAILABLE

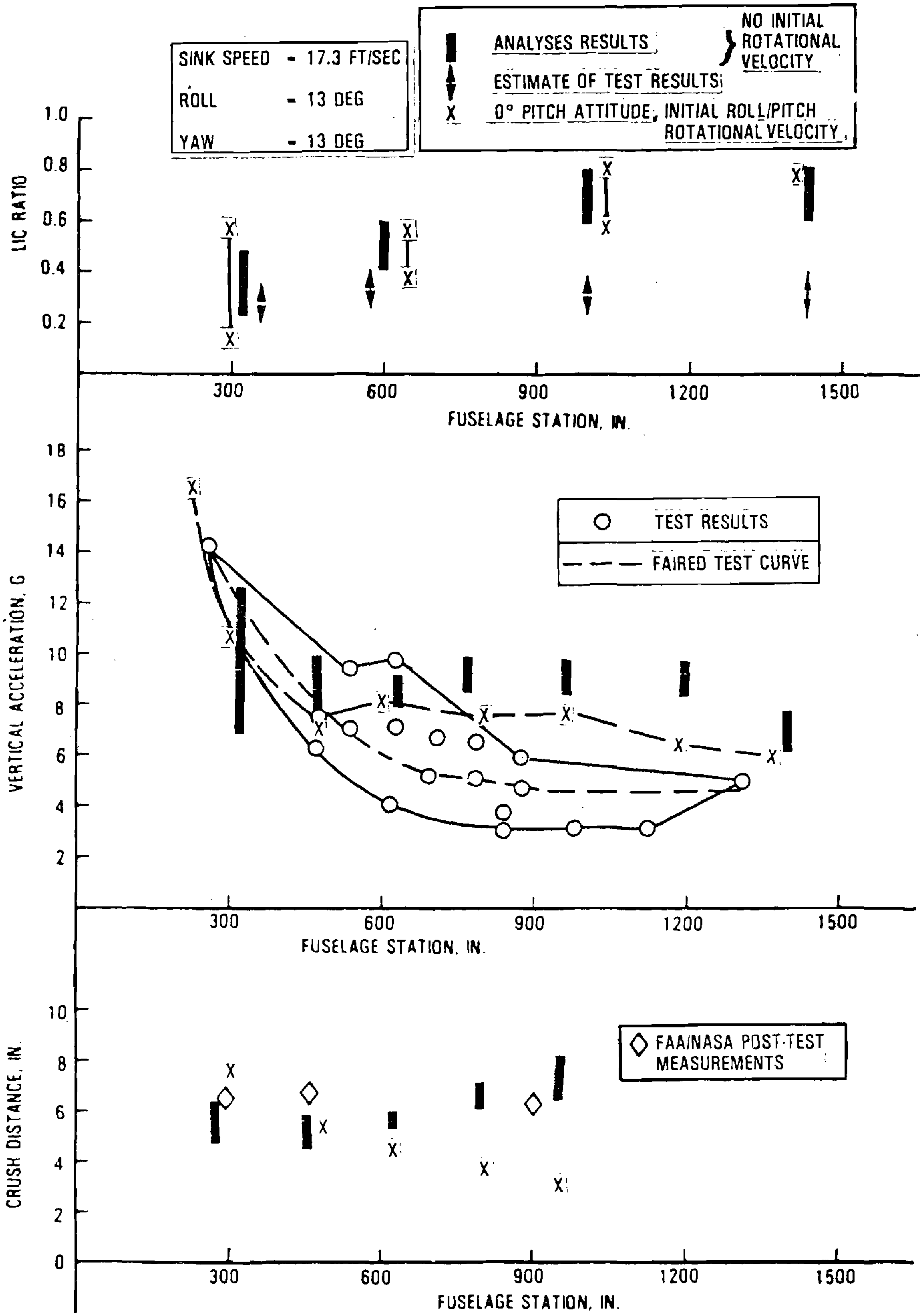

FIGURE 3-27. UNSYMMETRICAL IMPACT CONDITION COMPARISONS, INITIAL CONTACT ON ENGINE NO. 1, WITH AND WITHOUT INITIAL ROTATIONAL VELOCITIES, STICK MODEL

TABLE 3-10. COMPARISON OF ANALYSIS VERSUS TEST LONGITUDINAL AND LATERAL ACCELERATION RESULTS FOR THE UNSYMMETRICAL 17.3 FT/SEC IMPACT, STICK MODEL

LOCATION (F.S.)	ACCELERATION PULSE, TRIANGULAR(1) — KRASH ANALYSES PITCH ATTITUDE (DEGREES) (2): INITIAL ROLL/YAW RATES 0	NO INITIAL ROLL/YAW RATES 0	NO INITIAL ROLL/YAW RATES -1/2	NO INITIAL ROLL/YAW RATES -1	ESTIMATED TEST DATA RANGE
	LONGITUDINAL				
199	3.2 (.110)	3.3 (.140)	3.7 (.140)	3 (.160)	4.9–6.5 (FS 162)
300	3.2 (.110)	3.6 (.130)	3.7 (.130)	3.1 (.130)	2.5–4.0 (FS 340)
460	3.1 (.110)	3.6 (.130)	3.5 (.130)	2.8 (.160)	3.0–3.2 (FS 480)
620	2.8 (.150)	3.4 (.130)	3.4 (.130)	2.8 (.160)	2.5–3.1 (FS 540–600)
820	2.7 (.170)	3.4 (.130)	3.4 (.130)	2.9 (.156)	2.0–3.5 (FS 702–820)
960	2.6 (.160)	3.4 (.130)	3.4 (.130)	3. (.150)	2.2–4.2 (FS 960)
1200	2.8 (.140)	3.2 (.130)	3.4 (.130)	2.9 (.150)	2.0–4.0 (FS 1120)
1400	3.0 (.140)	4. (.080)	3.4 (.130)	4.0 (.100)	1.0–3.5 (FS 1380)
	LATERAL				
199	3.1 (.150)	4. (.050)	3. (.090)	2.9 (.100)	4.0–5.0 (FS 162)
300	2.1 (.150)	2. (.080)	2.1 (.100)	2.0 (.100)	3.0–4.0 (FS 340)
460	1.2 (.070)	1.4 (.100)	1. (.100)	1.4 (.100)	2.8 (FS 480)
620	1.0 (.070)	1.2 (.100)	1. (.100)	1.0 (.100)	1.5–2.5 (FS 540) 3.0 (FS 600)
820	1.6 (.100)	1.0 (.100)	1. (.100)	1.0 (.100)	1.5 (FS 702–820)
960	1.6 (.080)	1.5 (.100)	1. (.100)	1.0 (.100)	1.0 (FS 960)
1200	1.6 (.100)	1.5 (.120)	1.(.100)	1.0 (.100)	1.5 (FS 1120)
1400	1.6 (.100)	1.7 (.140)	1. (.200)	2.0 (.120)	1.5–2.5 (FS 1380)

(1) G(Δt); PEAK G $= \frac{\text{IMPULSE X 2}}{\Delta t}$, (Δt) = BASE DURATION FOR A TRIANGULAR PULSE, SEC.

(2) POSITIVE PITCH ATTITUDE IS NOSE-UP

fuselage through to the aft pressure bulkhead; both for the faired curve and the enveloped upper bound. The full duration unsymmetrical analysis generally shows lower crush except in the forward fuselage region where both analyses are in close agreement. The crush in the region from FS820 through to the aft fuselage for the symmetrical impact analysis is greater than that for the unsymmetrical analysis.

3.2.4 One-Degree Nose-Up Analyses Results

The planned impact, as noted previously, was to be symmetric with one-degree nose-up pitch attitude and a sink speed of approximately 17 ft/sec. The actual impact occurred with a sink speed close to the desired value, but

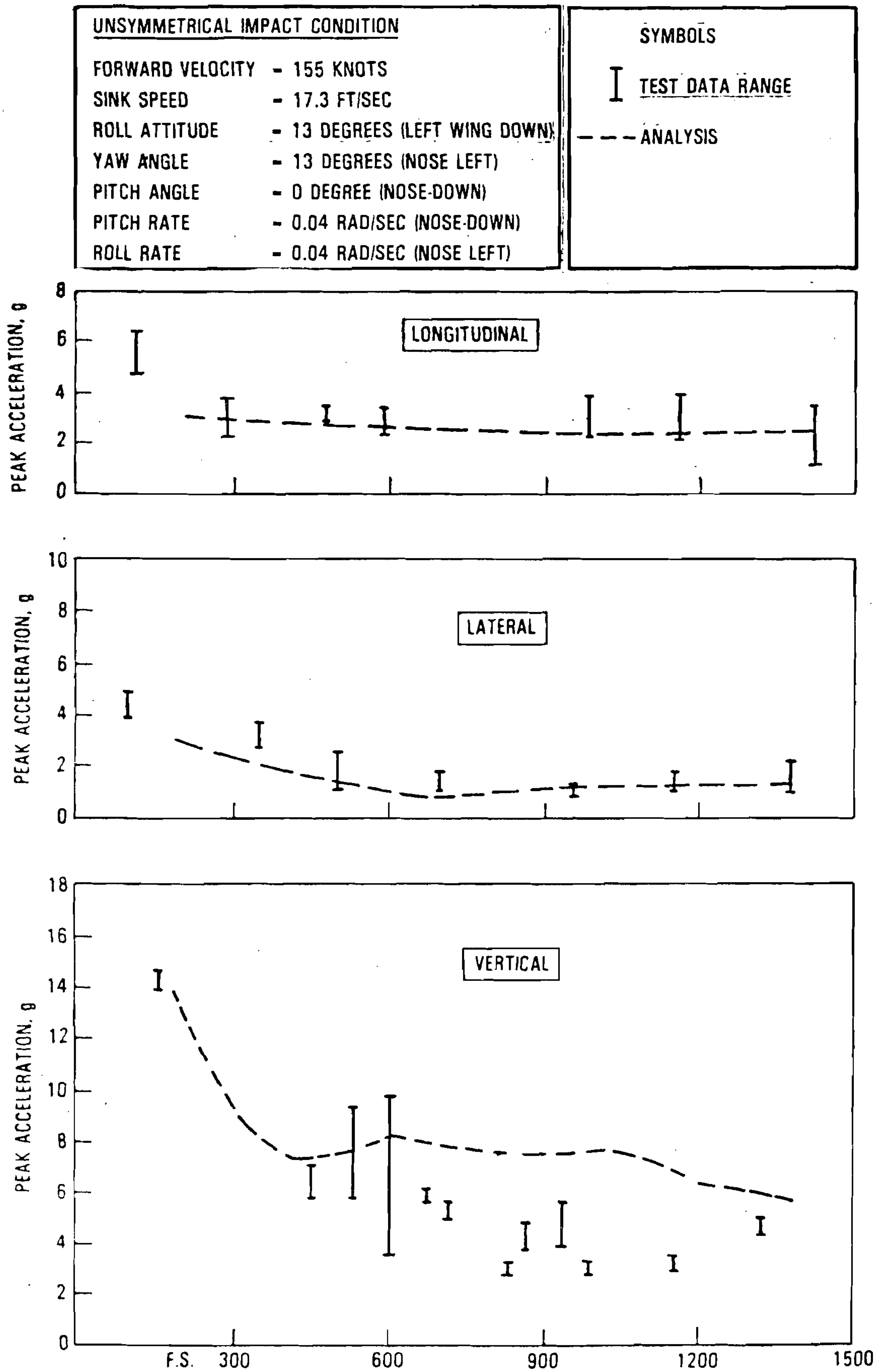

FIGURE 3-28. COMPARISON OF TEST VERSUS ANALYSIS RESULTS - UNSYMMETRICAL IMPACT, 0° PITCH ATTITUDE, INITIAL PITCH, ROLL RATES, STICK MODEL

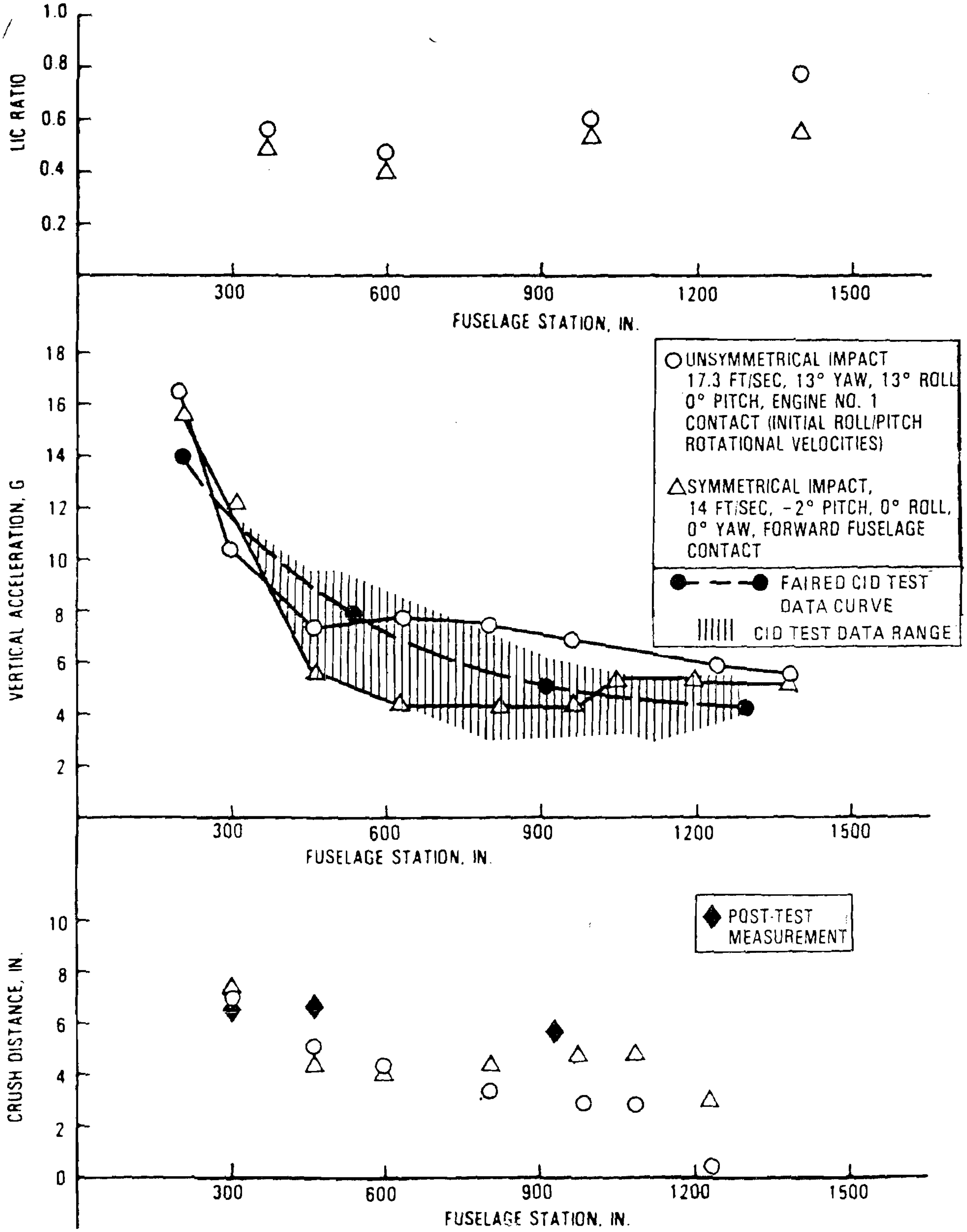

FIGURE 3-29. UNSYMMETRICAL IMPACT ON ENGINE AT 17.3 FT/SEC VERSUS SYMMETRICAL IMPACT ON FUSELAGE AT 14 FT/SEC, STICK MODEL

in an unsymmetrical attitude (yaw = 13°, roll = 13°), and at a flatter attitude (pitch = 0). Analyses were performed using the post-CID stick model to compare results between the planned and actual conditions. For this comparison presented in table 3-11 and figure 3-30 no initial rotational velocity was used. The engines do not crush much in the symmetrical impact as the fuselage, around FS1000, makes initial contact with the ground. For the unsymmetrical impact, the airplane initially impacts on the No. 1 engine and the No. 2 engine makes ground contact approximately 80 milliseconds later. The forward fuselage (FS300-460) contacts the ground aproximately 400 milliseconds after initial impact. The initial aerodynamic loading, as well as the location of the engine contact point, relative to the lowest extremity for the fuselage used in the model, will influence the contact sequence. The symmetrical model generally has higher accelerations from the mid fuselage (FS820) and aft, than the unsymmetrical model, since the initial contact is on the fuselage. The pulse durations are longer (130 - 160 milliseconds) in the symmetrical model than the pulse durations (120 milliseconds) obtained from the unsymmetrical model. Substantially more crushing is generated during the symmetrical impact. For reference, the "Laurinburg" crush range is shown in figure 3-30. The LICs for the symmetrical impact are generally lower than the corresponding LICs obtained from the unsymmetrical impact. However, the pulses for the former are broader in duration (approximately 0.150 seconds versus .120 seconds). The unsymmetrical impact appears to be more severe for the wing and associated wing related fuel containment concerns. Based on the results shown in figure 3-30, a comparison was made between the pre-CID 17 ft/sec symmetrical analyses with and without the revised (figure 3-24) engine crush characteristics. This comparison is also presented in figure 3-30. The post-CID acceleration responses are lower, particularly for the forward and rear extremes of the fuselage. The post-CID analytically obtained LIC values are also substantially lower. The post-CID analytically obtained crushing distances have increased when comparing symmetrical impacts. Based on the LIC values in table 3-11, the margin associated with the structural integrity of the airframe could be about 17 percent to 36 percent, whereas the pre-CID analysis indicates 0 to 20 percent margins. The extrapolation to a LIC value of 1.0 on a linear basis may be misleading.

TABLE 3-11. COMPARISON OF 17.3 FT/SEC SINK SPEED SYMMETRICAL AND UNSYMMETRICAL IMPACT ANALYSES RESULTS FOR +1° PITCH-UP ATTITUDE, STICK MODEL

LOCATION (F.S.)	SYMMETRICAL	UNSYMMETRICAL
	PEAK VERTICAL ACCELERATION, TRIANGULAR PULSE[(1)]	
199	18.7 (16, .130)[(1)]	10.6 (16., .120)[(1)]
300	11.5 (12.5, .140)	9.6 (12.4, .120)
460	11.7 (9.6, .160)	9.3 (10, .120)
620	9.1 (8.0, .150)	9.1 (9.2, .120)
820	7.2 (8.4, .150)	8.8 (9.2, .120)
960	6.8 (8.8, .140)	8.7 (9.2, .120)
1040	6.0 (8.0, .140)	8.0 (9.2, .120)
1200	7.7 (9.2, .140)	7.0 (9.0, .130)
1400	9.1 (9.0, .170)	5.7 (7.6, .180)
	L/C RATIO	
350	.52–.69	.27–.40
600–620	.67–.83	.80–.82
960–990	.51–.64	.73–.83
1210	.59	.75
1400	.65	.7
	CRUSH DISTANCE, IN.	
300	6.5	2.2
460	6.2	2.2
620	7.4	3.5
820	9.6	6.1
960	12.0	9.2
1040	13.4	10.0
1200	7.6	2.5

(1) A(B, C); A = 50 HZ FILTERED PEAK, B = $\frac{\text{IMPULSE X 2}}{\Delta t}$, C = IMPULSE DURATION, SECONDS

For the symmetrical impact crushing of the center section (FS820) and the main landing gear bulkhead (FS960) show 9.6 and 12.0 inches, respectively. If "bottoming out" occurs in these regions at crush distances reasonably close to these values, then there will be less available margin because the shear and moment loads could increase assympototically. Once again, a "Laurinburg" type test, to ascertain the limits of critical crush zones in both the fuselage center section and the engines, would be valuable. The symmetrical impact results in more fuselage crush, since the engines do not crush much, and higher peak accelerations (approximately 10-15 percent from FS460 to FS1400).

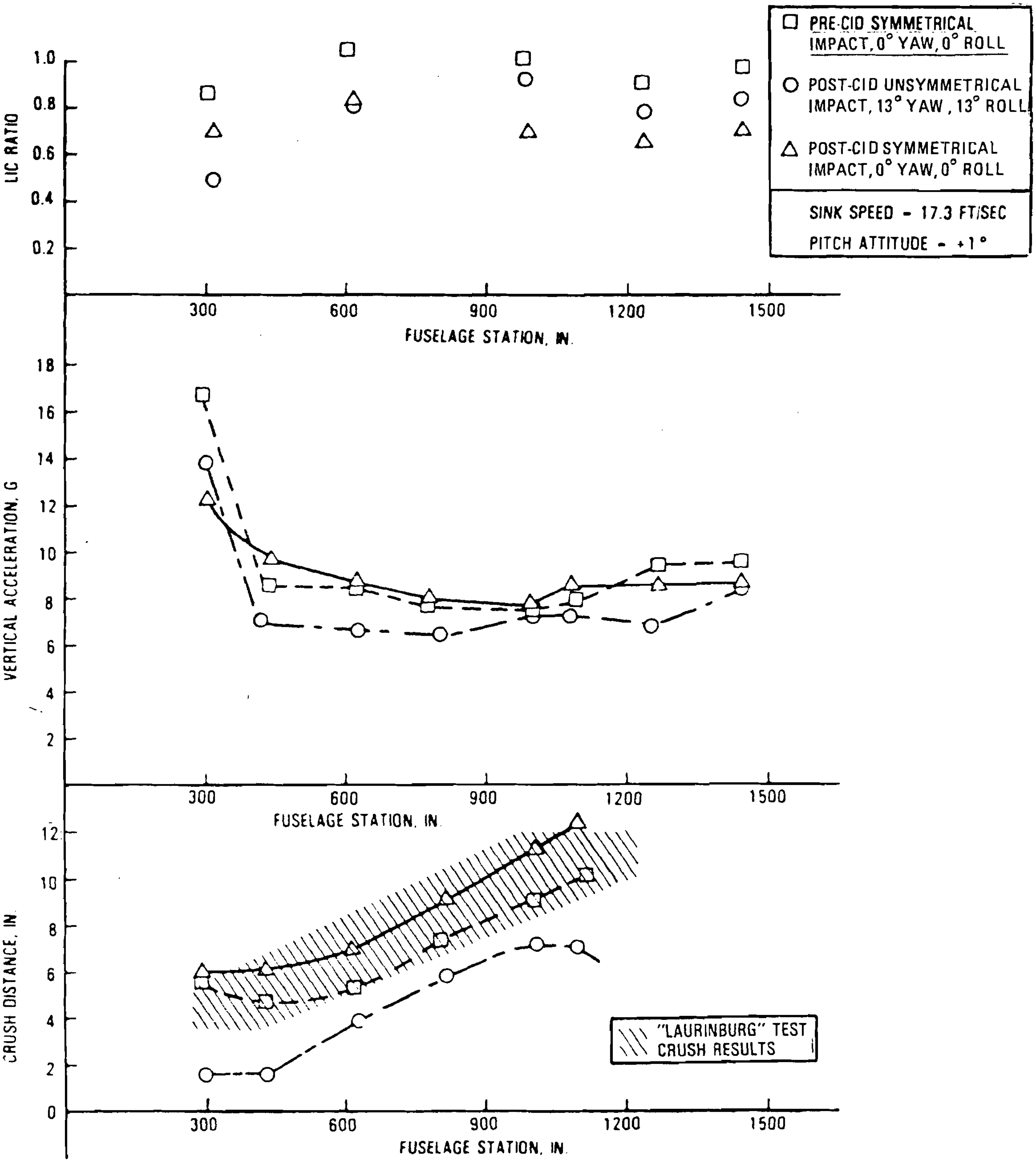

FIGURE 3-30. SYMMETRICAL VERSUS UNSYMMETRICAL IMPACT AT 17.3 FT/SEC SINK SPEED, +1° NOSE-UP ATTITUDE WITH ENGINES ON, STICK MODEL

3.2.5 Stick Versus Expanded Model Results

The expanded model versus stick model results for the 17 ft/sec, 1 degree nose-up attitude impact condition are shown in figure 3-31. The expanded model generally shows higher LIC ratios than the stick model. The one exception is at FS 600 - 620. There are several differences between the stick and expanded models which contribute to the discrepancies. Three notable differences are; (1) aerodynamic loading representation, (2) contribution of beams to LIC ratios, and (3) plasticity. A review of the two models shows an inadvertent difference in the time application of the aerodynamic forces. The expanded model, as intended, represents a fuselage section with several beams as opposed to one beam for the stick model. Thus, the LIC ratio is determined from several beam forces at each respective station. Some of these beams in the expanded model may yield. As noted in the pre-CID analyses, the representation of nonlinear beams does have an influence on the resultant loads and deflections. In the expanded model, the individual peak accelerations vary from 30 to 200 percent higher than the corresponding stick model peak levels. However, the higher peaks from the expanded model tend to be much shorter in duration. When comparing triangular pulses based on impulse data, the differences are not as great as noted in figure 3-31. The engines crush more in the expanded model which accounts for the lower fuselage crush throughout most of the length of the airplane. The expanded model shows yielding of some side fuselage structure and rupture of some longitudinal floor beams, as well as the inboard and outboard engine/wing attachment members. Concurrence that these failures will occur in a test is needed, perhaps from an additional planned "Laurinburg" type. Of interest, the range of crush distribution for the previously performed Laurinburg test is shown in figure 3-31. Unfortunately, no acceleration responses were obtained with which to compare with KRASH output. It may be that the beam failures are only model related since force cut-off levels are selected by the user.

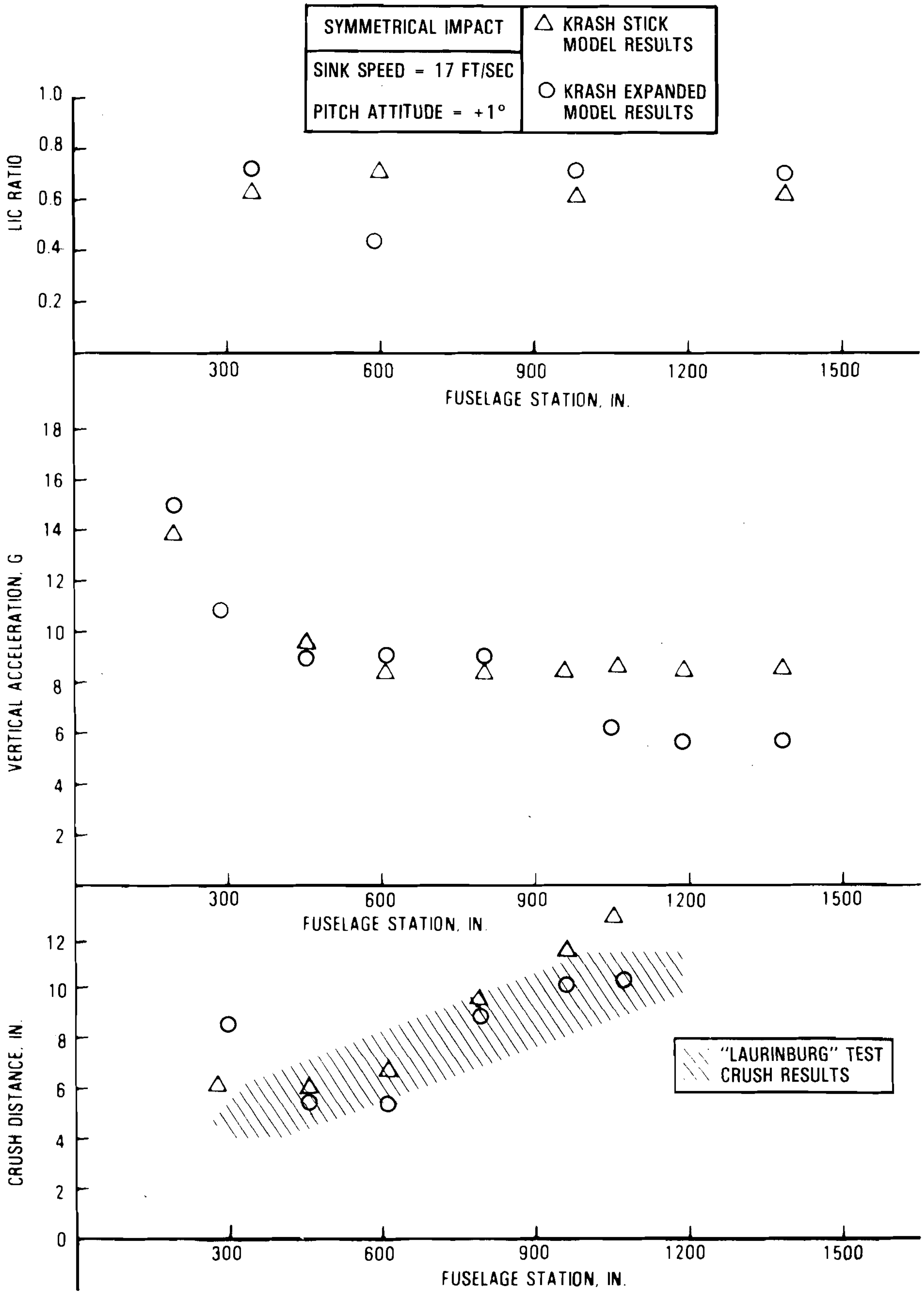

FIGURE 3-31. COMPARISON OF STICK VERSUS EXPANDED MODEL RESULTS - SYMMETRICAL IMPACT - 17 FT/SEC, +1° NOSE-UP

3.2.6 Wing and Engine Responses

Left and right wing and engine accelerations as well as wing bending moment responses were obtained from the CID test. The data points and their locations on the CID airplane are shown in table 3-12 for the 22 instrumentation channels. The wing and engine pylon accelerometer data traces are shown in figures 3-32 through 3-36. The wing bending moment responses are shown in figure 3-37. The airplane impact sequence was described earlier in this section. As was previously stated the initial impact was on the left wing outboard engine. The left wing accelerometers responses reflect this impact in that they exhibit significant high frequency ringing and in some instances overload of the accelerometers, which in effect, results in loss of data. The left wing tip (outboard of the number 1 engine) fails and the engines also during the crash sequence depart the aircraft. The left engine data indicate more significant responses at the forward section of the pylon as compared to the rear section of the pylon. The engine attachment to the wing at the front spar failed in both the 'Laurenburg' drop test and CID test. The right wing and engine accelerometers show lower amplitudes and their responses, for the most part, reflect the fundamental low frequency wing bending mode. Several right wing channels (No. 180, 182, 183) either show loss of data or an intermittent transient peak with no appreciable time duration. The right engine rear pylon response (Ch. 342) shows a high peak (28.5g) after fuselage impact. However, this data is suspect because the area under the curve integrates to an approximate ΔV of 58 ft/sec. The results of the KRASH unsymmetrical impact, using a 24-mass, 25-beam KRASH stick model described earlier, are summarized in tables 3-13 through 3-16. Included in tables 3-13 and 3-14 are estimated wing allowable strengths. The acceleration responses shown in table 3-15 tend to be relatively low in magnitude, particularly for the left wing where initial impact occurred. Table 3-16 shows the engine beam loads that are developed in the analytical model. The KRASH model has, for each engine, only one engine to wing attachment beam. The crush of the engine is most likely relatively soft compared to the 'real world' since with one beam, if failure occurs, the beam ruptures and the airplane will not rotate properly. A more realistic approach for a wing-engine response study is two attachment beams per engine. As noted earlier, the emphasis is on aircraft fuselage

TABLE 3-12. WING AND ENGINE RESPONSE MEASUREMENT INSTRUMENTATION LOCATIONS

CHANNEL	PARAMETER	DIRECTION	LOCATION	
			BS	BL
172	LEFT WING – TIP	NORMAL	1214	-733
173	LEFT WING – FWD. SPAR INBOARD	NORMAL	806	-318
174	LEFT WING – FWD. SPAR OUTBOARD	LONGITUDINAL	1020	-540
175	LEFT WING – REAR SPAR OUTBOARD	NORMAL	1090	-540
176	RIGHT WING – REAR SPAR INBOARD	NORMAL	940	+318
177	LEFT WING – REAR SPAR INBOARD	NORMAL	940	-318
178	RIGHT WING – REAR SPAR OUTBOARD	NORMAL	1090	540
179	RIGHT WING – TIP	NORMAL	1214	733
180	RIGHT WING – FWD. SPAR INBOARD	NORMAL	806	318
181	RIGHT WING – FWD. SPAR INBOARD	LONGITUDINAL	806	318
182	RIGHT WING – FWD. SPAR OUTBOARD	NORMAL	1020	540
183	RIGHT WING – FWD. SPAR OUTBOARD	LONGITUDINAL	1020	540
184	LEFT WING – FWD. SPAR INBOARD	LONGITUDINAL	806	-318
185	LEFT WING – FWD. SPAR OUTBOARD	NORMAL	1020	-540
332	LEFT ENGINE – FWD. PYLON	NORMAL	494	-324
336	LEFT ENGINE – REAR PYLON	NORMAL	569	-333
339	RIGHT ENGINE – FWD. PYLON	NORMAL	494	328
342	RIGHT ENGINE – REAR PYLON	NORMAL	569	319
343	LEFT WING – BRIDGE, INBOARD	LATERAL	700/870	-160/162
344	LEFT WING – BRIDGE, OUTBOARD	LATERAL	830/870	360/384
345	RIGHT WING – BRIDGE, INBOARD	LATERAL	700/870	160/162
346	RIGHT WING – BRIDGE, OUTBOARD	LATERAL	830/960	-360/384

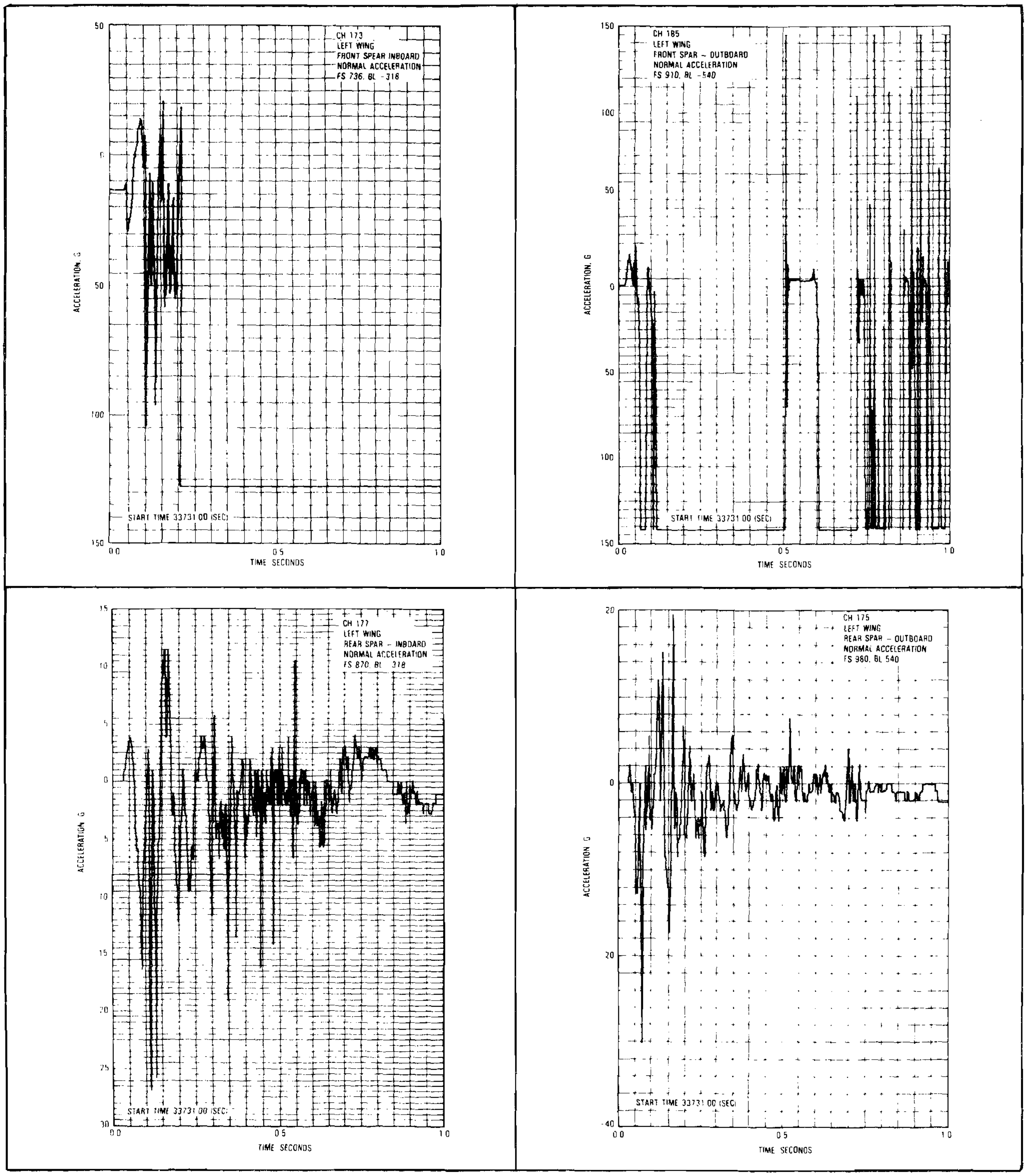

FIGURE 3-32. LEFT WING NORMAL ACCELERATIONS AT BL±318, BL±540, CID TEST DATA

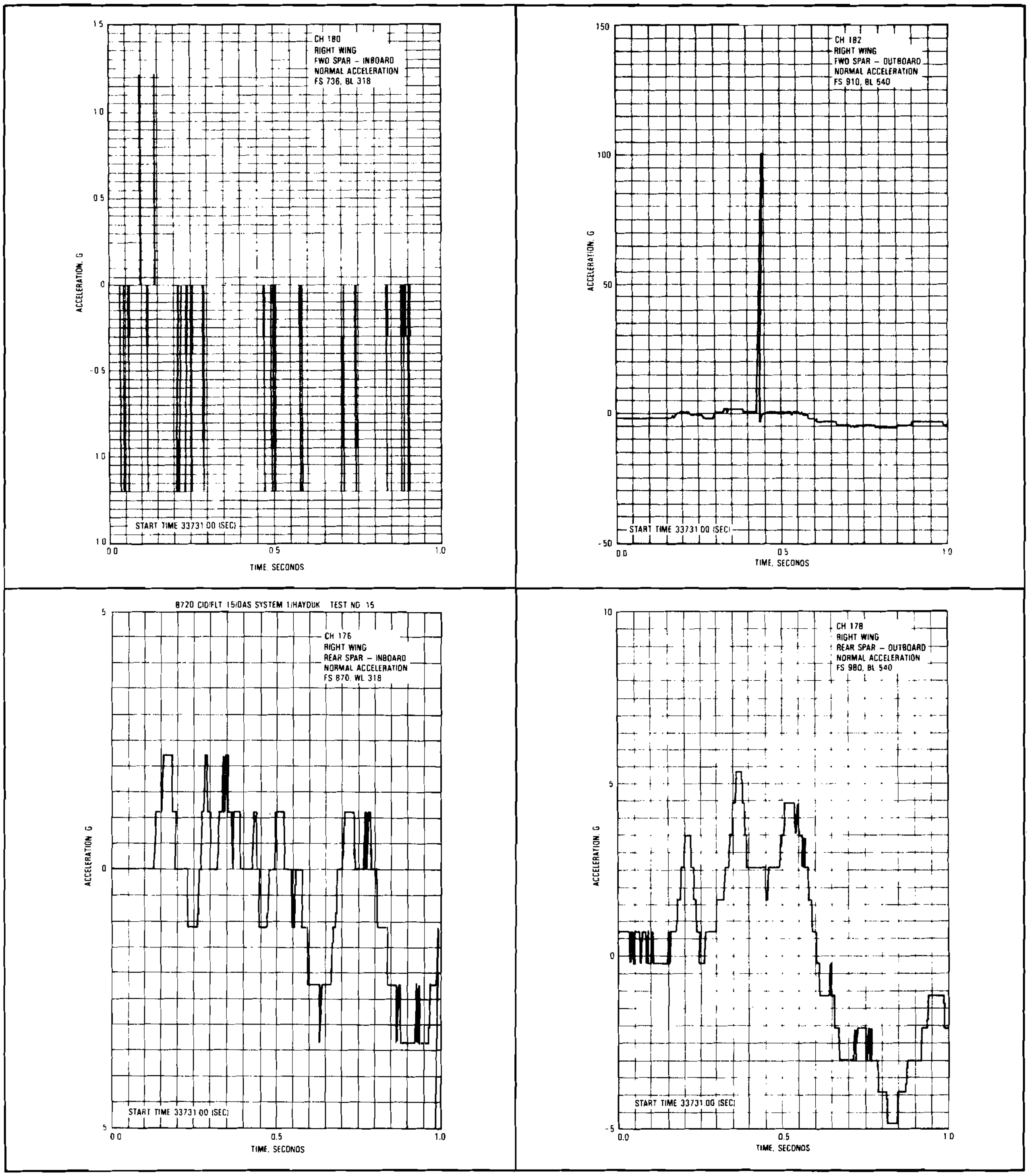

FIGURE 3-33. RIGHT WING NORMAL ACCELERATIONS AT BL±318, BL±540, CID TEST DATA

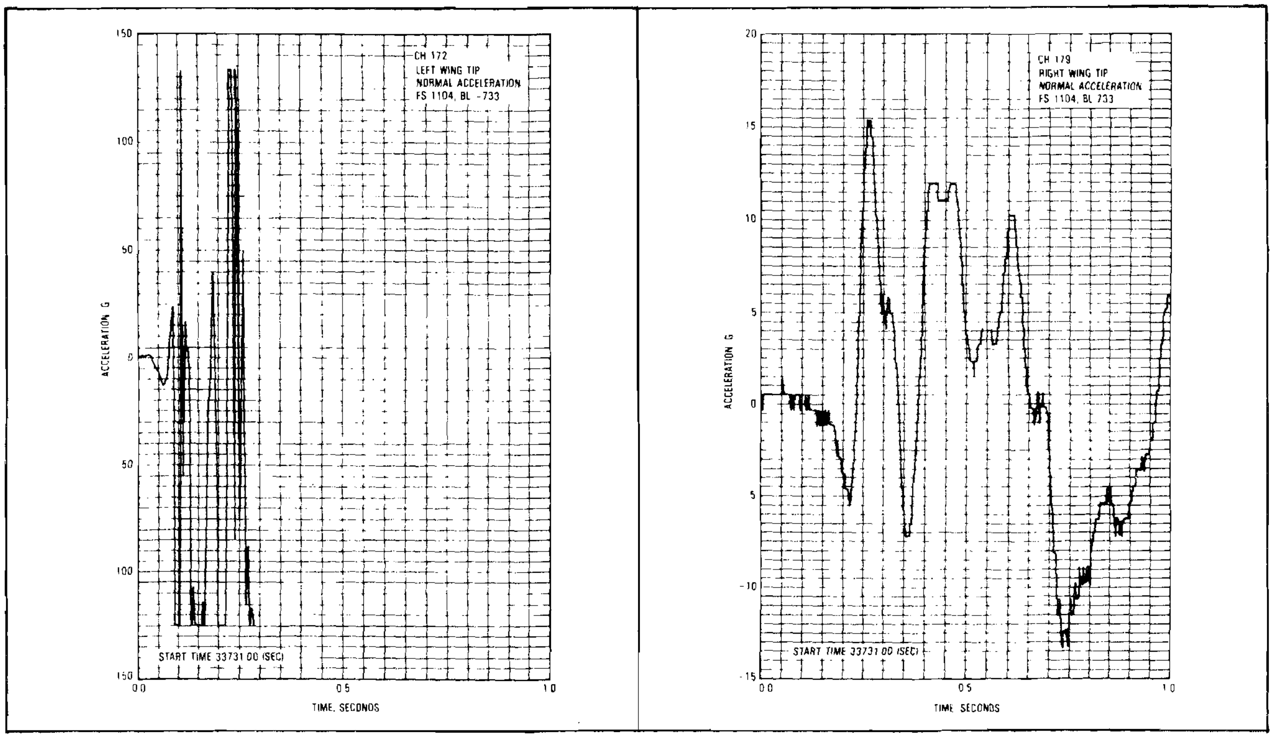

FIGURE 3-34. LEFT AND RIGHT WING TIP NORMAL ACCELERATIONS (BL±733), CID TEST DATA

impact and floor responses, which is why a modification was not pursued. It is, however, suggested for future analytical development.

The KRASH model for the CID unsymmetrical impact condition assumes that the initial aerodynamic forces acting on the left and right wings differ in the following two respects:

1. There is more lift acting on the right wing;
2. The lift acting on the left wing decays to zero at 1 second after impact, while the lift on the right wing remains constant.

The loss of lift on the left wing reflects the fact that the left wing pylons/engines impact the ground. The application of unsymmetrical lift forces allows the airplane to keep the right wing from impacting the ground which reflects the test results. The lift is applied at the four-engine mass locations so as to result in bending moment distributions which approximate the initial loading exhibited in the test data. The analysis results show

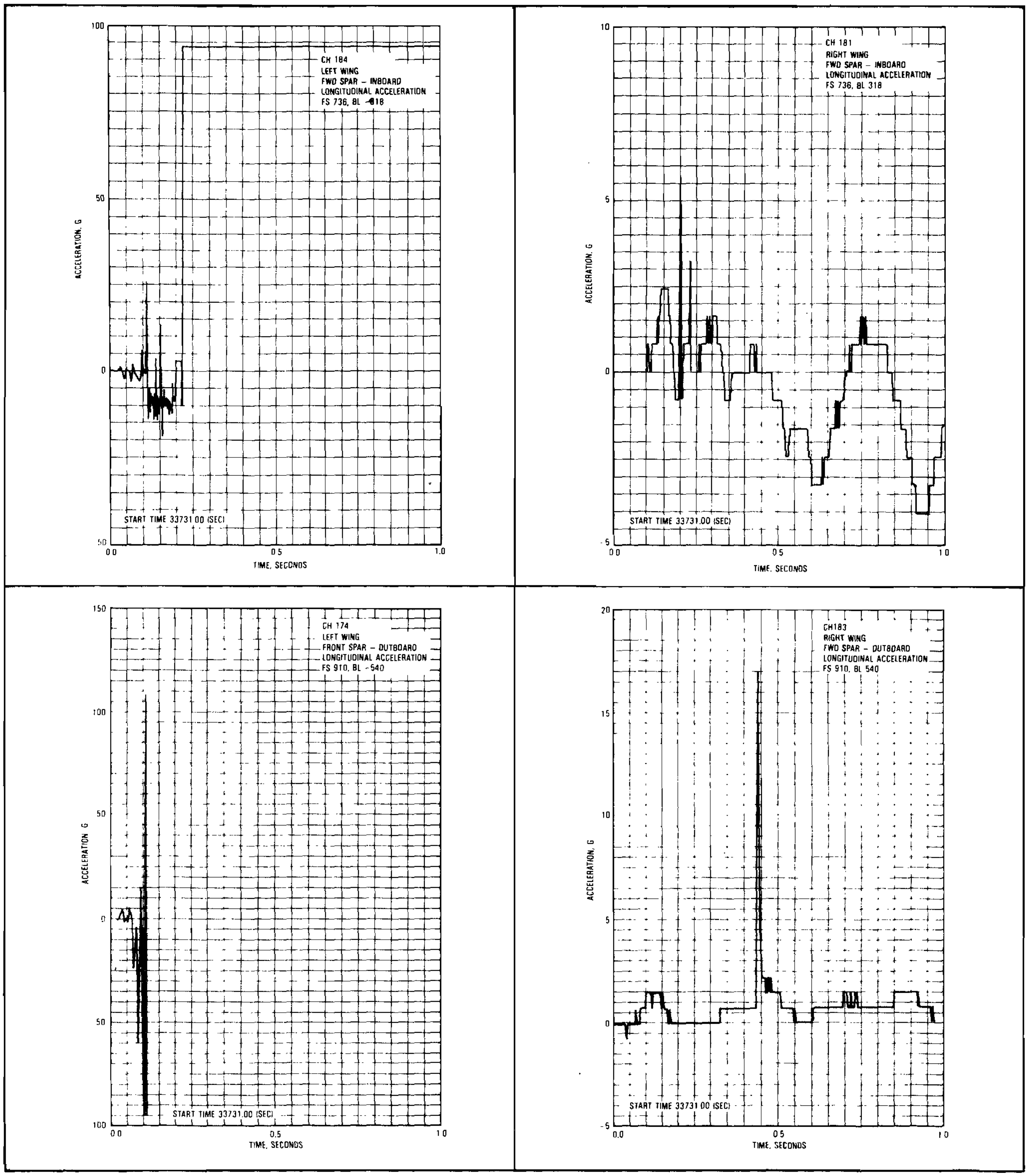

FIGURE 3-35. LEFT AND RIGHT WING LONGITUDINAL ACCELERATIONS, CID TEST DATA

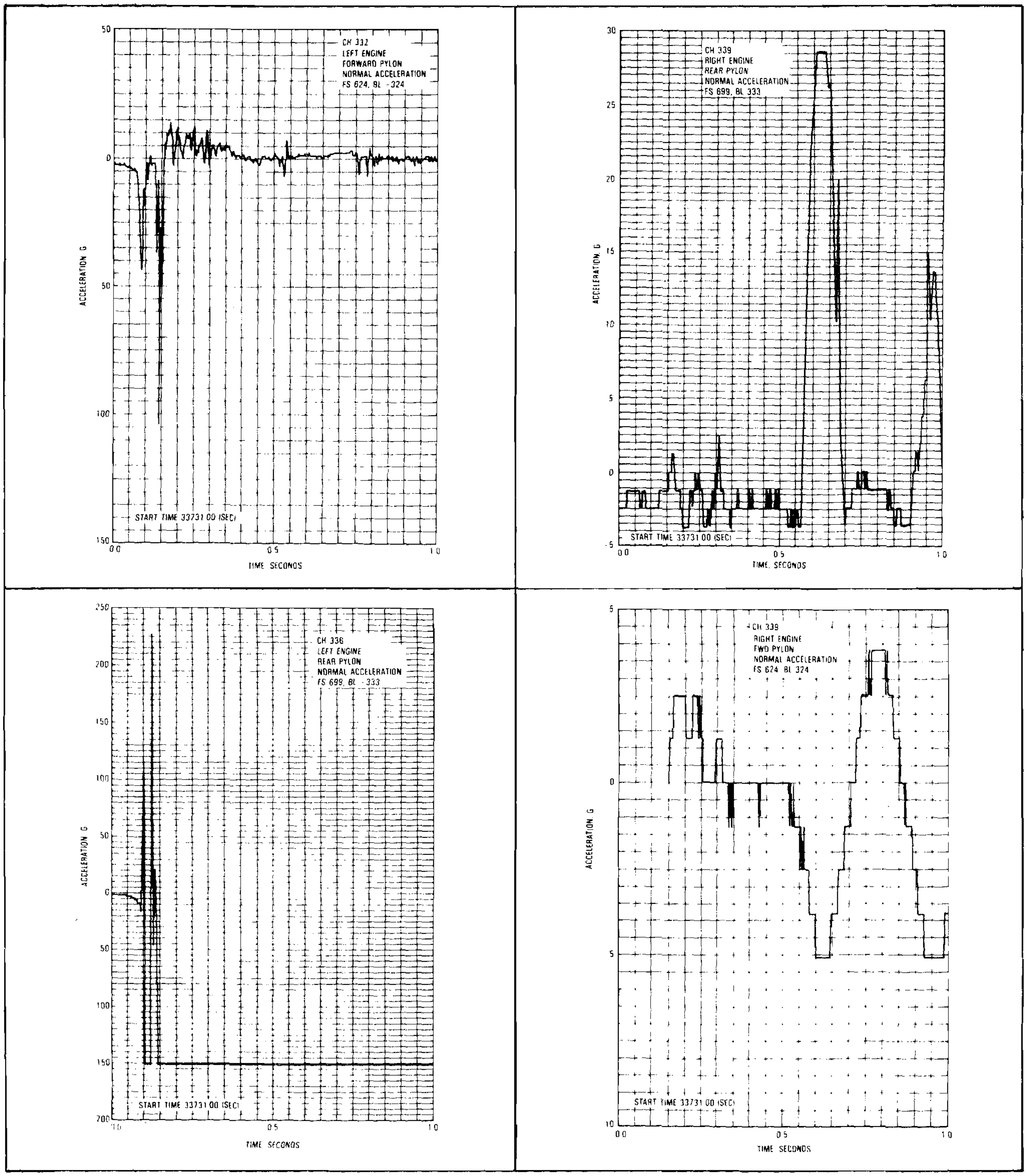

FIGURE 3-36. LEFT AND RIGHT WING ENGINE PYLON ACCELERATIONS, CID TEST DATA

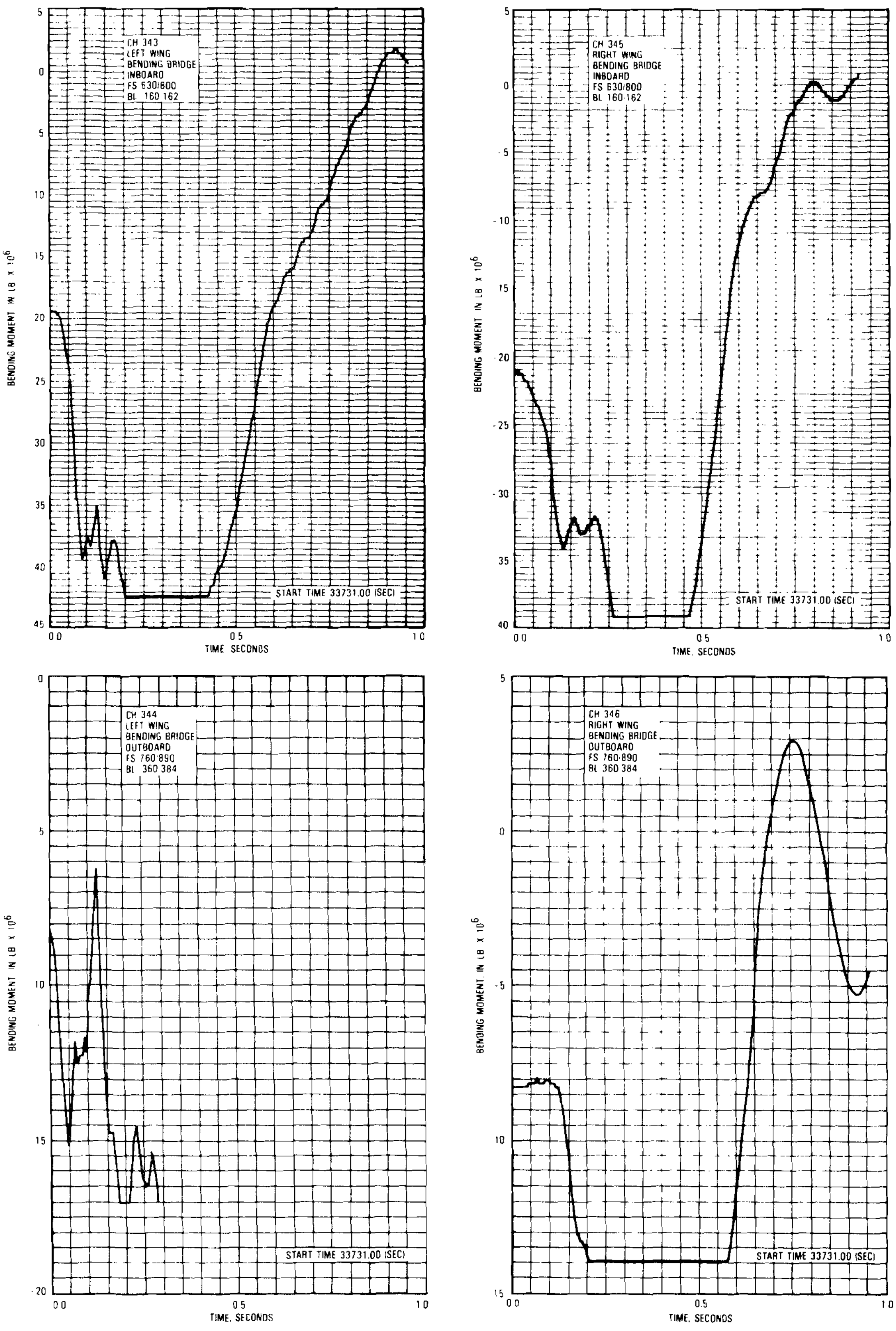

FIGURE 3-37. LEFT AND RIGHT WING BENDING MOMENT RESPONSES, CID TEST DATA

TABLE 3-13. KRASH WING BENDING MOMENT RESPONSE, STICK MODEL

MASS NO.	BL (a)	BENDING MOMENT, IN-LB X 10^6	
		ANALYSIS	ESTIMATED ULTIMATE
11	-118	41.4	50.
12	-271	28.2	30.
13	-430	19.7	15.
14	-583	7.4	10.
15	-740	1.0	5.
21	118	39.1	50.
22	271	24.9	30.
23	430	10.2	15.
24	583	4.7	10.
25	740	0.2	5.

(a) NEGATIVE DENOTES LEFT WING

TABLE 3-14. KRASH WING SHEAR RESPONSE, STICK MODEL

$MASS_{i-j}$	BL (a)	SHEAR, LB X 10^3	
		ANALYSIS	ESTIMATED ULTIMATE
FUSEL. – 11[b]	- 0/-118	200.	250
11 – 12	-118/-271	139.	200
12 – 13	-271/-430	94.	110.
13 – 14	-430/-583	90.3	40.
14 – 15	-583/-740	44.	10.
FUSEL. – 21	0/ 118	195.	250.
21 – 22	118/ 271	106.	200
22 – 23	271/ 430	84.	110.
23 – 24	430/ 583	86.	40.
24 – 25	583/ 740	19.5	10.

(a) NEGATIVE DENOTES LEFT WING
(b) TWO ATTACHMENT BEAMS

TABLE 3-15. KRASH WING AND ENGINE ACCELERATIONS, STICK MODEL

MASS NO.	BL(a)	PEAK ACCELERATION, G (50 HZ FILTERED)	
		VERTICAL	LONGITUDINAL
11	-118	6.1	1.8
12	-271	8.0	3.5
13	-430	9.7	4.5
14	-583	13.5	5.6
15	-740	29.	11.2
16(b)	-321	5.6(c)	2.5(c)
17(b)	-551	6.7(c)	3.2(c)
21	118	9.0	2.3
22	271	7.1	2.3
23	430	7.4	2.3
24	583	5.7	1.5
25	740	15.9	5.7
26(b)	321	7.3	4.0
27(b)	551	6.2	2.1

(a) NEGATIVE DENOTES LEFT WING
(b) ENGINE MASS
(c) ACCELERATION PEAK VALUES EXCEED 50 G VERTICAL AND 25 G LONGITUDINAL AT FAILURE

TABLE 3-16. KRASH ENGINE BEAM FORCES, STICK MODEL

WING	ENGINE LOCATION	PEAK VERTICAL FORCE OCCURRENCE		PEAK LONGITUDINAL FORCE OCCURENCE	
		VERTICAL FORCE, LB	LONGITUDINAL FORCE, LB	VERTICAL FORCE, LB	LONGITUDINAL FORCE, LB
LEFT	INBOARD	101500	26500	44800	57700
LEFT	OUTBOARD	106700	18700	43600	74000
RIGHT	INBOARD	59290	3229	17790	20660
RIGHT	OUTBOARD	69840	8118	30740	9950

predominantly up shear and bending on both wings. The duration of the loading is between 0.460 seconds and 0.700 seconds, which appears consistent with the wing bending moment responses obtained from the CID test (figure 3-30).

Comparisons of test and analytically obtained wing response results are presented in figures 3-38 and 3-39. Figure 3-38 shows the wing peak bending moment distribution. The analysis results are not simultaneous values. In general, the analysis and test comparison is in good agreement. The one discrepancy is at BL-430 (left side) which is located between the two engines which impact the ground. The engine-wing attachment modeling, as noted earlier, has to be further evaluated, and may be responsible for the difference. However, this one data point not withstanding, the analysis indicates bending moments reasonably close to the estimated wing strength.

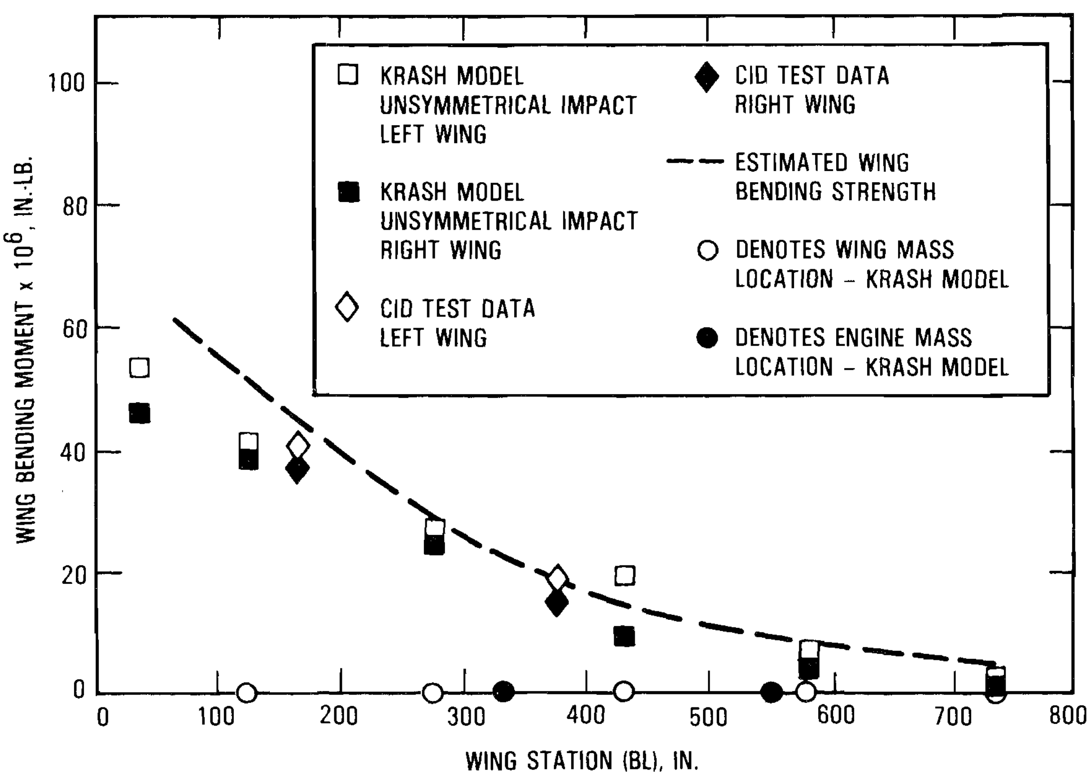

Figure 3-38. COMPARISON OF KRASH ANALYSIS AND CID AIRPLANE TEST WING BENDING, STICK MODEL

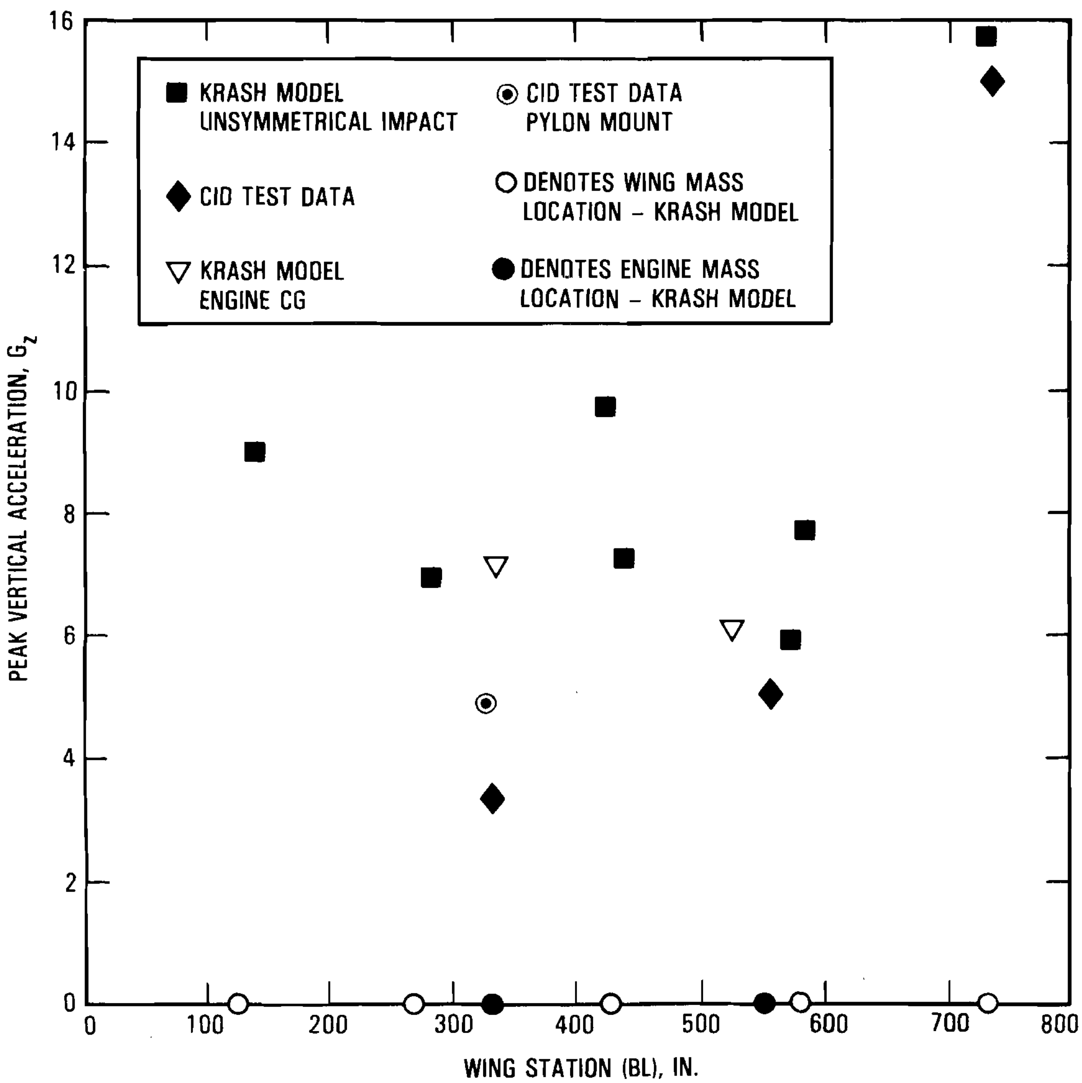

FIGURE 3-39. COMPARISON OF KRASH ANALYSIS AND CID AIRPLANE TEST RIGHT WING VERTICAL ACCELERATIONS, STICK MODEL

Figure 3-39 shows a comparison of peak vertical accelerations. As stated earlier, the left wing measured responses, because of transient ringing behavior and overload, are difficult to assess. The right wing, because it did not impact the ground, provides responses which can be more directly compared to the analysis results. The analysis indicates somewhat higher peak values than shown in the test data.

Figure 3-40 shows the wing shear distribution. Once again, the trend is generally good. The analysis results suggest that failure can be expected outboard of the number 1 engine (BL 551). Based on the data in table 3-14, the most vulnerable region for failure to occur is at the left wing tip. Indeed, the left wing tip did fail during the initial stage of impact. No right wing failure occurred during the test and the analysis, in this respect, predicts too high a loading. The estimated shear strength could also be lower than exists. For example, if the strength curve were modified, as noted in figure 3-40, then only the wing failure potential would exist. Once again, engine-wing modeling represents an area that could be further explored.

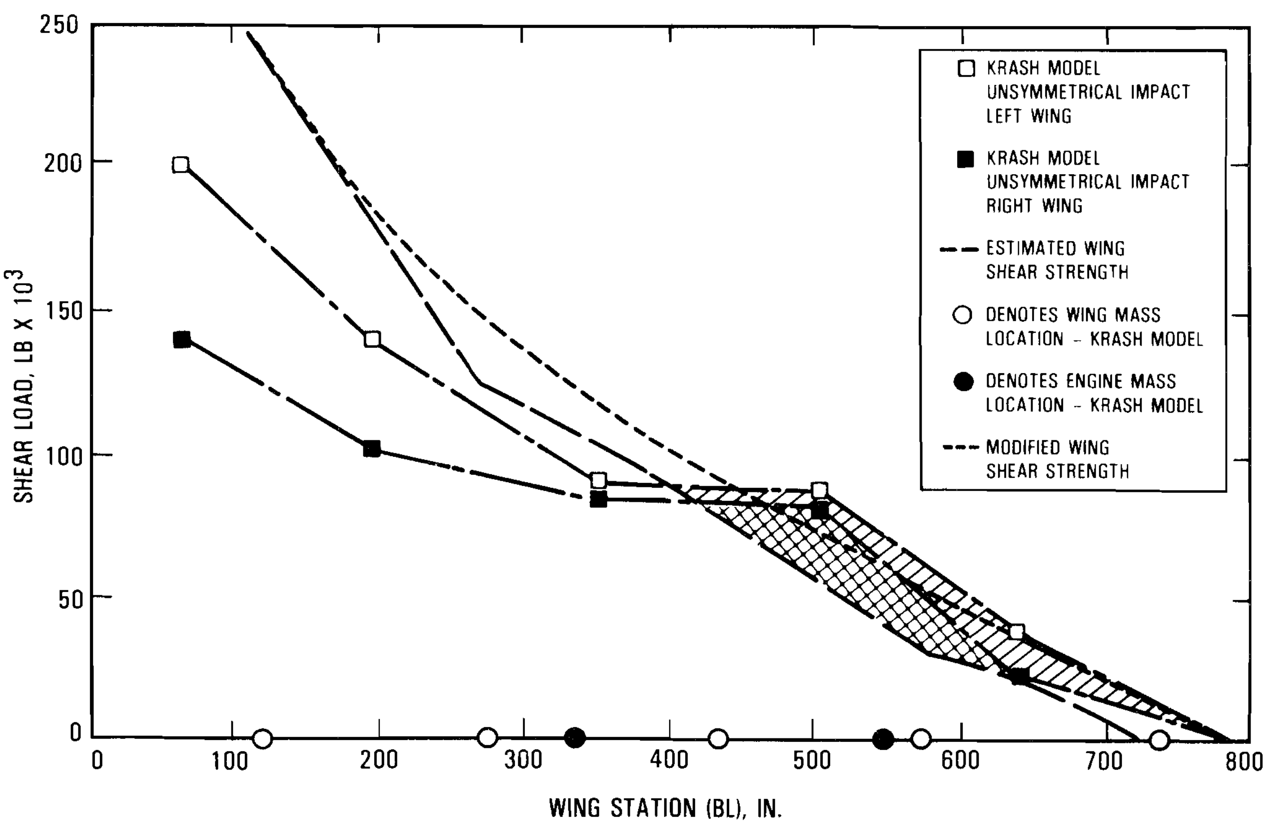

FIGURE 3-40. KRASH ANALYSIS WING SHEAR DISTRIBUTION FOR CID TEST CONDITION, STICK MODEL

The pre-CID symmetrical KRASH stick model analysis wing and engine responses for the planned CID impact conditions (17 ft/sec sink speed, +1 degree pitch, zero yaw and roll) are shown in figures 3-41 through 3-43. Figure 3-41 shows the moment distribution obtained from the model, as well as the estimated strength. The analysis shows margins of at least 10 percent. The analysis, to determine fuselage responses for the symmetrical impact, is presented in table 3-11 and figure 3-30. In the pre-CID analysis the fuselage LICs indicated zero margins. The post-CID analysis shows at least 17 percent margin for the fuselage. Figure 3-42 shows the shear distribution obtained

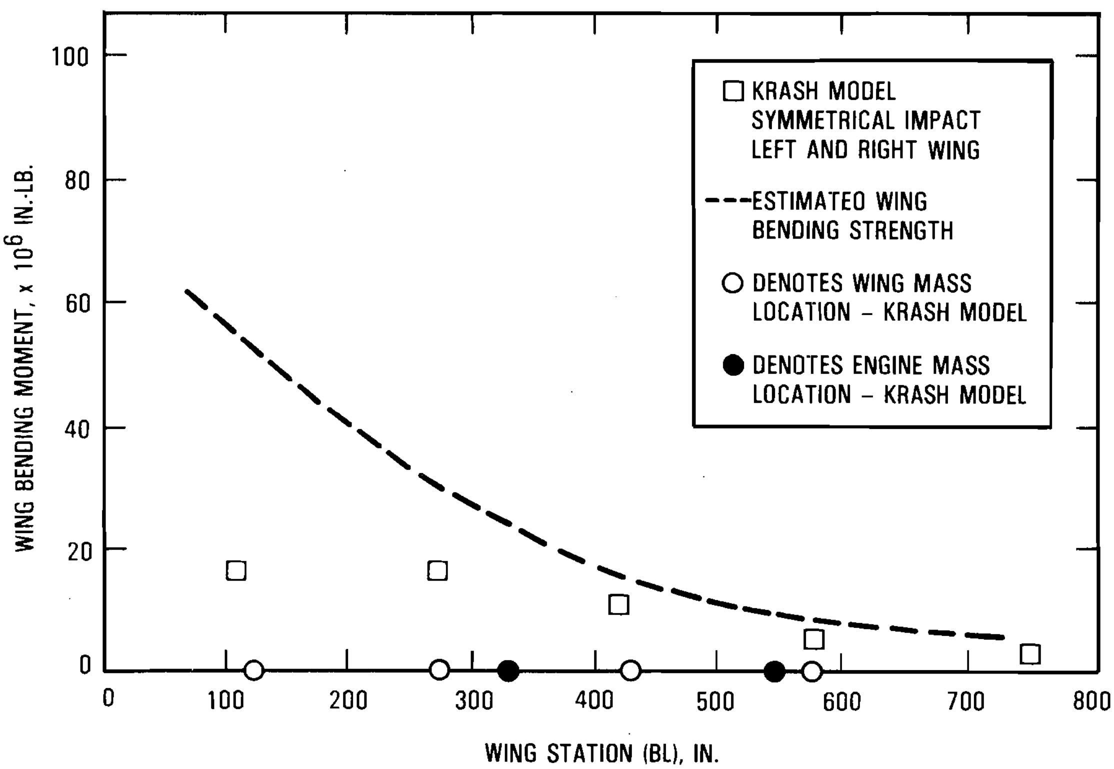

FIGURE 3-41. KRASH ANALYSIS WING SHEAR DISTRIBUTION FOR SYMMETRICAL IMPACT; 17.3 FT/SEC SINK SPEED, +1 DEGREE PITCH ATTITUDE, STICK MODEL

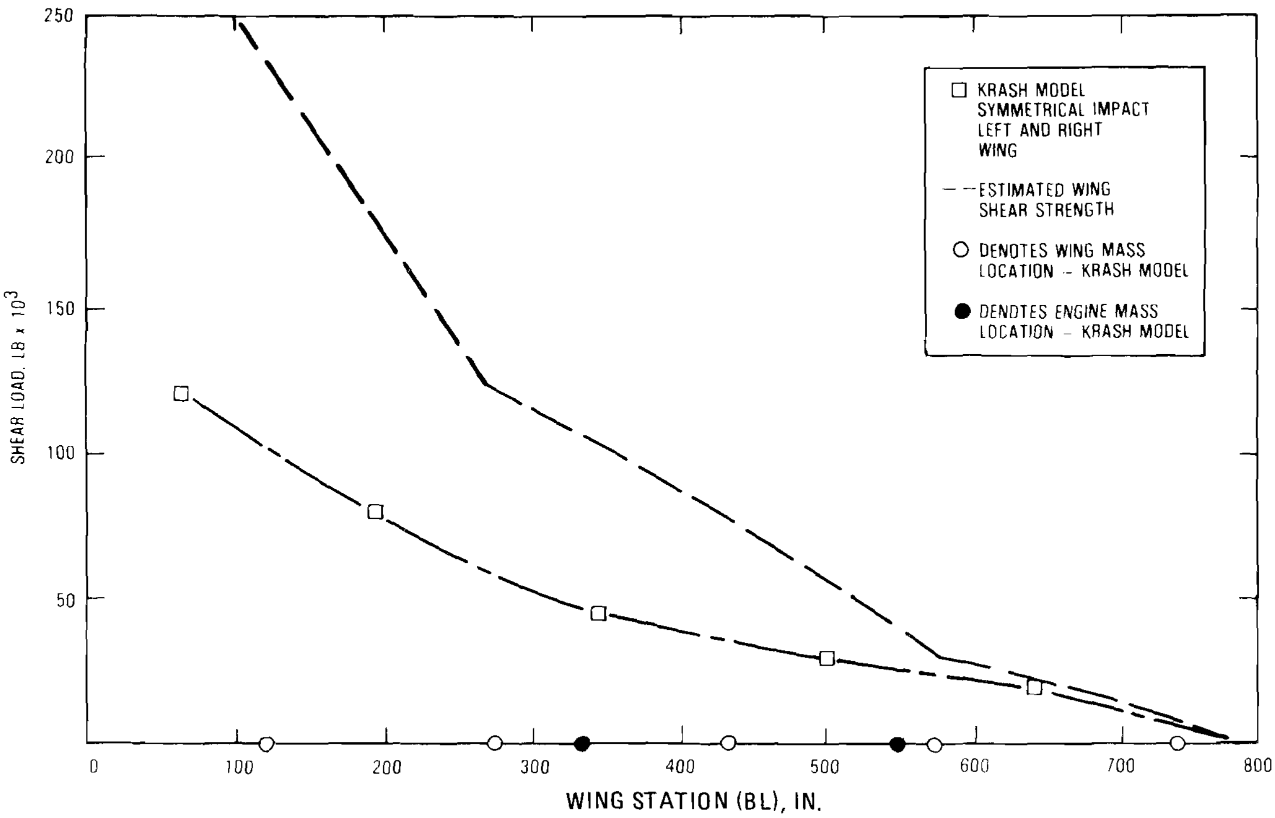

FIGURE 3-42. KRASH ANALYSIS WING SHEAR DISTRIBUTION FOR SYMMETRICAL IMPACT; 17.3 FT/SEC SINK SPEED, +1 DEGREE PITCH ATTITUDE, STICK MODEL

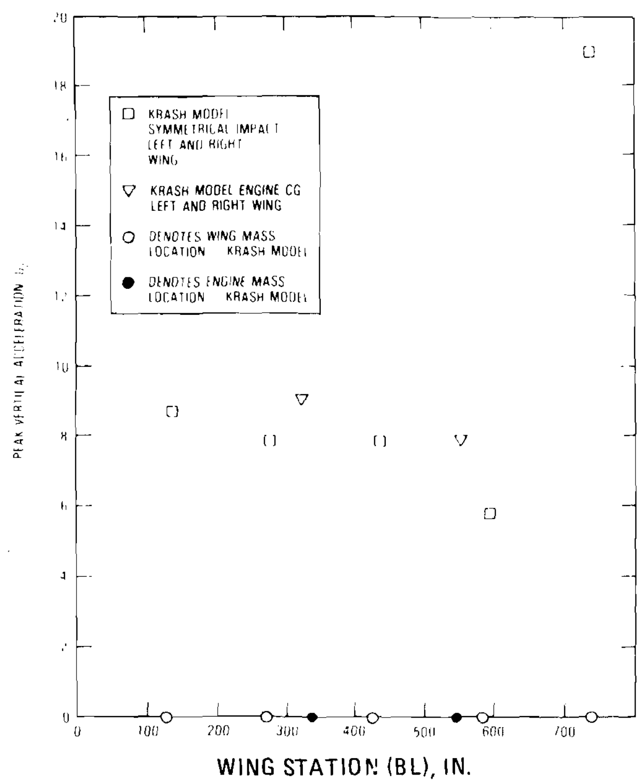

FIGURE 3-43. KRASH ANALYSIS WING VERTICAL ACCELERATIONS IMPACT; FOR SYMMETRICAL 17.3 FT/SEC SINK SPEED, +1 DEGREE PITCH ATTITUDE, STICK MODEL

from the model as well as the estimated strength. Positive margins exist from BL 583 inboard. At the outboard tip the margin is negative. Either the analysis predicts the loads too high or the wing shear strength is greater than shown. Figure 3-43 shows the peak vertical acceleration along the wing span. In general, the value is between 8g and 9g except at the tip, where it is 18.9g. The peak vertical acceleration, at the two wing attach points, are approximately 8.5g and 8.0g, respectively, for the pre-CID analysis. The corresponding post-CID analysis values are 9.1g and 7.2g.

The KRASH stick model for this impact condition has an assumed aerodynamic loading distribution which is similar to the pre-CID analyses. The lift load is assummed to remain constant throughout the impact. The magnitude of the lift forces, the distribution along the airplane and the time application of the lift forces differ from the CID correlation model described earlier in this section. These differ along with a different impact sequence account for the lower wing bending and shear responses experienced in the 17 ft/sec, +1 degree symmetrical impact versus the CID unsymmetrical impact.

SECTION 4
SUMMARY OF RESULTS

The KRASH stick model (figure 2-1) depicting the fuselage initial impact with the ground at 14 ft/sec in a symmetrical attitude shows agreement with the CID test data with regard to peak vertical accelerations and crush distances. The analysis indicates higher LIC values than are estimated from the test bending bridge data. The analytically determined LIC values show that airframe strength has not been exceeded.

The KRASH stick model results depicting the CID unsymmetrical air-to-ground impact from engine No. 1 contact on and through to fuselage contact shows agreement with the sequence and time of occurrence of significant events such as engine No. 1, engine No. 2 and fuselage ground contact. The airplane cg velocity is reduced from an initial 17.3 ft/sec to approximately 14 ft/sec when the fuselage hits the ground which is consistent with the test data. The crush magnitudes and distribution, as well as the LIC values which indicate fuselage airframe strength margins which exist at that impact level, are also consistent with the test results. However, the fuselage vertical accelerations from the mid-fuselage (FS820) through to the aft-fuselage (FS1400) are higher than the levels recorded during the test, which also differs from the results obtained from the abbreviated 14 ft/sec fuselage impact analysis results. Acceleration response comparisons for the fuselage initial impact are described in Section 3.2.1 and are shown in figures 4-1 and 4-2. The analyses showed that the responses are somewhat sensitive to the initial loading (aerodynamics) conditions and the manner in which those loads change. The difference in acceleration responses noted may be due to the manner in which these external forces are represented in the KRASH model.

The fuselage vertical acceleration responses obtained from the post-CID analyses, both the symmetrical impact on the fuselage at 14 ft/sec, and the unsymmetrical impact on the No. 1 engine at 17.3 ft/sec are shown in figure 4-3, along with the measured test data range. The acceleration values shown in figure 4-3 represent peak g's for a triangular pulse with a base

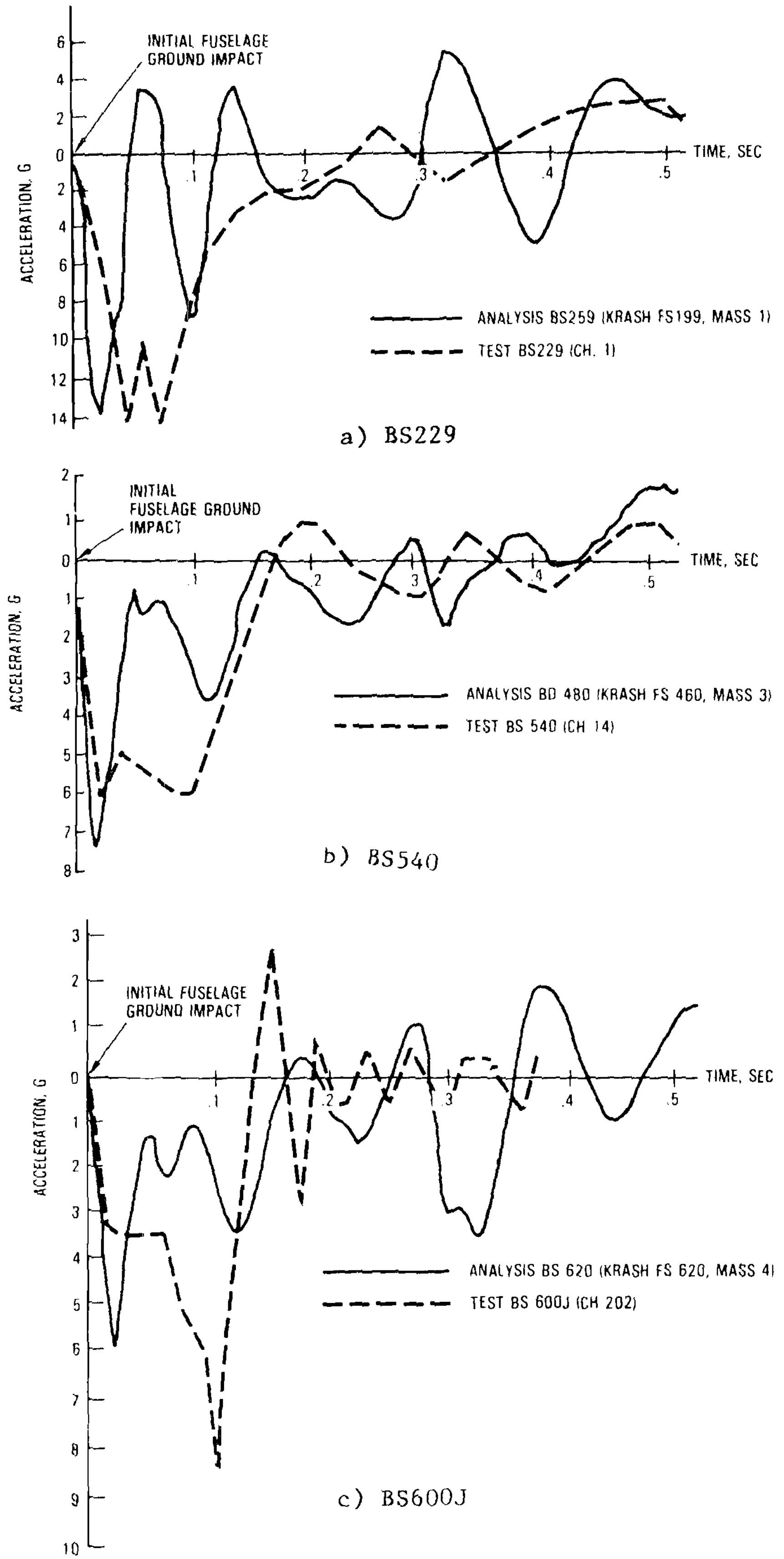

FIGURE 4-1. COMPARISON OF KRASH STICK MODEL AND CID ACCELERATION TIME HISTORIES: BS229, 540, 600J

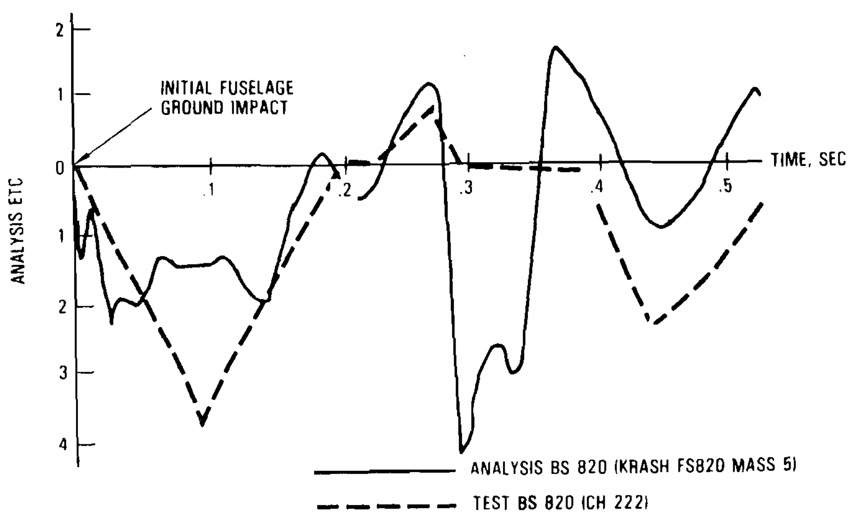

a) BS820

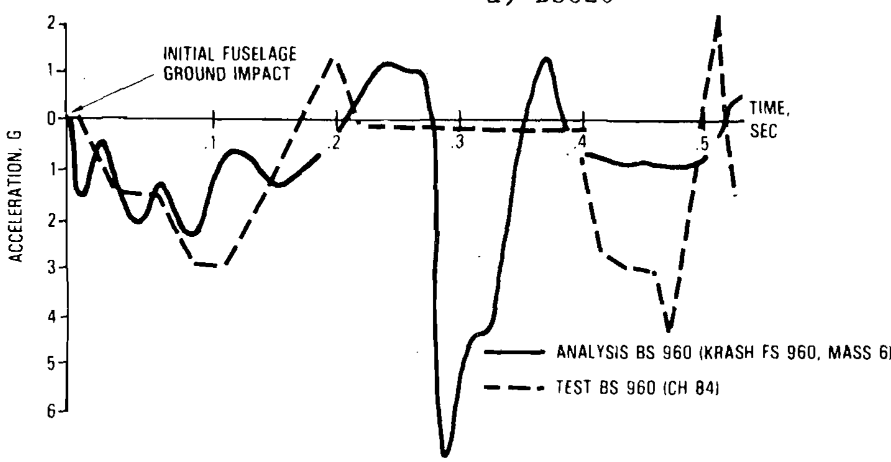

b) BS960

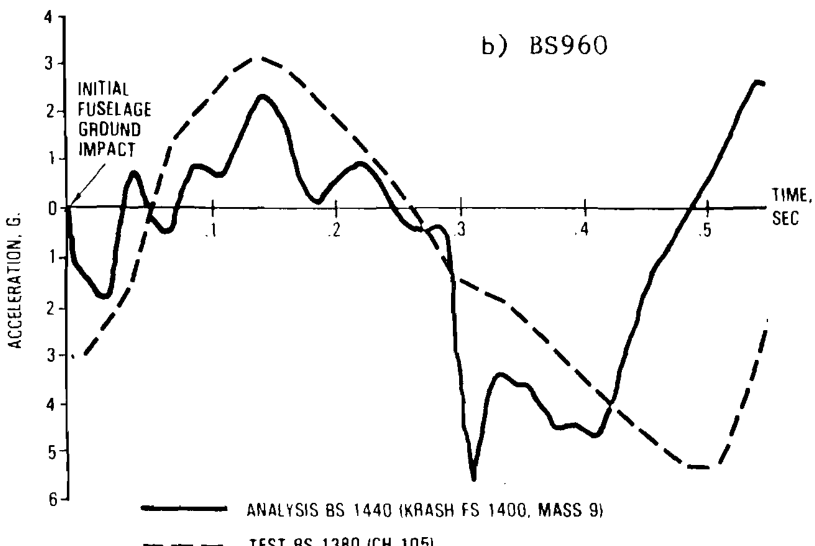

c) BS1380

FIGURE 4-2. COMPARISON OF KRASH STICK MODEL AND CID ACCELERATION TIME HISTORIES: BS820, 960, 1380

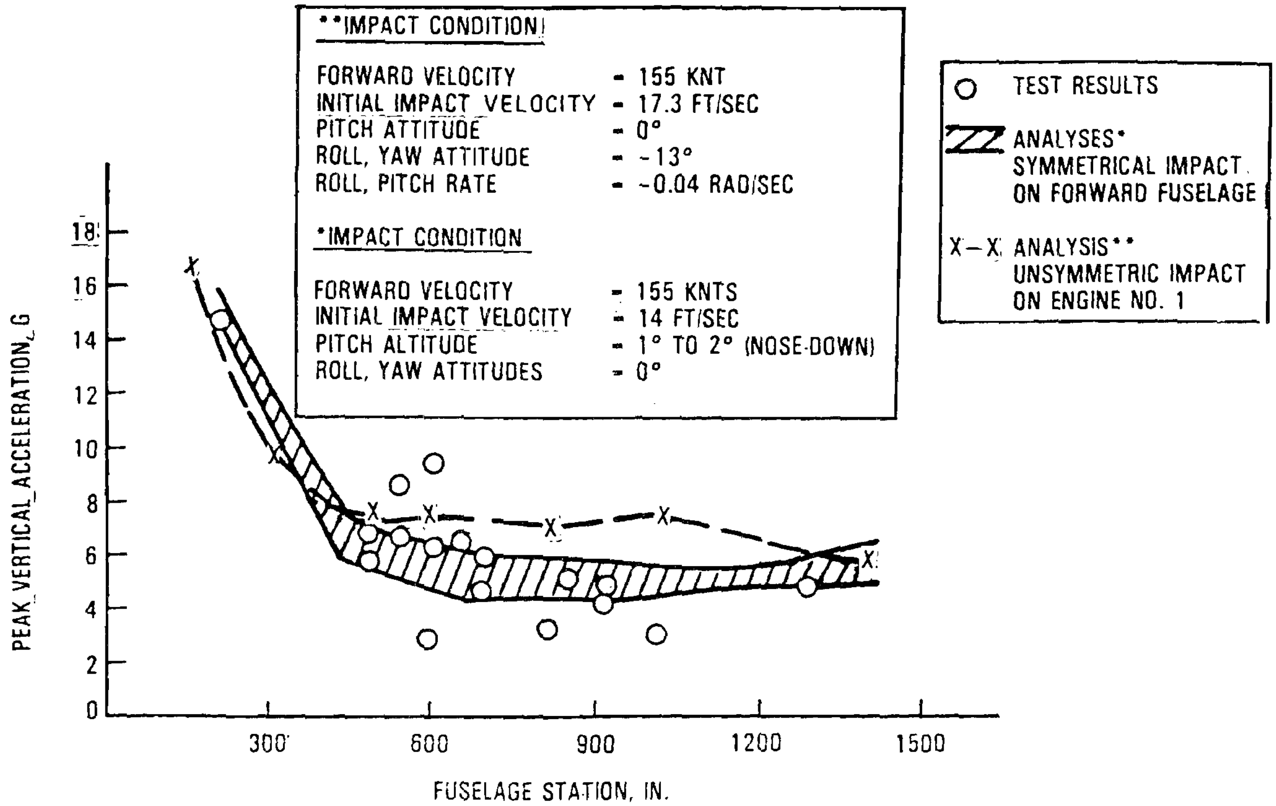

FIGURE 4-3. COMPARISON OF POST-TEST CID KRASH STICK MODEL ANALYSIS AND TEST RESULTS FOR FUSELAGE IMPACT

duration between 0.100 and 0.150 seconds. The longitudinal pulses are approximately 3 to 4 g's along the fuselage.

The analyses results for both the planned symmetrical (0^{o} roll, yaw) and the actual unsymmetrical (-13_{o} roll, yaw) impact conditions with the one-degree nose-up and a 17.3 ft/sec sink rate are shown in figure 4.4. The fuselage peak triangular vertical responses generally are higher for the planned symmetrical impact than for the actual CID unsymmetrical. The LIC ratios are higher; however, for the aft fuselage impact for the unsymmetrical impact. The LIC ratio for the symmetrical impact reaches a maximum of 0.78 at around FS960 (Main Landing Gear Bulkhead). The crush distribution is similar to the "Laurinburg" results for the symmetrical impact and lower for the unsymmetrical impact. The LIC ratios, crush distances, as well as the "Laurinburg" crush range are shown in figure 4-4. It should be noted that when the fuselage impacts the ground at 14 ft/sec with the engines having

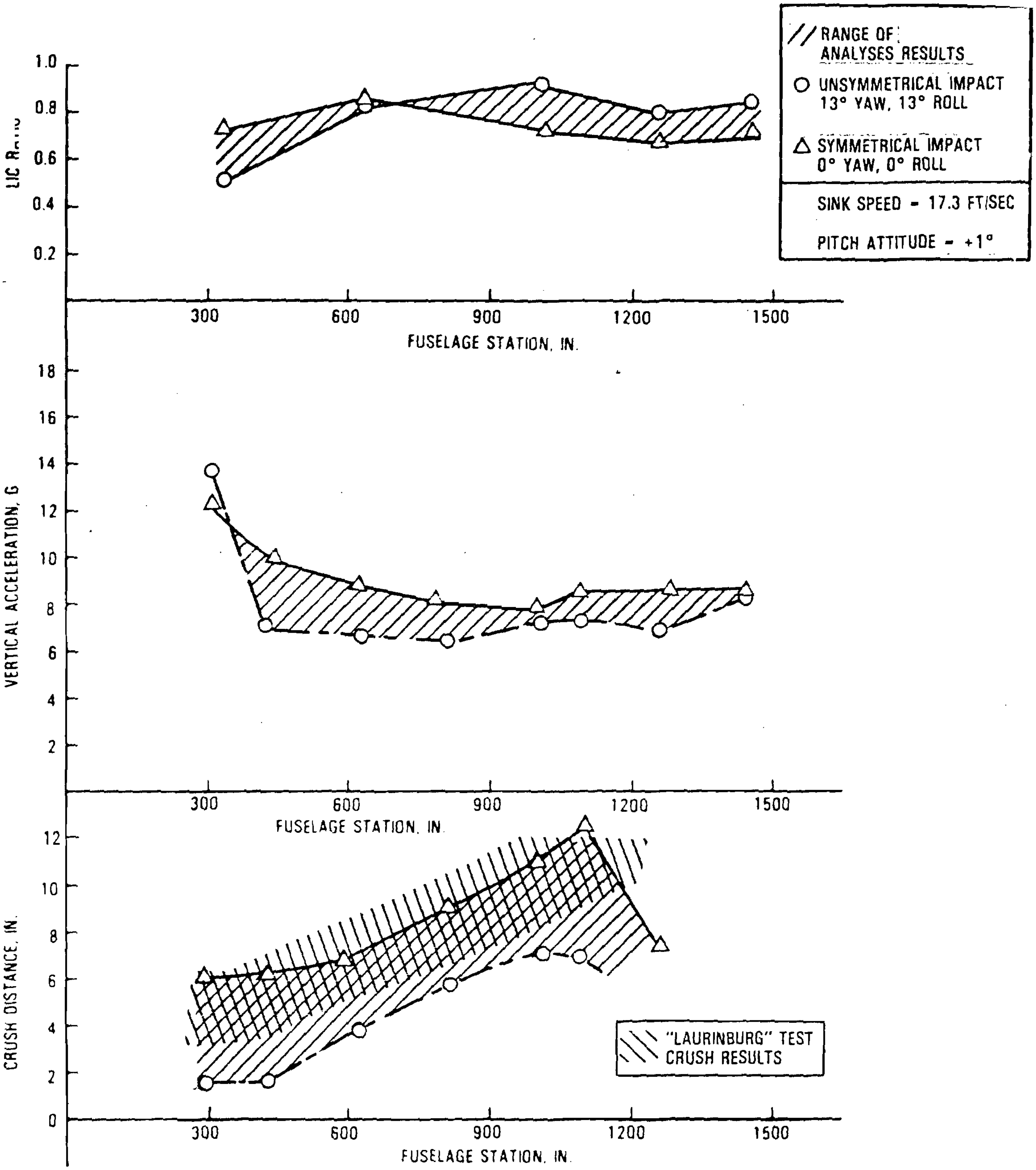

FIGURE 4-4. SYMMETRICAL VERSUS UNSYMMETRICAL IMPACT AT 17.3 FT/SEC SINK SPEED, +1° NOSE-UP ATTITUDE WITH ENGINES ON, STICK MODEL

already crushed and failed, the LIC reaches a maximum value of 0.6. By linear extrapolation this data suggests that a LIC ratio of 1.0 would be reached at a sink speed of 20 ft/sec.

Comparisons of the stick versus expanded model fuselage results for a symmetrical 17 ft/sec impact with a 1 degree nose-up altitude engines-on are shown in figure 4-5. As noted earlier a major discrepancy exists for the LIC ratios at FS600. Other than that the LIC values range between 0.60 and 0.70, the peak vertical accelerations, also shown in figure 4-5, are reasonably close through to fuselage station 960. Aft of this station the expanded model responses are approximately 2/3 of the stick model values. The crush distribution for both stick and expanded models exhibit the same trend. They are both within the crush distances observed for the "Laurinburg" test, which was performed under the same impact conditions, excluding aerodynamic loading and forward velocity. As noted in Section 3.2.5 there are differences in the stick and expanded model representations. These differences need to be further investigated to ascertain their influence on the respective results.

The fuselage peak vertical g versus base duration for the triangular pulses associated with the analyses and test results are shown in figure 4-6. The acceleration responses are shown for the passenger cabin region only (FS460-FS1400). As expected there is substantial scatter. For the most part the results; test and analyses fall in the shaded area which is between 4g to 10g peak and 0.100 to 0.170 second base duration.

The major discrepancy between analysis and test results for the fuselage is the high peak vertical accelerations obtained from the full unsymmetrical analysis. Several areas in the model and impact condition representation may contribute to this difference. These include:

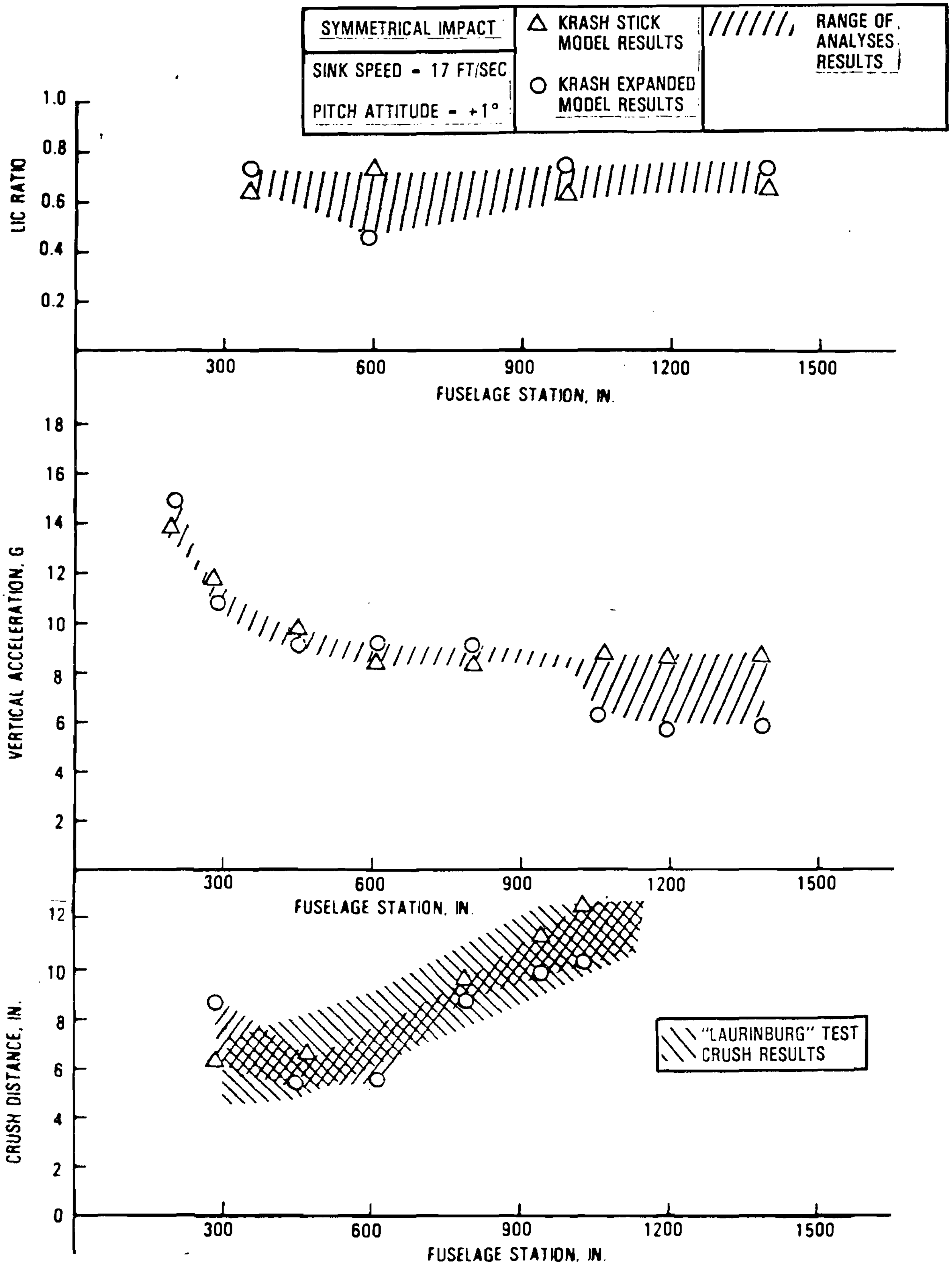

FIGURE 4-5. STICK MODEL VERSUS EXPANDED MODEL RESULTS FOR A SYMMETRICAL IMPACT - 17 FT/SEC, +1° NOSE-UP ATTITUDE

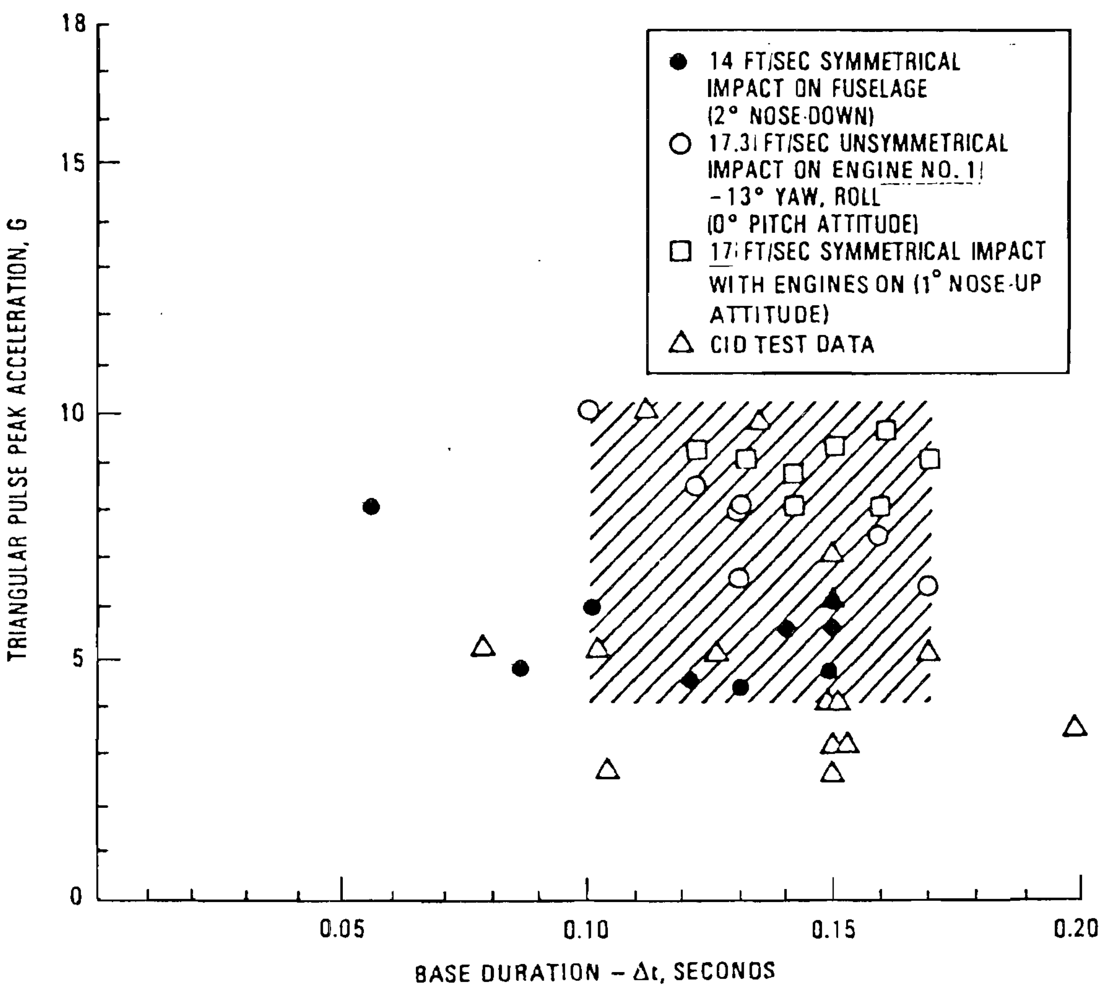

FIGURE 4-6. TRIANGULAR SHAPED VERTICAL ACCELERATION RESPONSES FROM ANALYSES AND TEST; PEAK MAGNITUDE VERSUS BASE DURATION, PASSENGER REGION FS460-1400

- The effect of both the initial and time varying aerodynamic loading - For example, the moment response data from figure 3-2 is repeated in figure 4-7. The symmetrical model analysis starts at the point designated "nose-impact," with an aerodynamic loading applied so as to develop the moment distribution measured. The unsymmetrical model analysis starts at the point noted "initial engine impact." For the analyses to be identical the moments would have to be developed from "initial engine impact" through "nose-impact" as shown in figure 4-7. This does not occur in the model. Model revisions to allow more detail in engine/wing attachment and application of aerodynamic loading are needed to evaluate this effect.

- Representation of engine/wing/fuselage attachments - For example, the unsymmetrical model results indicate that a pitch rotational velocity developes at the time the fuselage impacts; it is approximately 0.05 to 0.10 rad/sec. The actual contact velocity at the fuselage mass at time of ground contact in some cases is noted to be higher than the cg velocity, resulting in higher peak g values. When initial pitch and roll rotational velocity were included such that the resultant 17.3 ft/sec vertical contact velocity consisted of both translational and rotational components, the results were in better agreement with the test data (figure 3-28).

The analytical wing response results are of interest, in light of the measured and observed CID test data. The analytically obtained moment and shear distributions, along with estimated strength levels and available test data, were shown in figures 3-38 and 3-40, respectively. These data are reproduced in figures 4-8 and 4-9, respectively. The curves suggest that for the 13 degree roll, 17.3 ft/sec sink speed condition the wing structural integrity is at or near its limit. For this impact condition, the left outboard wing section has the highest potential for failure. Failure initiated at the left wing tip would progressively work its way inboard. Since there was no fuel tank rupture, or significant fuel spill as a result of this failure, it is presumed that the wing fuel containment requirements are met for this crash scenario. Anaytical studies, described in reference 11, were performed for a gear-up airplane contacting the ground with one-wing low. The pitch attitude was level, or slightly nose-up. These conditions are similar to the CID test. The report goes on to state that crushing and wearing-off the tip and outer wing will begin when contact is made with the ground and will progress along the wing until a fuel tank is opened, the wing is broken off, or the airplane is righted by the loads which are crumbling the outer

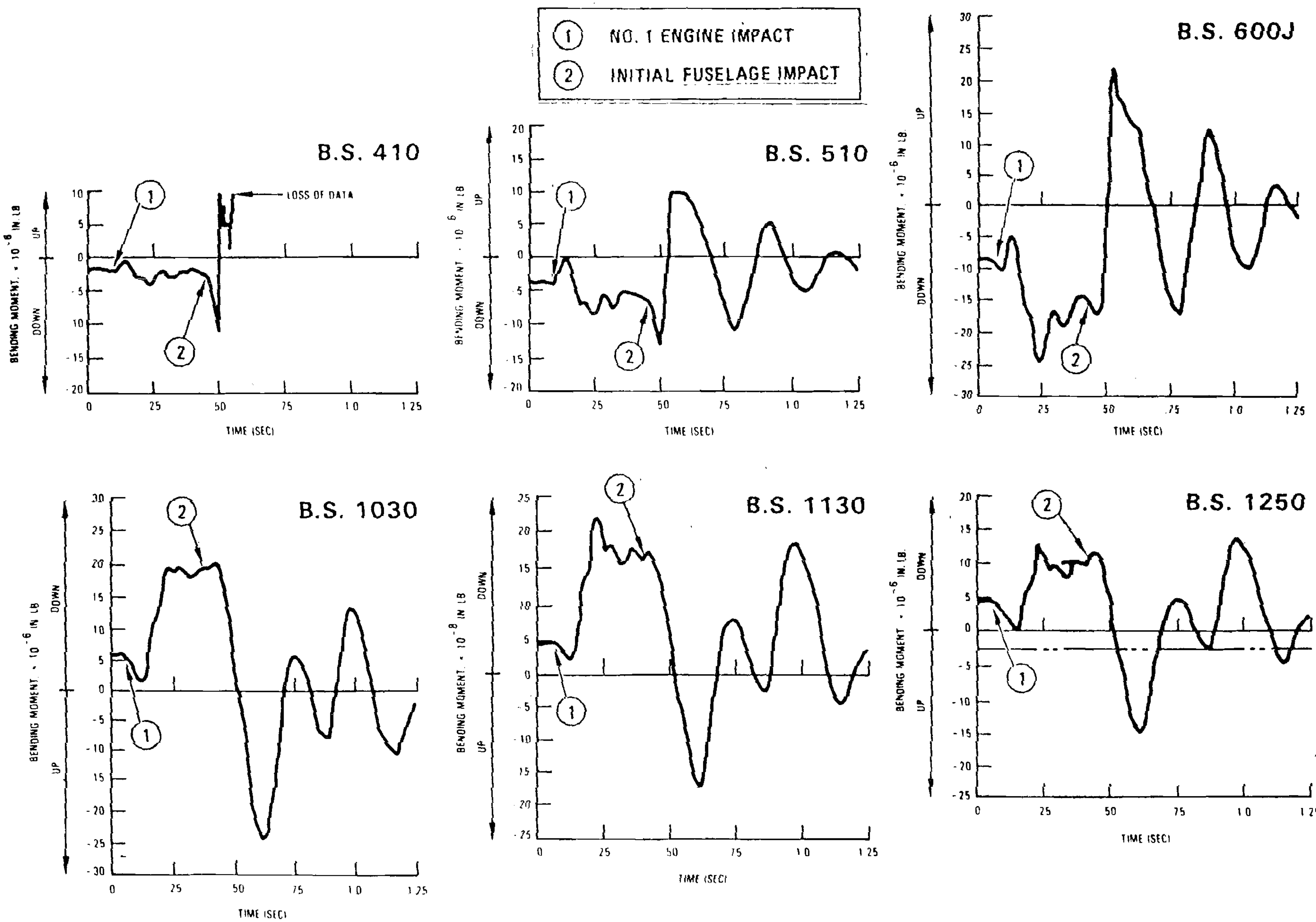

Figure 4-7. CID Test Results, Moment Responses

wing. The study concluded that for an airplane carrying fuel, the entire span of structural box, the fuel can be contained at roll attitude up to 12 degrees, independent of descent angle. With no fuel carried outboard of the 80 percent semi-span location, the fuel can be contained at roll attitudes up to 15 or 16 degrees. The CID test, at a roll attitude of 13 degrees and the extent of wing damage experienced at impact, appears to confirm these earlier findings.

The analyses results showed that for symmetrical impact at 17.3 ft/sec impact and a +1 degree pitch attitude, the moment and shear distribution along the wing will be substantially below the estimated strength (figures 4-10 and 4-11).

The correlation results, described in this report, suggest several concerns that need to be addressed with additional analyses and/or test. The following is a brief discussion of these items:

- How sensitive are the responses to assumed external loading (aerodynamics) and initial rotational velocities (pitch, roll, yaw) within the range of survivable impact speeds and attitudes. Analysis, as opposed to testing, is a more practical attempt to clarify this item.

- What is the trend of the response of the airframe as a function of pitch attitude? For example, do the fuselage extremities respond in the manner as indicated by the results of the limited range of analyses performed during this study and reported in Section 3.0? Additional analysis supported by limited testing is necessary.

- What is the appropriate representation of the engine/wing and wing/fuselage attachments to provide better agreement with test data, both during initial engine ground contact and subsequent fuselage ground contact? While the effort, described in Section 3.0, did not dwell on the engine or wing representation the results indicate that this is an area that needs further effort. Model improvements in this area could be beneficial to wing fuel containment studies. More detailed analysis, with some limited testing, appears desireable for this issue.

- Formulate a crash dynamics manual which, as a minimum, describes crash scenarios, available test data, modeling approaches, structural element representations, and fuselage crush characteristics.

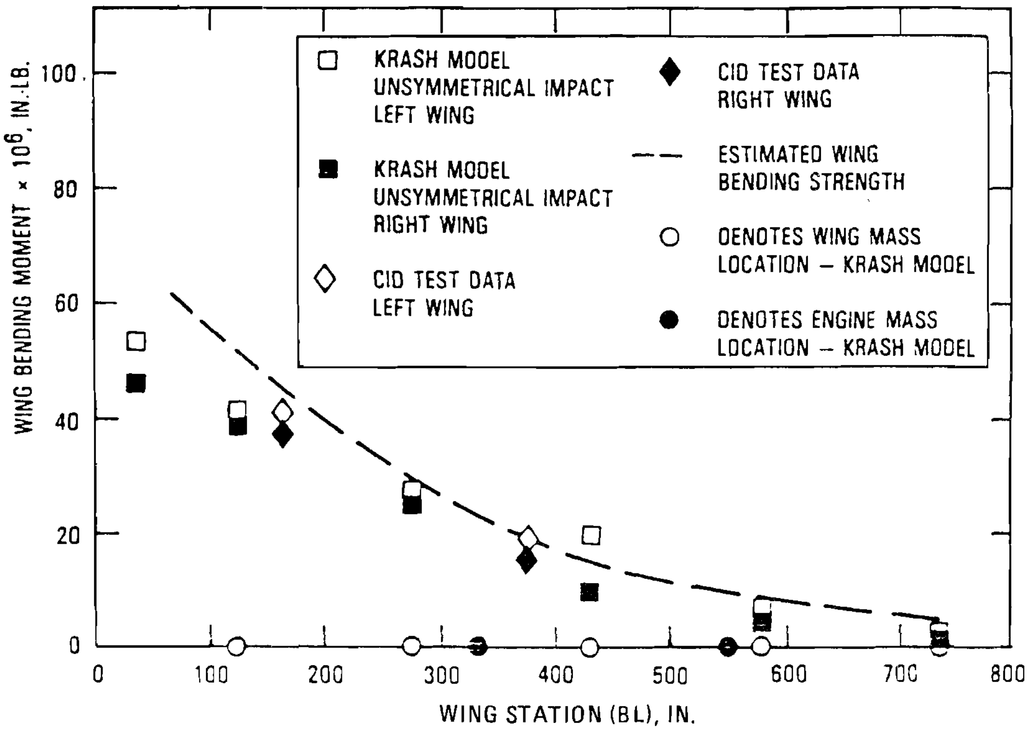

FIGURE 4-8. COMPARISON OF KRASH ANALYSIS AND CID AIRPLANE TEST WING BENDING, STICK MODEL

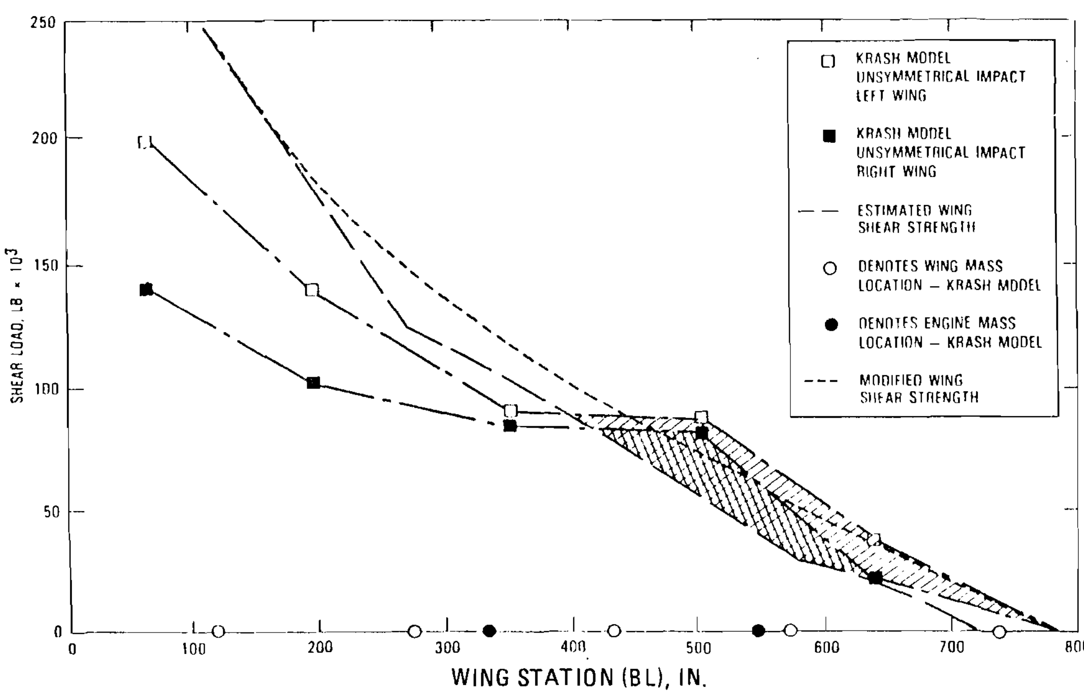

FIGURE 4-9. KRASH ANALYSIS WING SHEAR DISTRIBUTION FOR CID TEST CONDITION, STICK MODEL

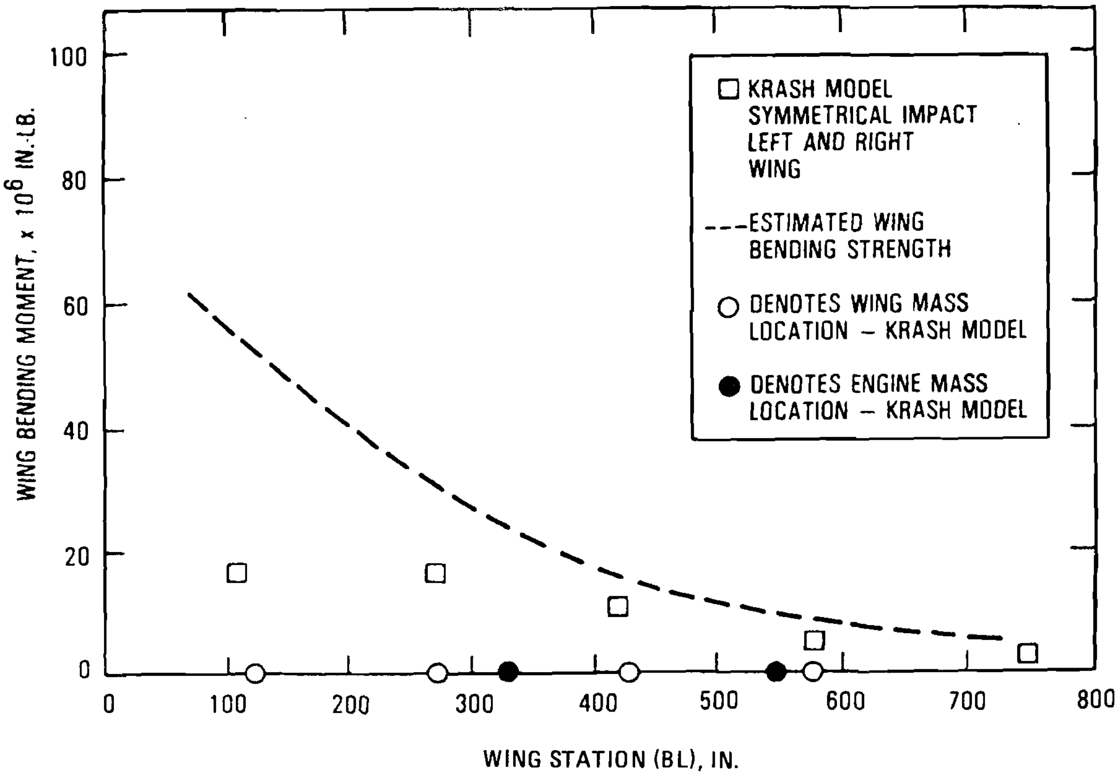

FIGURE 4-10. KRASH ANALYSIS WING BENDING DISTRIBUTION FOR SYMMETRICAL IMPACT; 17.3 FT/SEC SINK SPEED, +1 DEGREE PITCH ATTITUDE, STICK MODEL

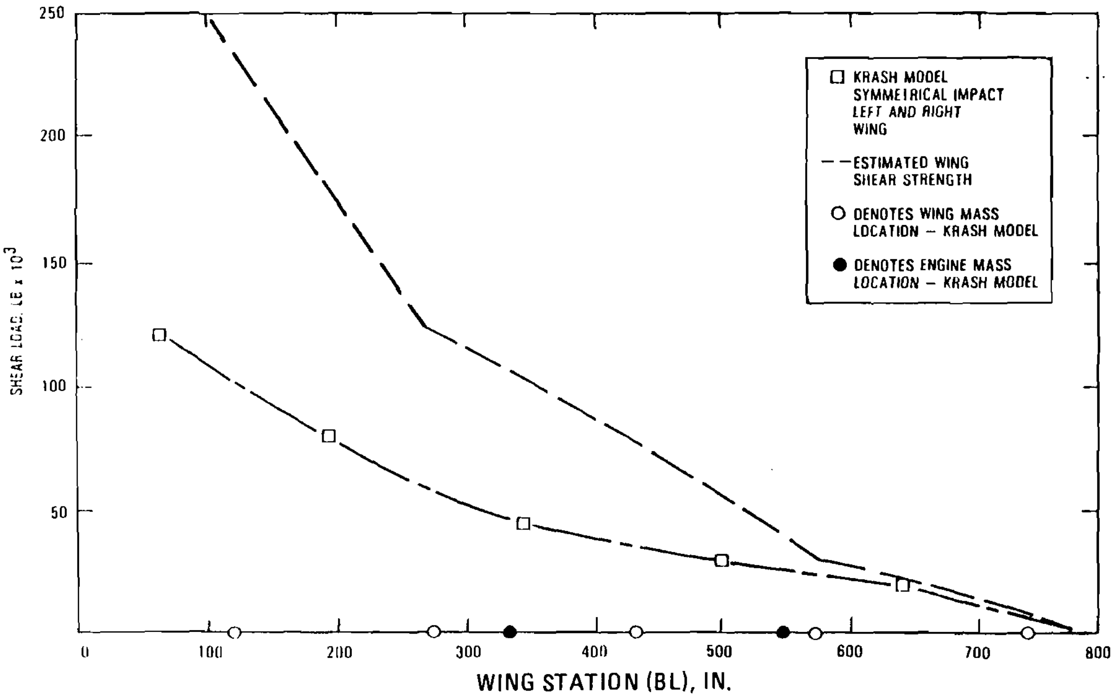

FIGURE 4-11. KRASH ANALYSIS WING SHEAR DISTRIBUTION FOR SYMMETRICAL IMPACT; 17.3 FT/SEC SINK SPEED, +1 DEGREE PITCH ATTITUDE, STICK MODEL

SECTION 5

CONCLUSIONS

5.1 CONCLUSIONS

Comparison of KRASH modeling results, with CID test data, has shown the capability to depict the significant responses and events.

- The analysis of the symmetrical impact on the fuselage at a 14 ft/sec sink speed and with a 1° to 2° nose-down attitude shows good agreement with acceleration pulse magnitudes, durations, and distribution, as well as fuselage crush. The LIC ratios, while higher for the analyses, still indicate that the test impact levels are well within airframe structural integrity.

- The analysis of the unsymmetrical impact initiating with engine No. 1 contact with the ground at 17.3 ft/sec and subsequent rotation onto the No. 2 engine and fuselage, indicates agreement with regard to airframe structural integrity and fuselage crush. However, the fuselage peak vertical accelerations are higher than those measured and obtained from the symmetrical fuselage impact analyses from the mid-fuselage and aft.

- The stick model is adequate for obtaining basic data such as floor pulses, airframe integrity and fuselage crush.

- The expanded model results which were obtained for the 14 ft/sec fuselage symmetrical impact show reasonable agreement with the stick model results. However, the relatively low level of fuselage impact loads do not result in fuselage airframe failures and thus substantiation of the adequacy or desirability of the need for additional detail modeling is lacking.

- While the analytically obtained wing and engine responses show agreement with the test data, they also indicate that improved/wing/engine and wing/fuselage interface representations are desirable.

SECTION 6

REFERENCES

1. "Full-Scale Transport Controlled Impact Demonstration Program," FAA Report No. DOT/FAA/CT-82/151, FAA Technical Center, Atlantic City Airport, NJ, January 1984.

2. "Draft Advisory Circular on Human Exposure to Impact; and a Preview of the Agency's Crash Dynamics Program," Federal Register, Vol. 49, No. 185, September 21, 1984.

3. "Transport Aircraft Crash Dynamics," Lockheed-California Company, NASA Contractor Report 165851, FAA Report DOT-FAA-CT-82/69, March 1982.

4. "Commercial Jet Transport Crashworthiness," Boeing Commercial Airplane Company, NASA Contractor Report 165849, FAA Report DOT-FAA-CT-82/86, March 1982.

5. "Transport Aircraft Accident Dynamics," Douglas Aircraft Company, NASA Contractor Report 165850, FAA Report No. DOT-FAA-CT-82/70, March 1982.

6. Caiafa, C. and Thomson, R. G.: "Structural Response of Transport Airplanes in Crash Situations," NASA Technical Memorandum 85654, National Technical Information Service, Springfield, VA, June 1983.

7. Stauffer, W. A. and Wittlin, G.: "Transport Crash Dynamics Airframe Structural Integrity, Design Criteria," Flight Safety Foundation, Inc., Conference and Workshop on Cabin Safety, Arlington, VA, December 1984.

8. Soltis S., Caiafa C., Wittlin G.: "FAA Structural Crash Dynamics Program Update," SAE October 16, 1985, Long Beach, Ca.

9. Gamon, M. A., Wittlin, G. and LaBarge, W. L.: "KRASH85 User's Guide - Input/Output Format," Lockheed-California Company, DOT/FAA/CT-85/10, May 1986.

10. Wittlin, G. and LaBarge, W. L.: "KRASH Dynamics Analytical Modeling - Transport Airplane Controlled Impact Demonstration Test," Lockheed-California Company, Report DOT/FAA/CT-85/9, May 1986.

11. Nissely, P. M., Heid, T. L., "Structural Design For Fuel Containment Under Survivable Crash Conditions", General Dynamics/Convair, FAA Technical Report ADS-19, August 1964.

APPENDIX A

CID TEST DATA

TABLE A-1 CID FUSELAGE FLOOR RESPONSE DATA

CHANNEL NO.	DESIGNATION	DIRECTION	LOCATION		
			BS	BL	WL
1*,2,3	PILOT-FLR	N,L,T	228	-12	0
14*,15*	SITE3-LFLR	N,L	540	-25	4
29*,30,31	SITH5-LFLR	N,L,T	600J	-25	4
45*	SITF6-RFLR	N	660	25	0
49*,50	SITD7-LFLR	N,L	702	-25	0
65*,66	SITG9-LFLR	N,L	820	-25	4
80*	SITB11-LFLR	N	920	-25	0
84*,85	SITI12-RFLR	N,L	960	25	0
95,96	SITN14-RFLR	N,L	1220	25	0
105*,106,107	SITT15-LFLR	N,L,T	1380	-25	0
118,119	FR#2-FLRLW	N,L	540	-70	4
120,121	FR#2-FLRRW	N,L	540	70	4
138,139	FR#4-FLRLW	N,L	820	-70	6
140,141	FR#4-FLRRW	N,L	820	70	6
147,148	FR#6-FLRLW	N,L	1120	-70	4
186*,187,188	SITA3-RFLR	N,L,T	540	25	4
198*	SITC4-LFLR	N	600	-25	0
202*,203	SITB5-RFLR	N,L	600J	25	4
218*	SITI6-LFLR	N	660	-25	0
222	SITC9-RFLR	N	820	25	4
234	SITA10-LFLR	N	860	-25	0
238*	SITH11-RFLR	N	920	25	0
242*,243	SITF12-LFLR	N,L	960	-25	4
254*	SITD7-RFLR	N	696	25	0
258	SITN14-LFLR	N	1220	-25	4
271,272	FR#1-FLRLW	N,L	400	-70	4
278,279	FR#1-FLRRW	N,L	400	-70	4
288	FR#3-FLRLW	N	600J	-70	4
290	FR#3-FLRRW	N	600J	70	4
300,301	TAIL	N,T	1608	0	52
316	FR#7-FLRLW	N	1220	-70	4

*PRESENTED IN SECTION 3

N = NORMAL T = LATERAL
L = LONGITUDINAL

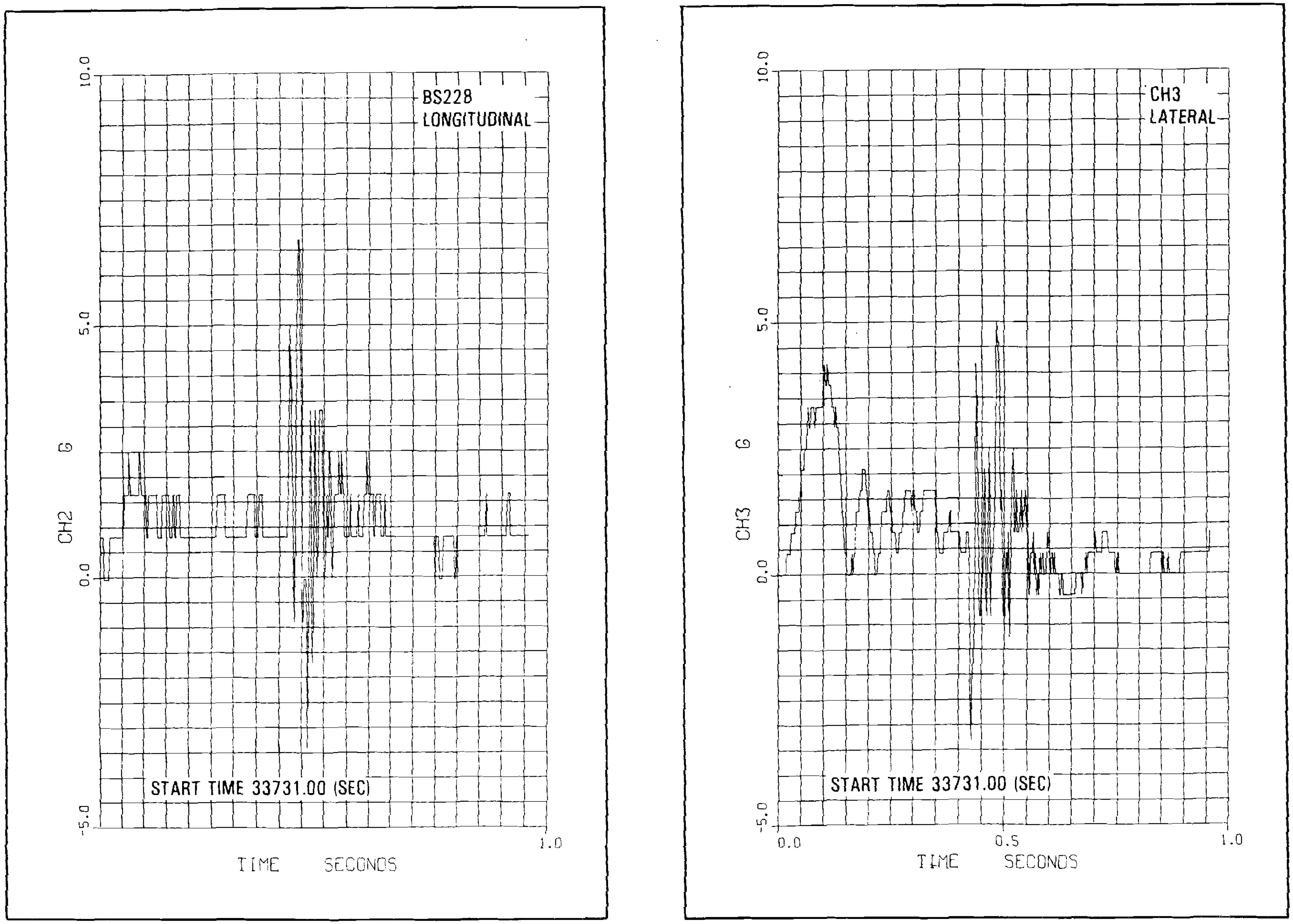

FIGURE A-1. CID TEST DATA, BS228

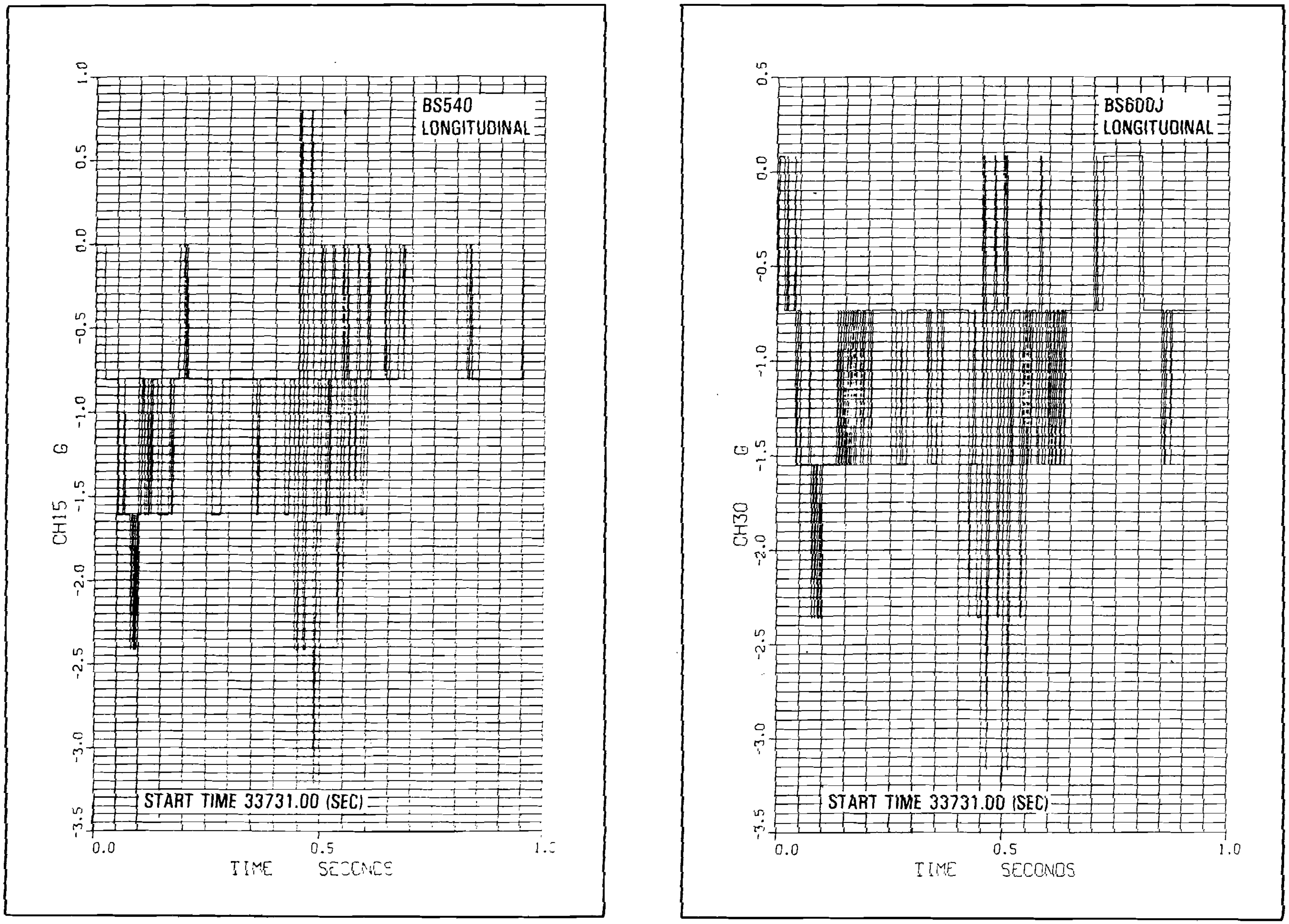

FIGURE A-2. CID TEST DATA, BS540 – BS600J

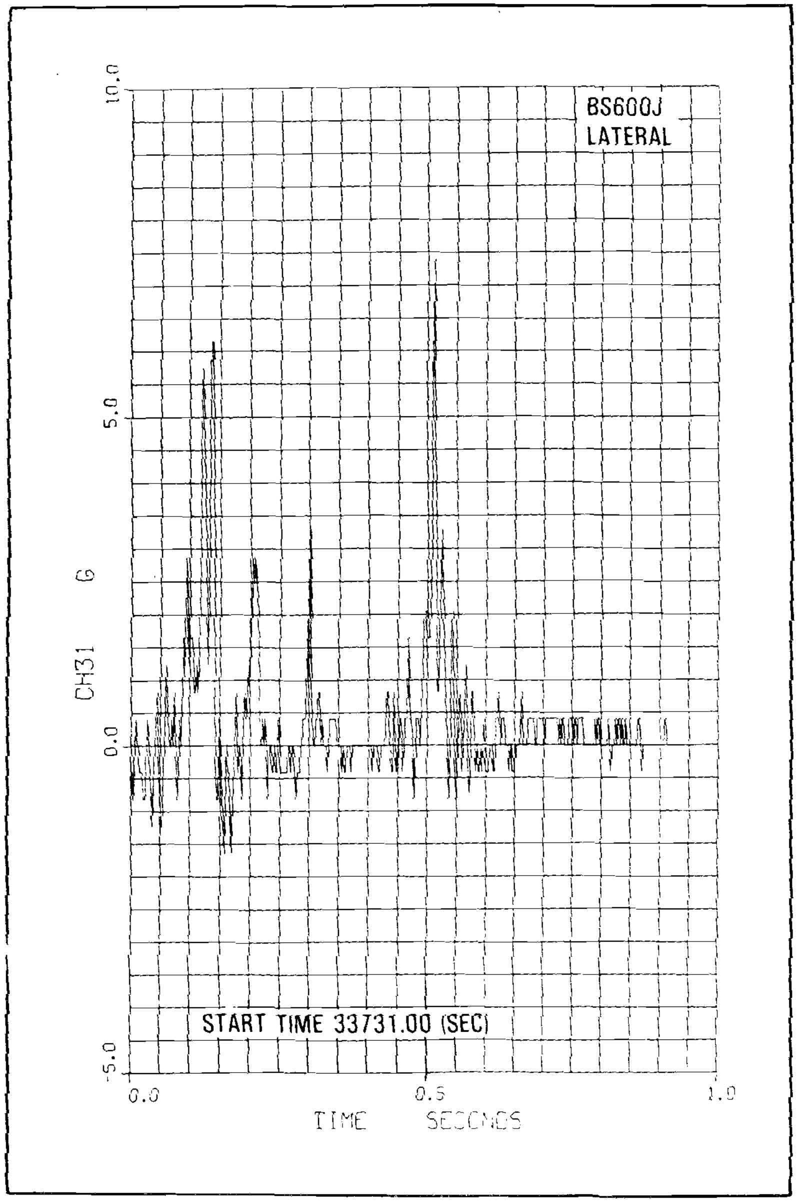

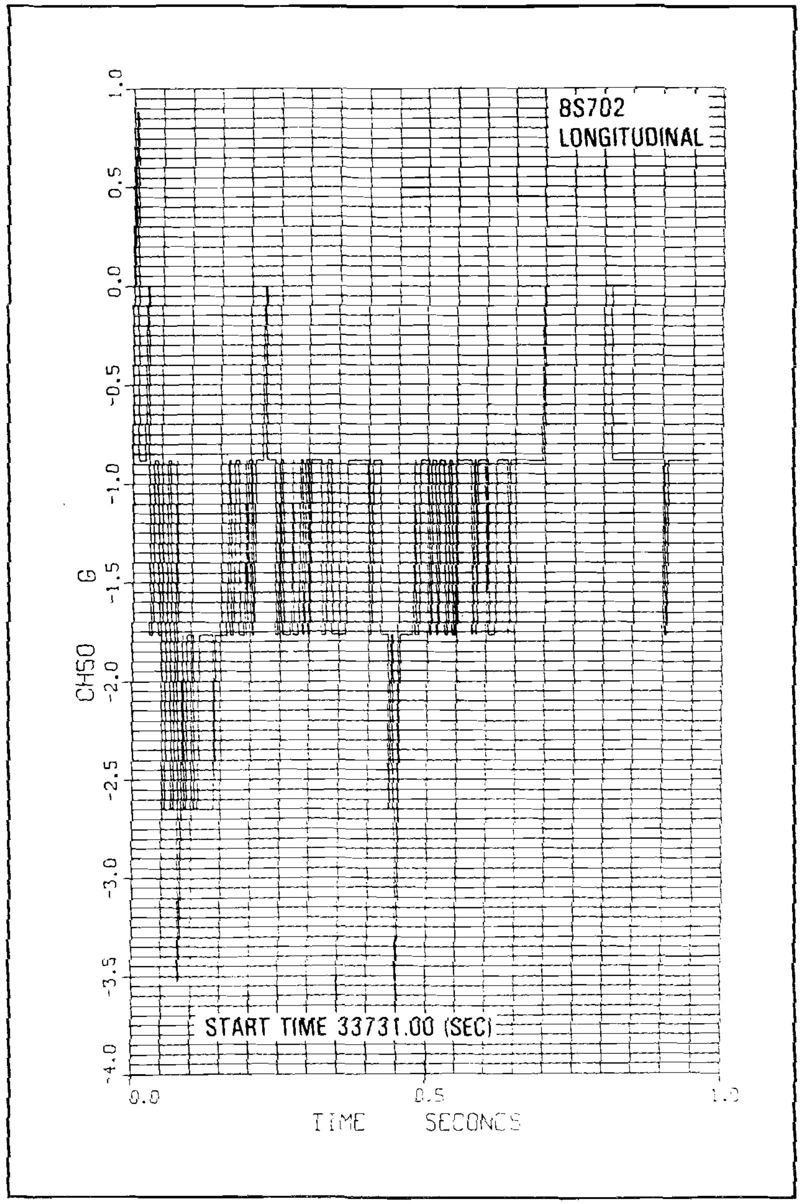

FIGURE A-3. CID TEST DATA, BS600J – BS702

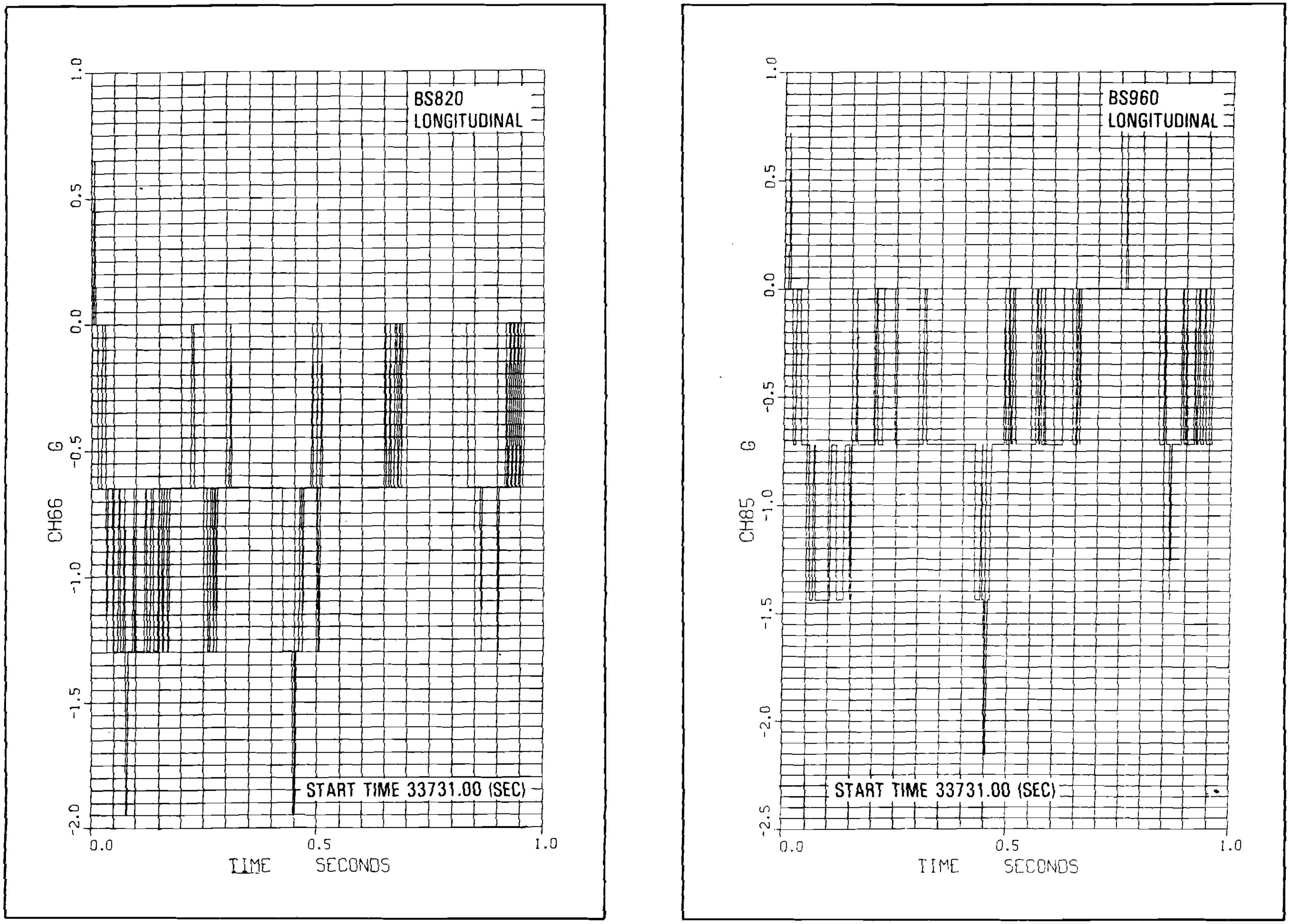

FIGURE A-4. CID TEST DATA, BS820 - BS960

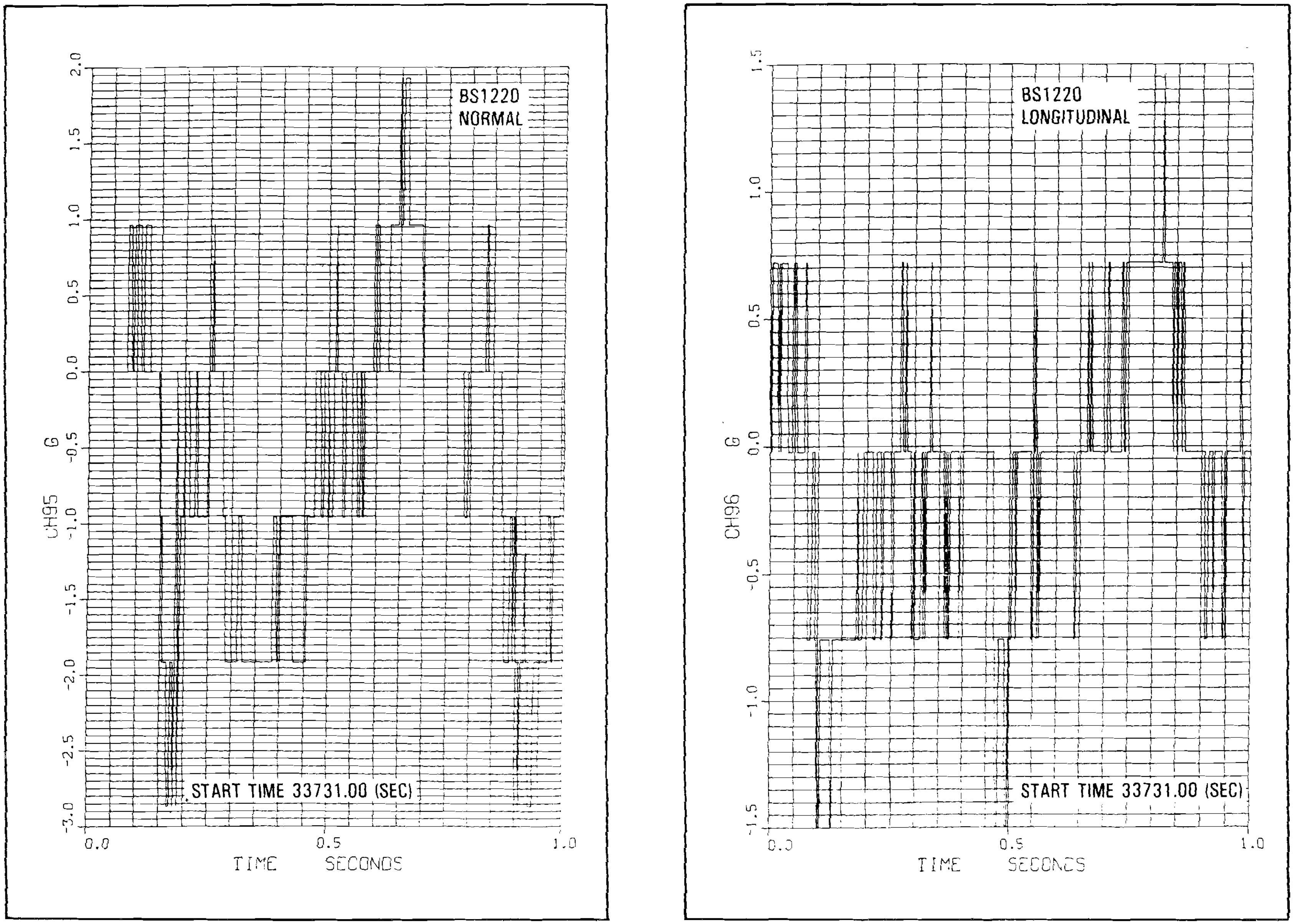

FIGURE A-5. CID TEST DATA, BS1220

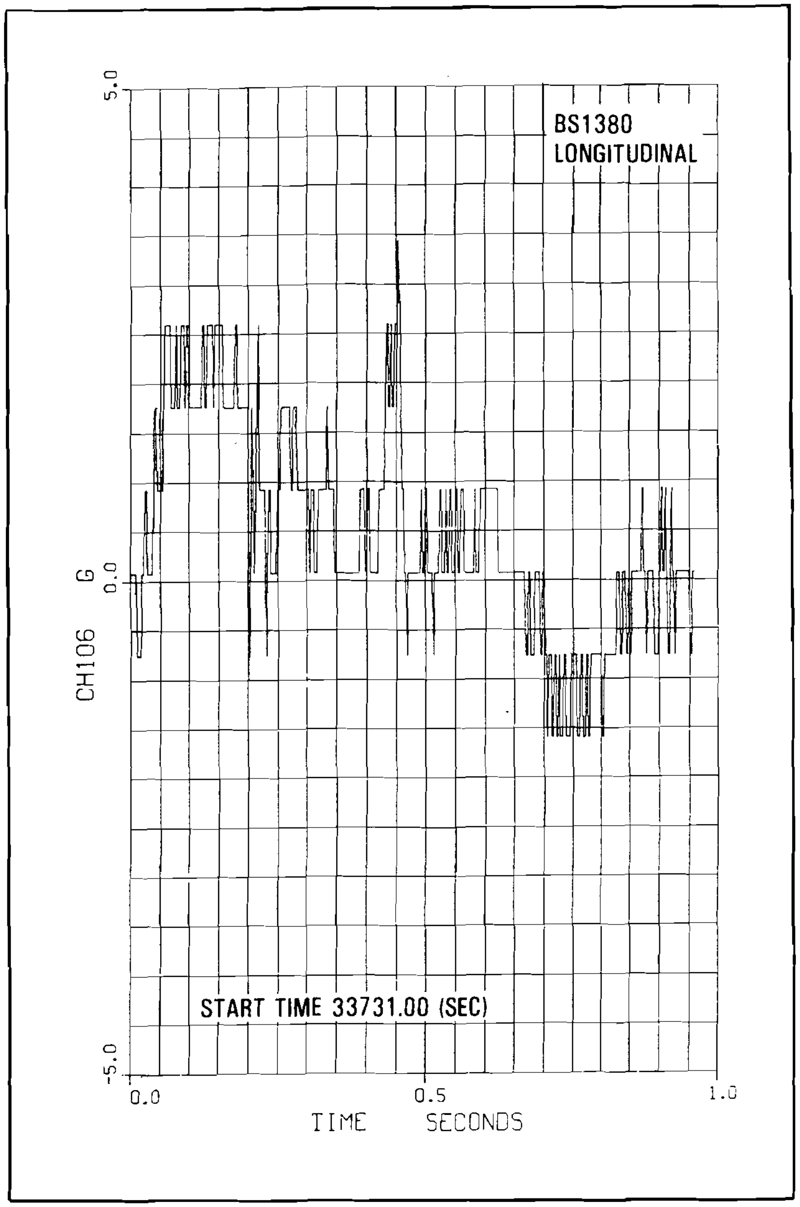

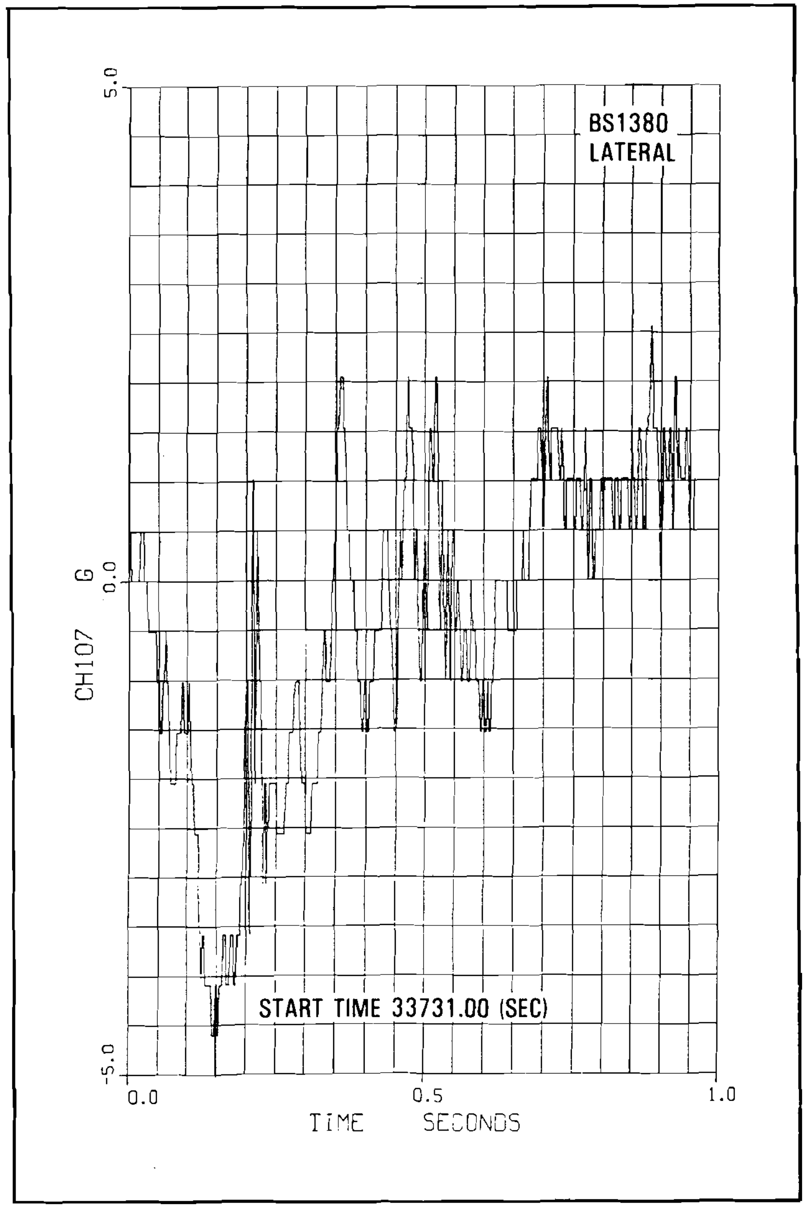

FIGURE A-6. CID TEST DATA, BS1380

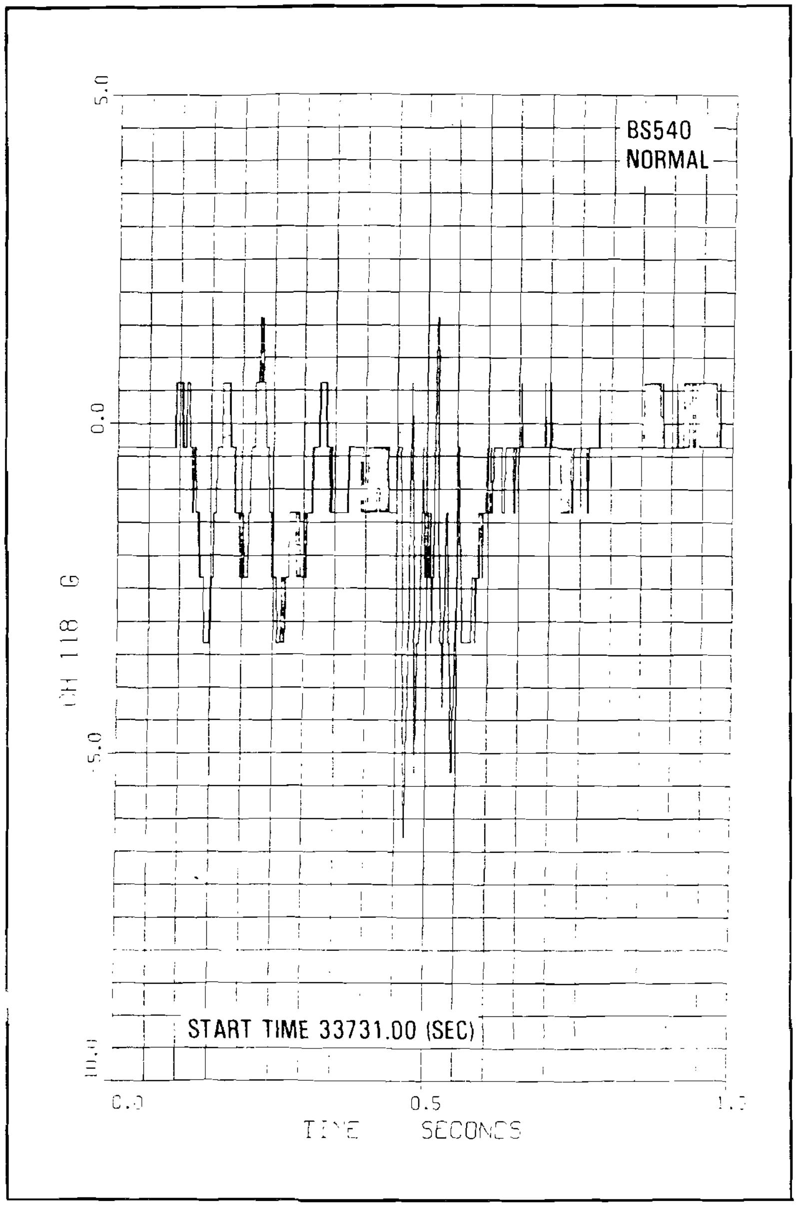

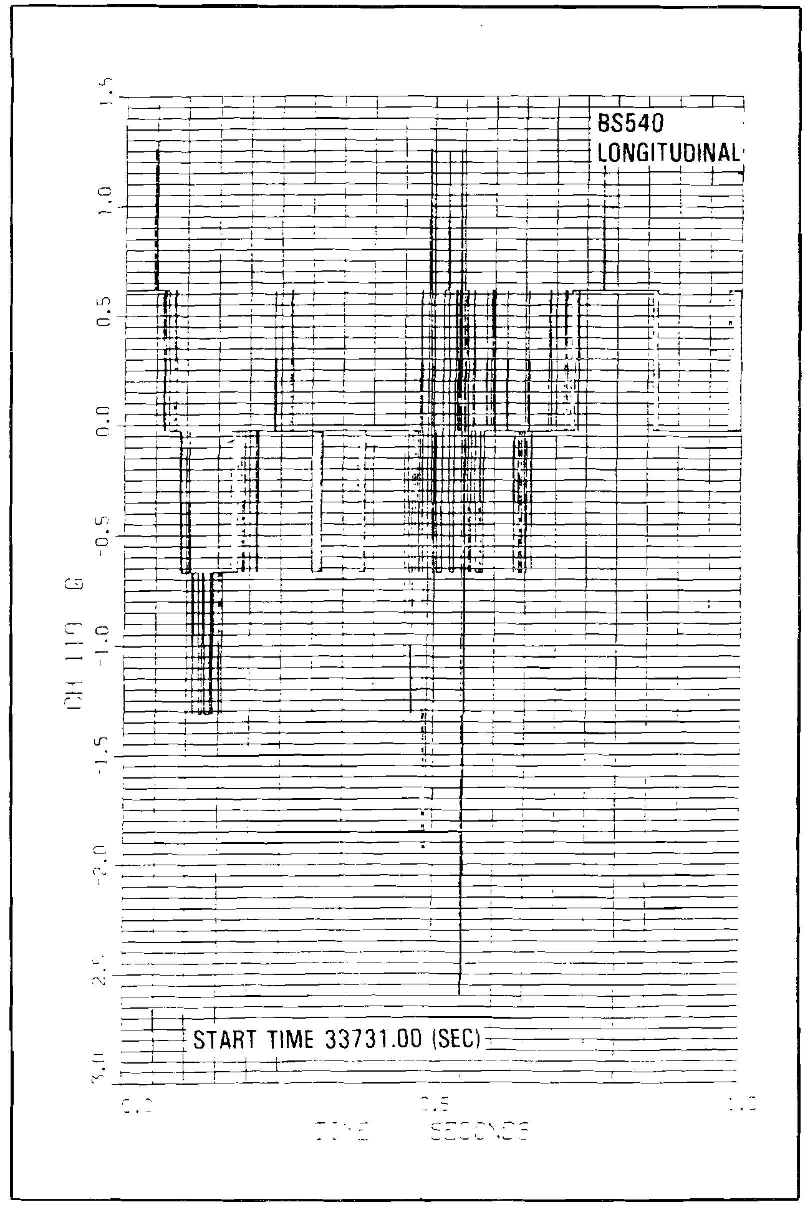

FIGURE A-7. CID TEST DATA, BS540

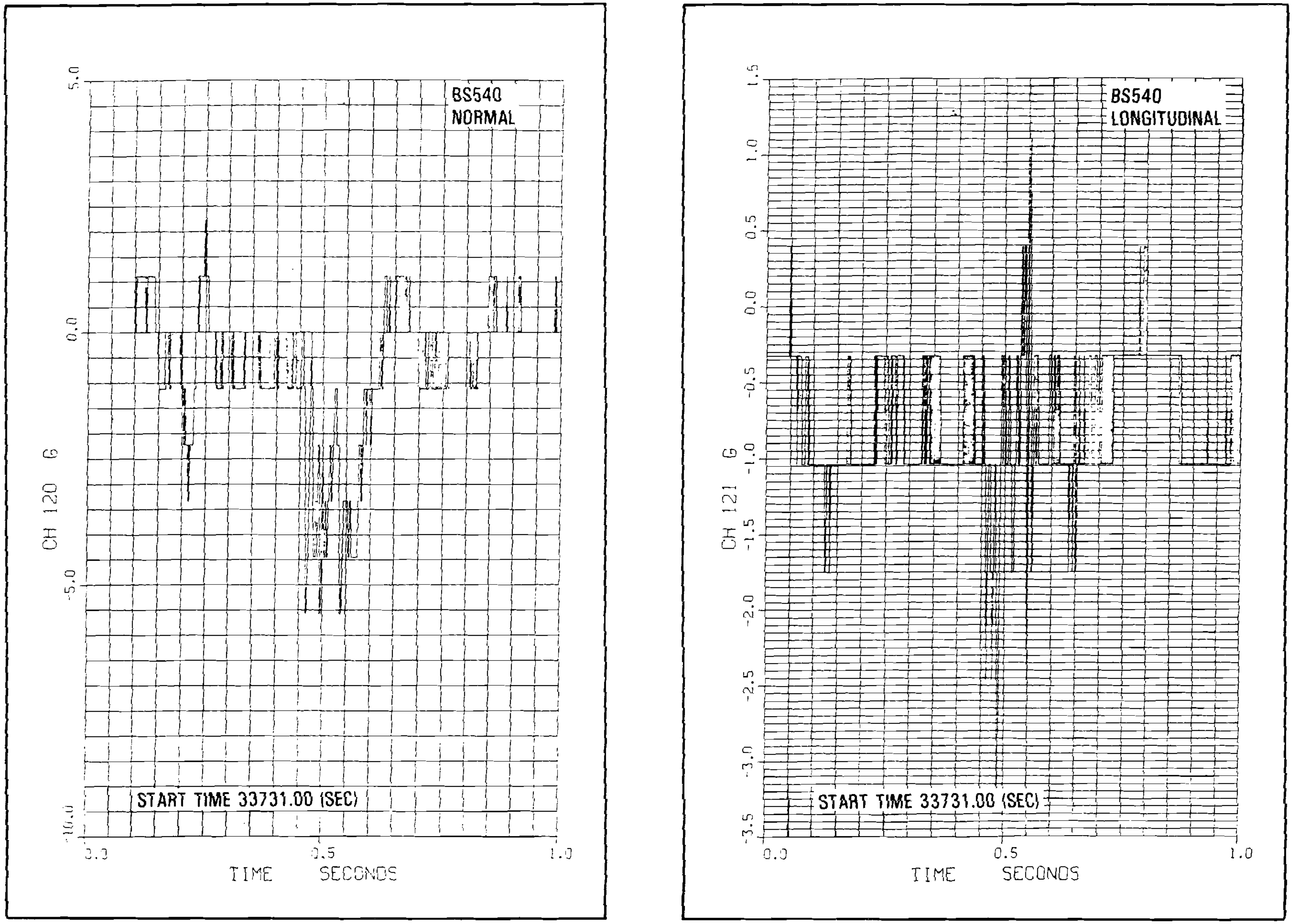

FIGURE A-8. CID TEST DATA, BS540

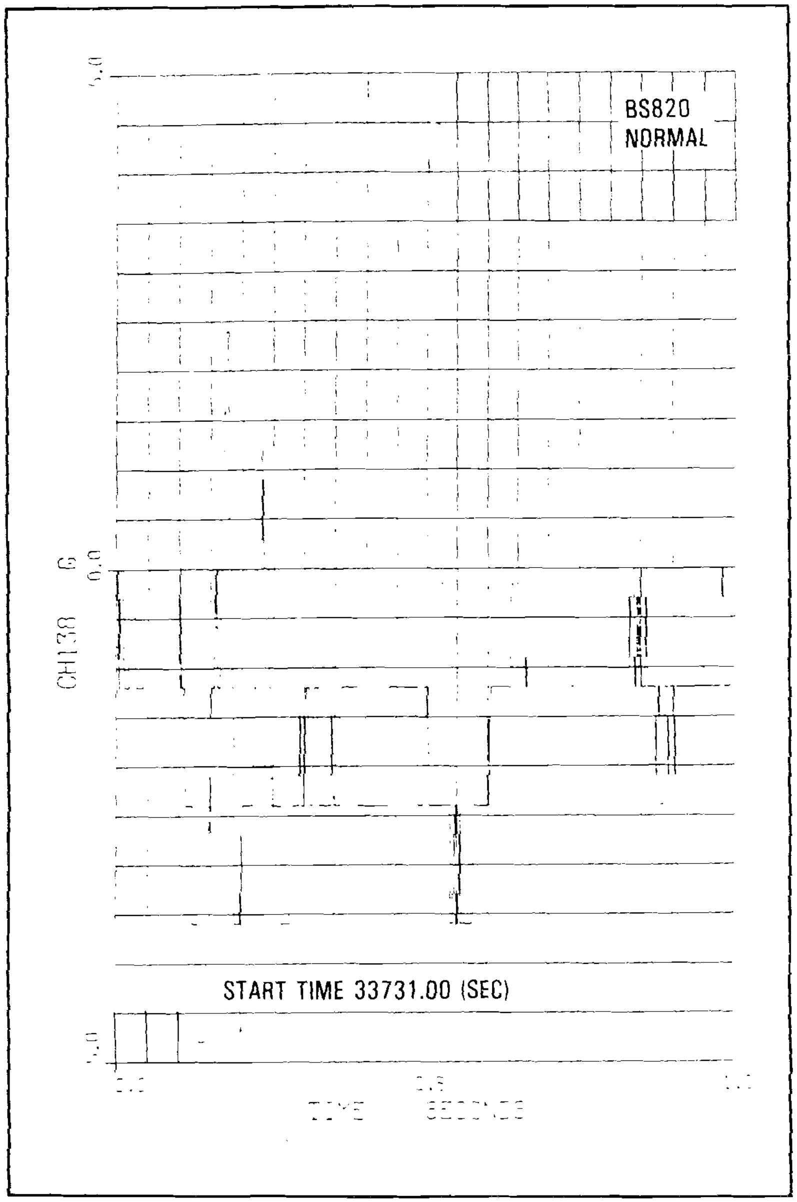

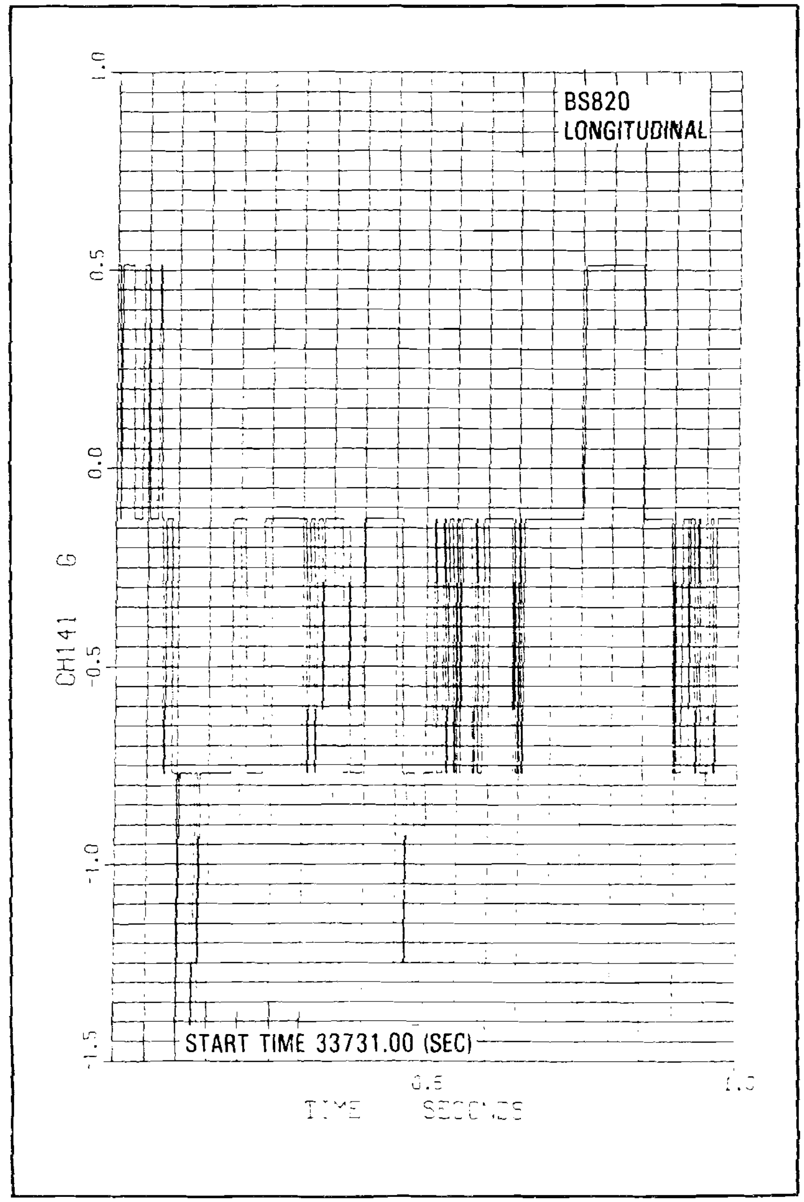

FIGURE A-9. CID TEST DATA, BS820

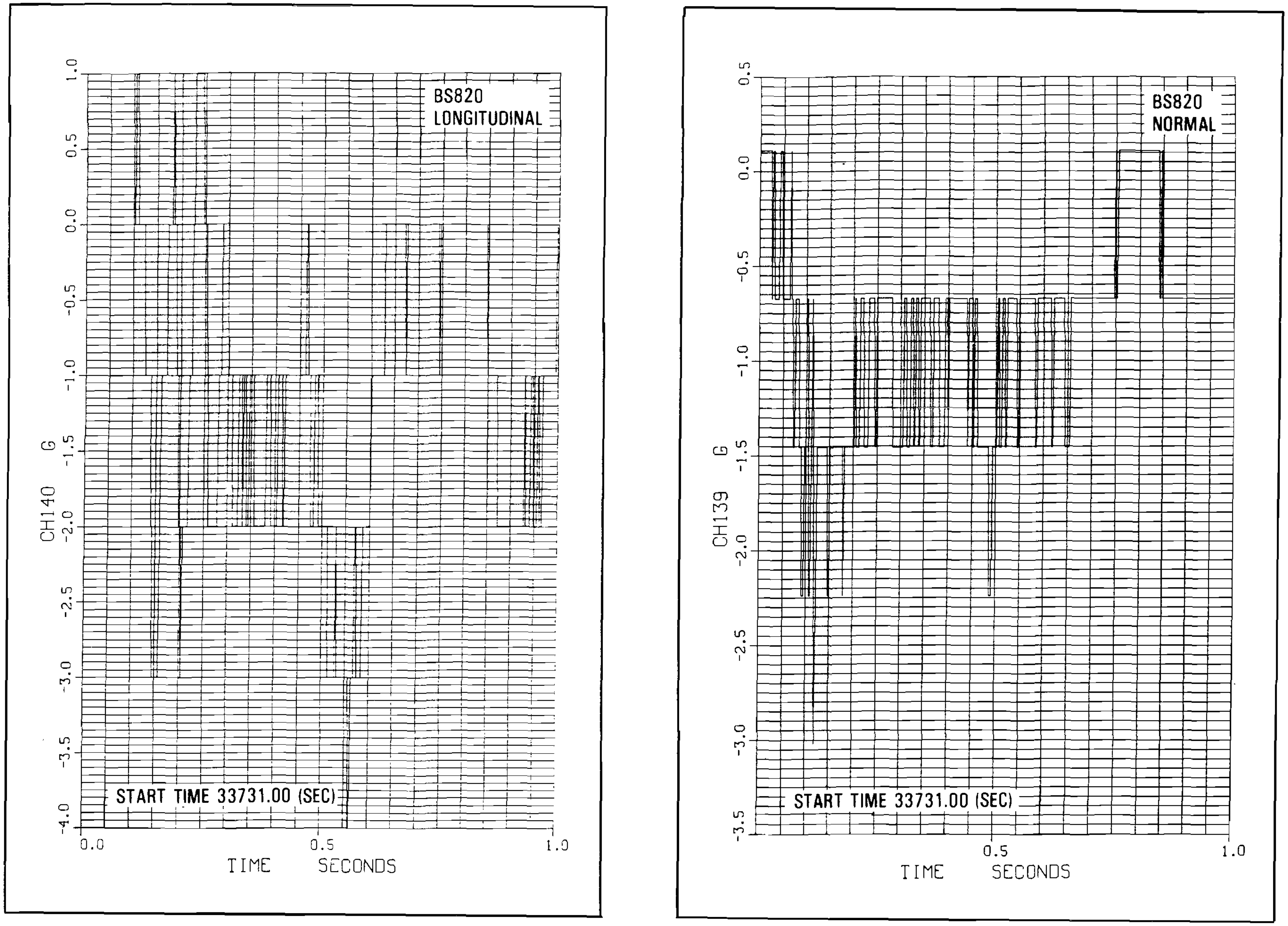

FIGURE A-10. CID TEST DATA, BS820

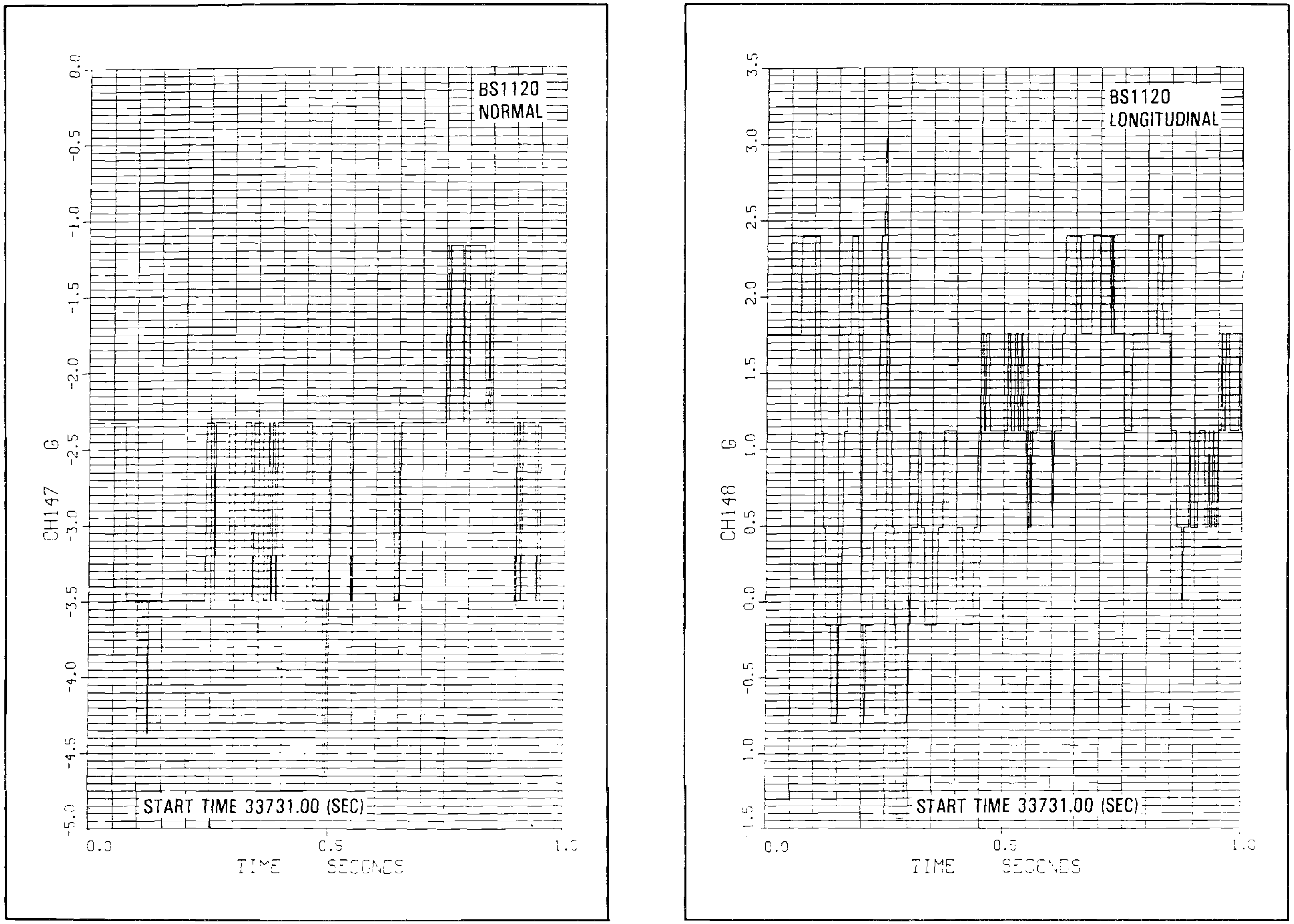

FIGURE A-11. CID TEST DATA, BS1120

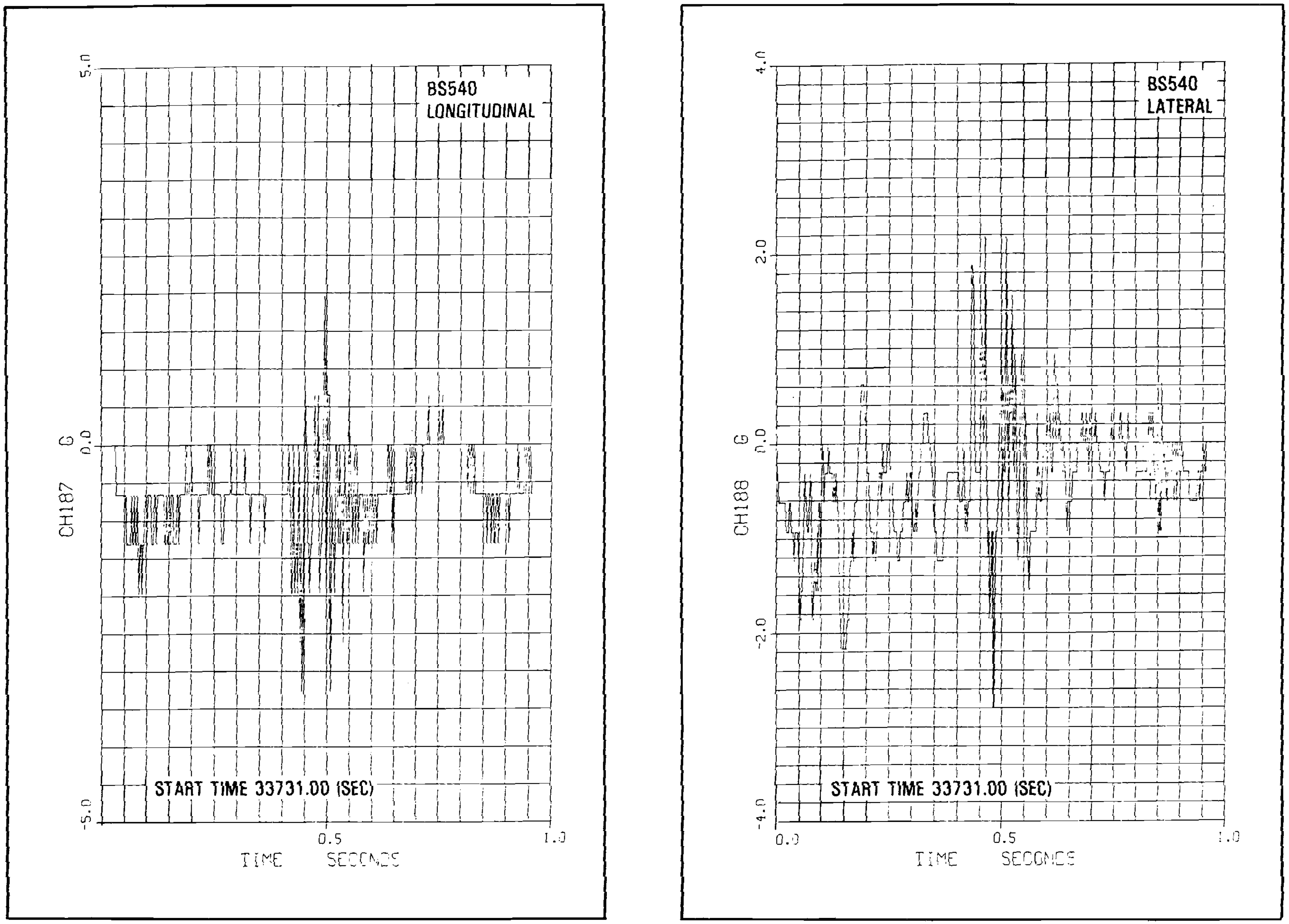

FIGURE A-12. CID TEST DATA, BS540

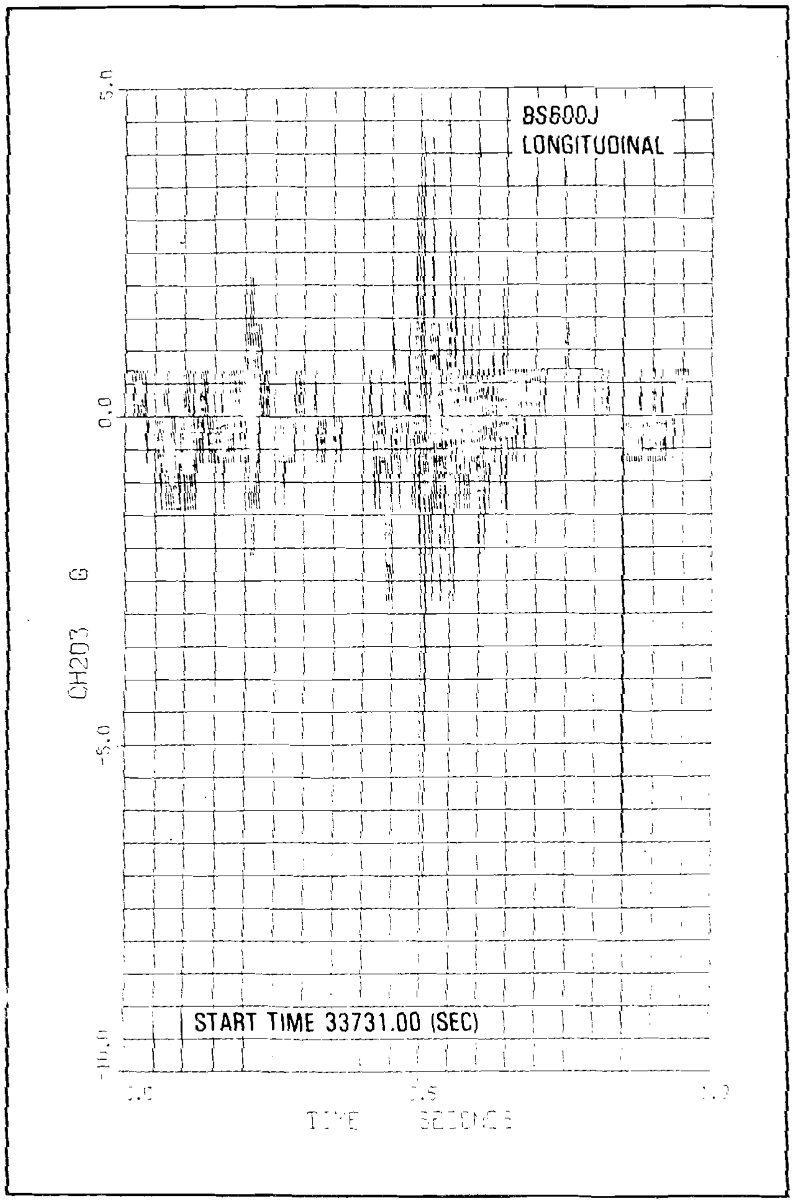

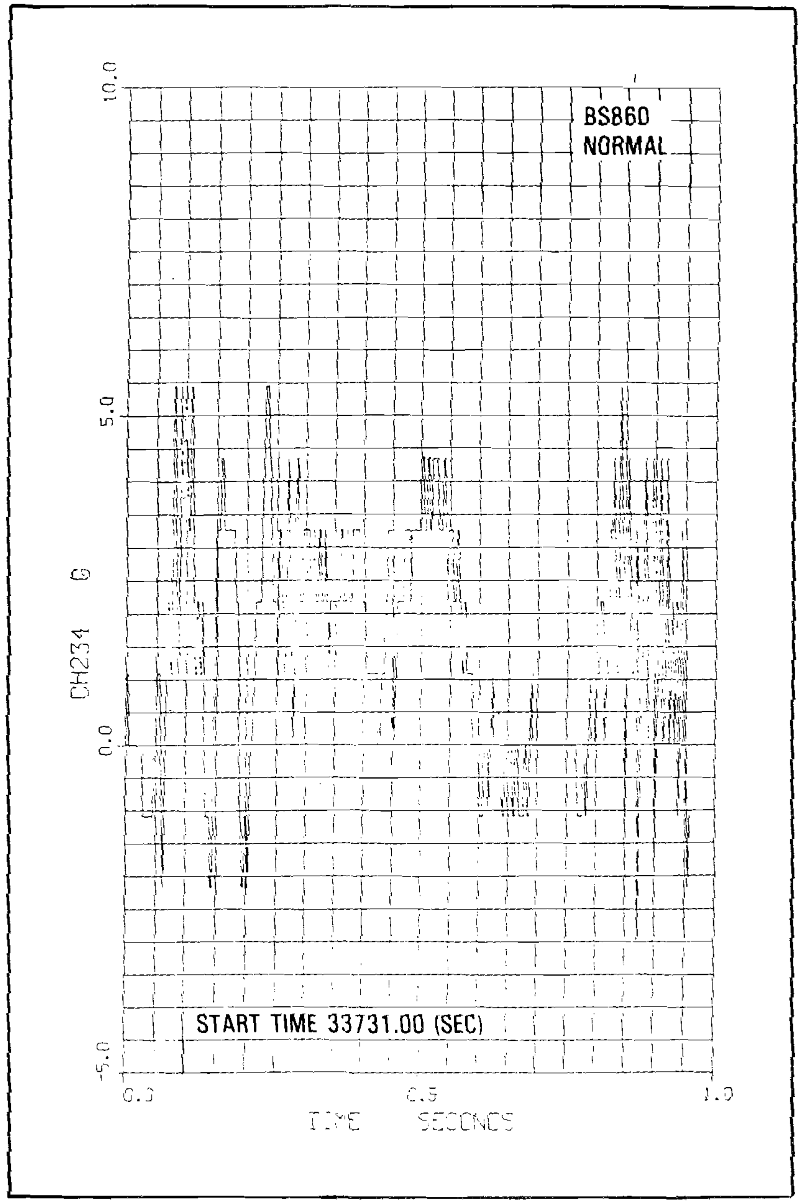

FIGURE A-13. CID TEST DATA, BS600J – BS860

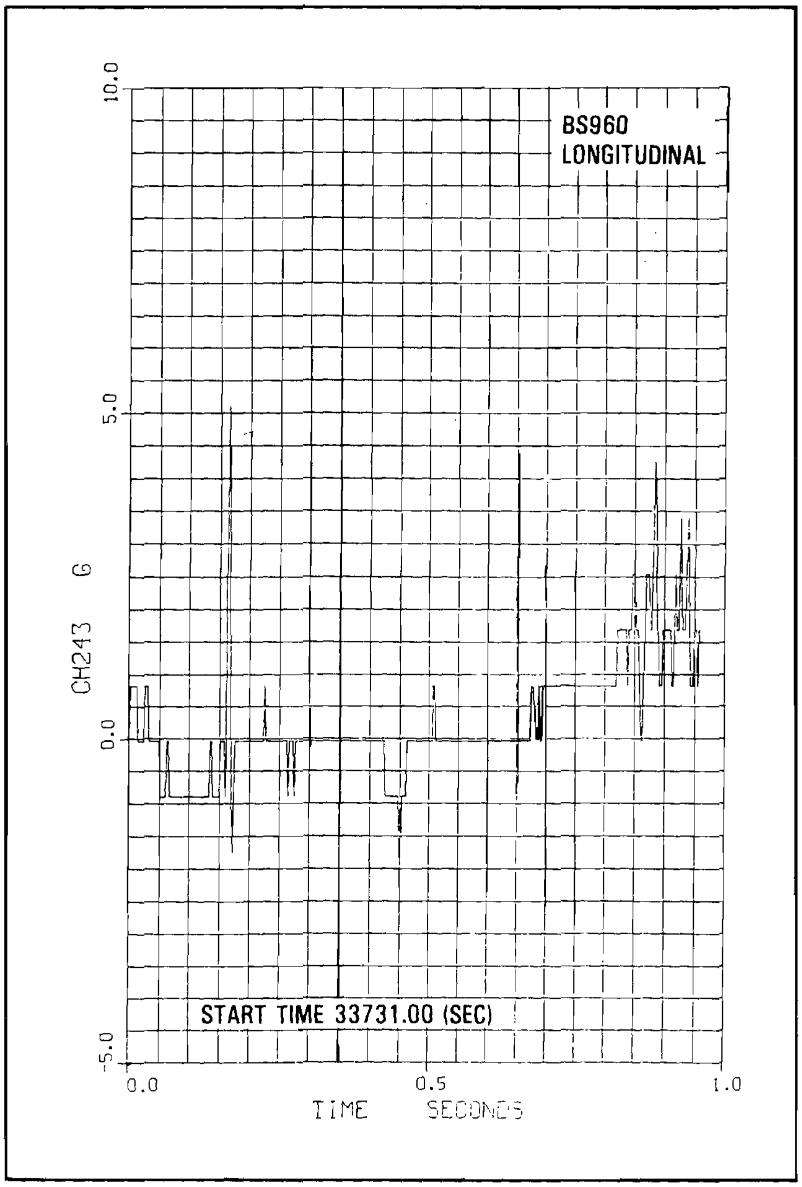

FIGURE A-14. CID TEST DATA, BS960

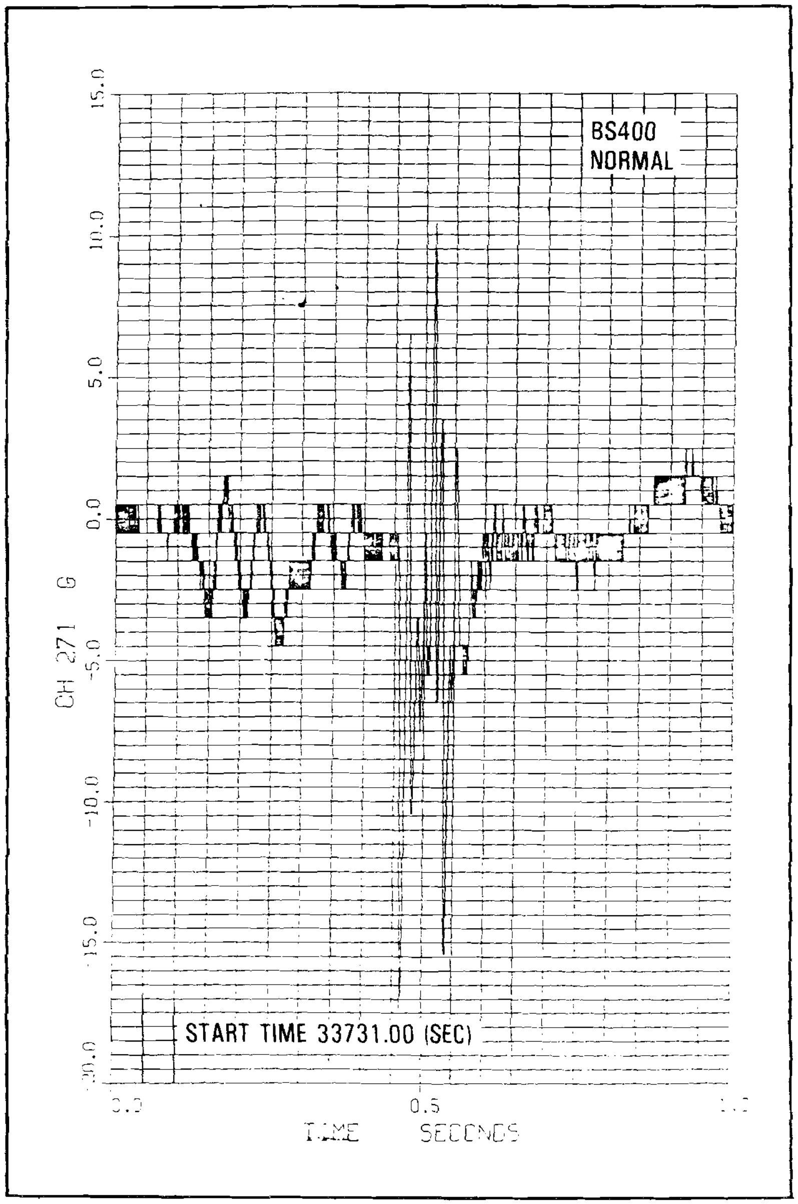

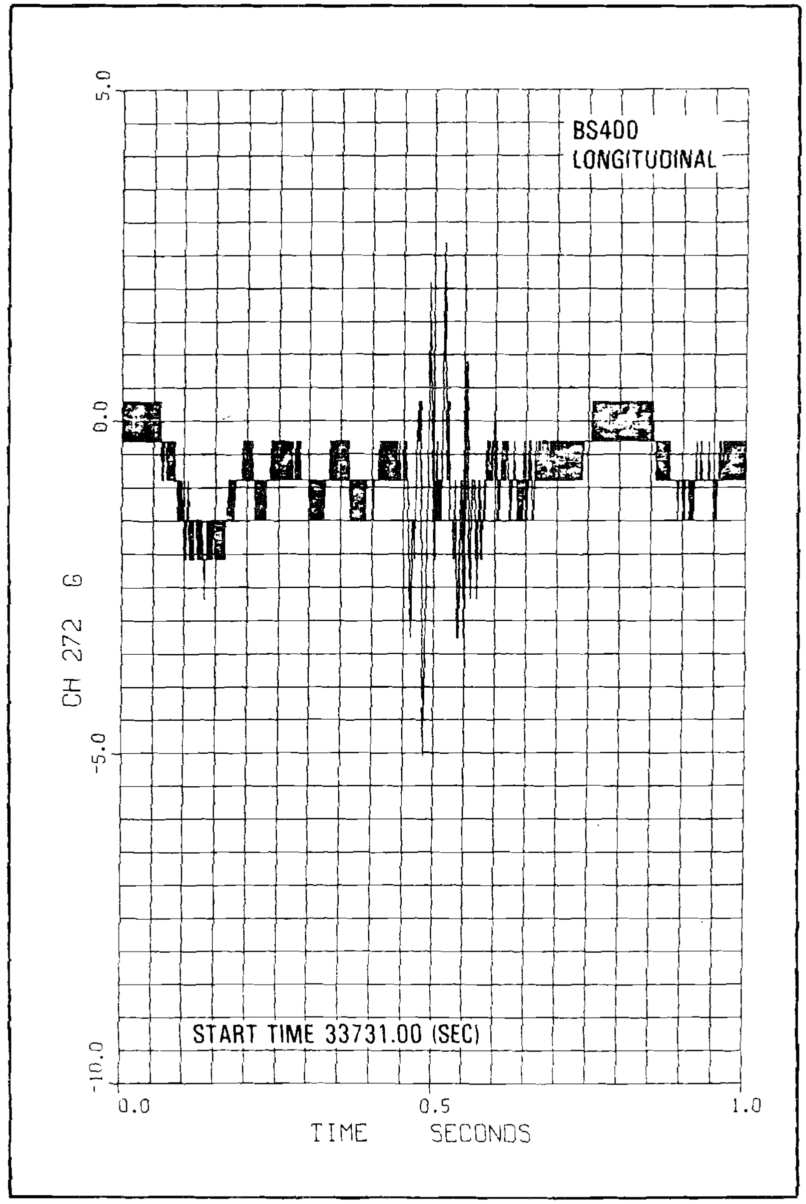

FIGURE A-15. CID TEST DATA, BS400

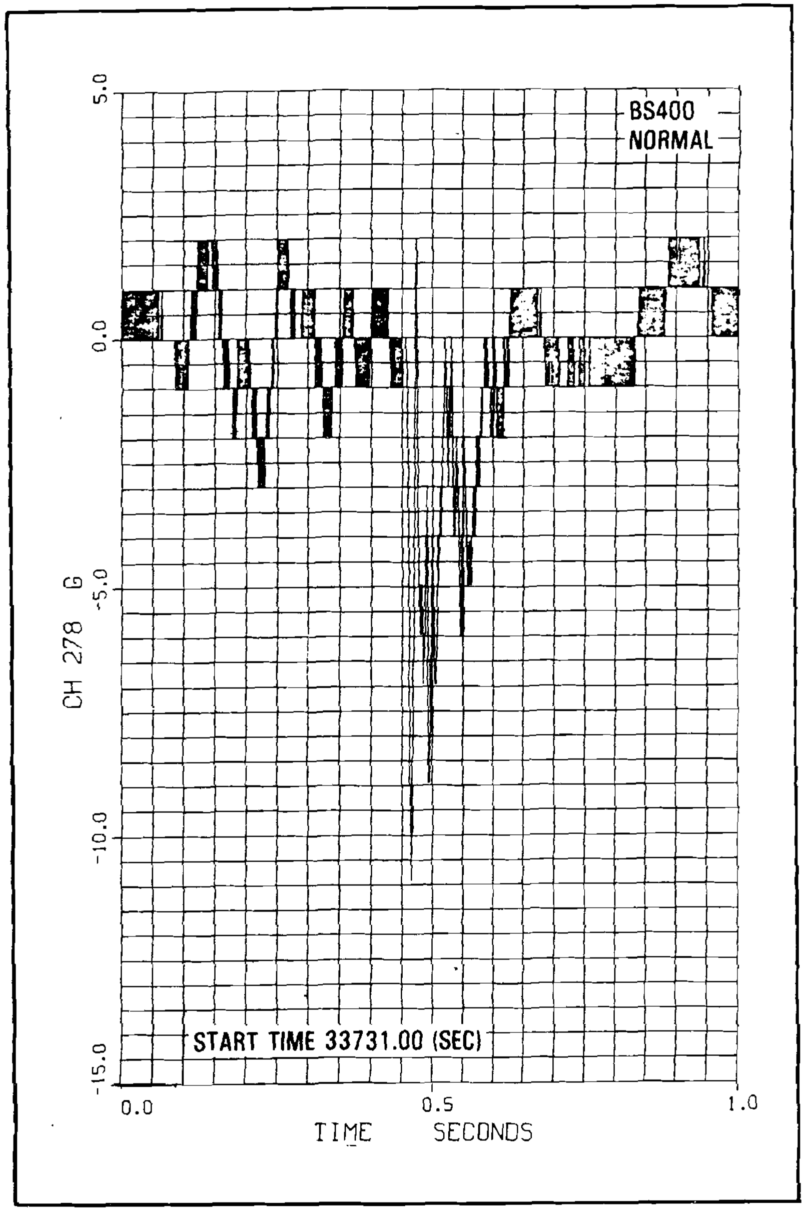

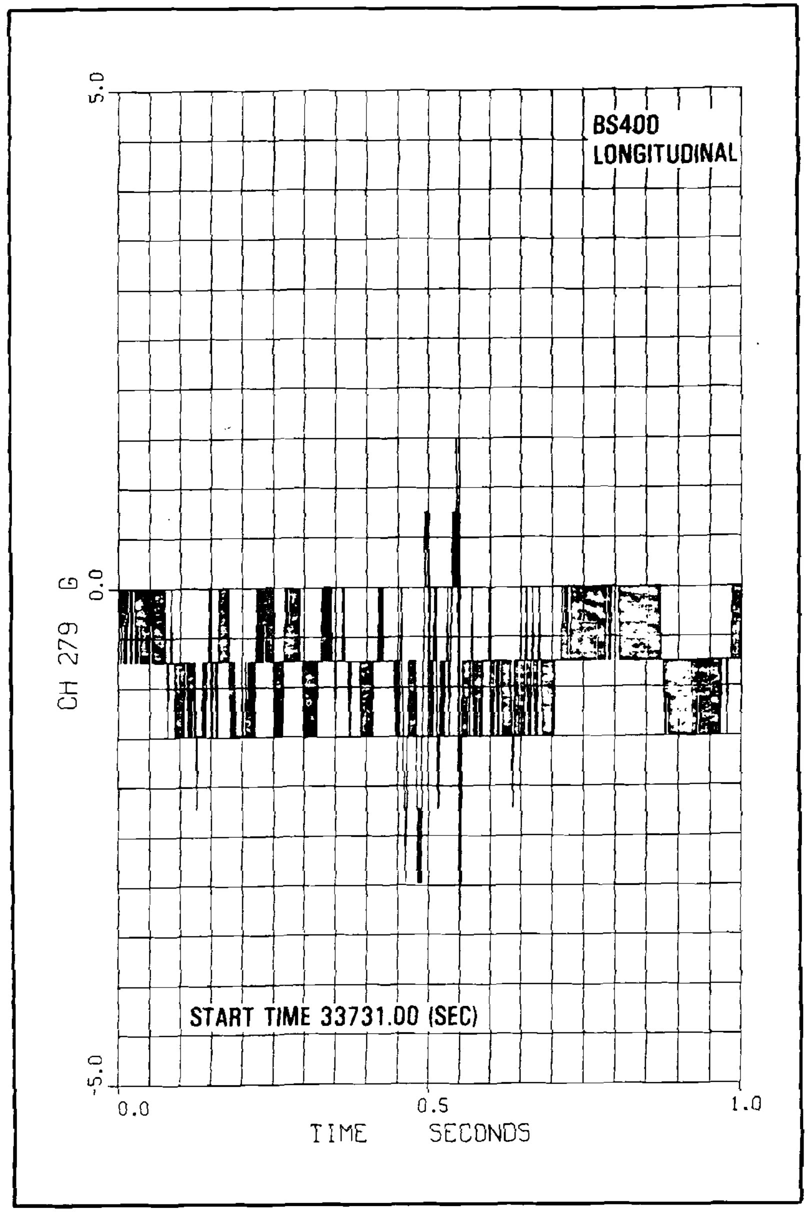

FIGURE A-16. CID TEST DATA, BS400

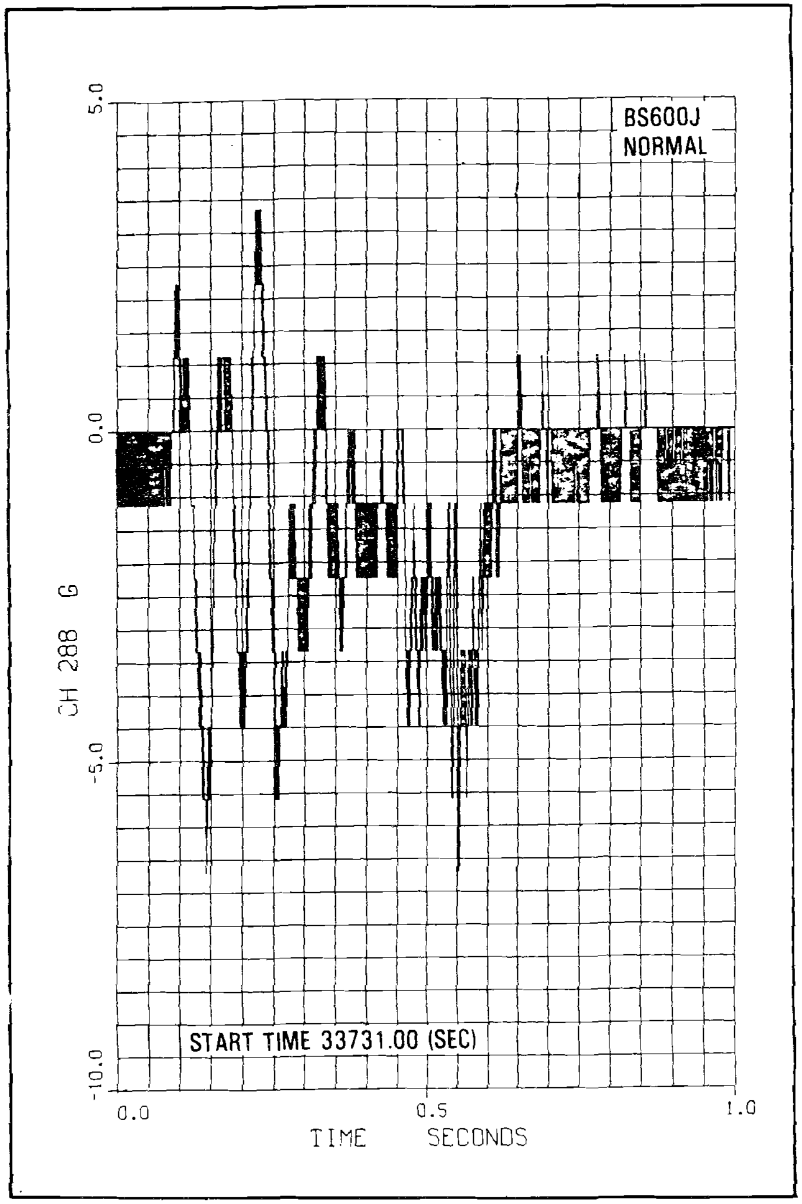

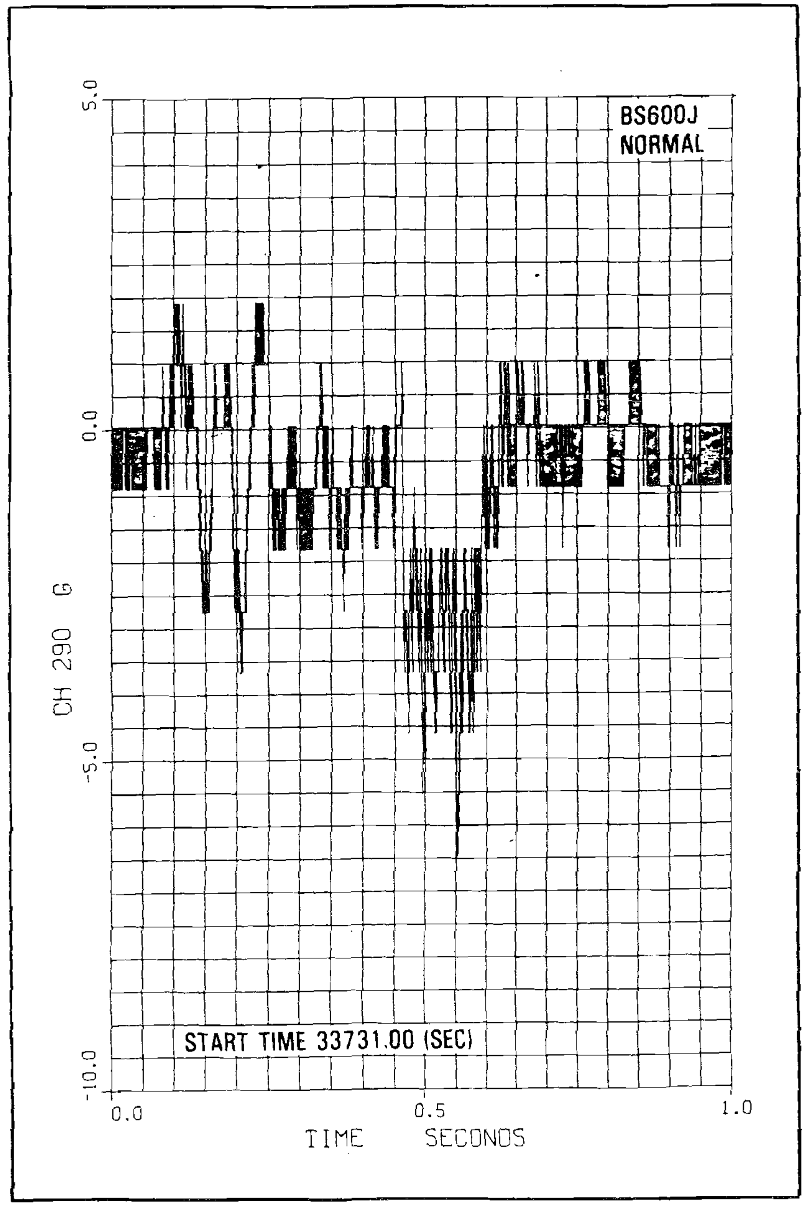

FIGURE A-17. CID TEST DATA, BS600J

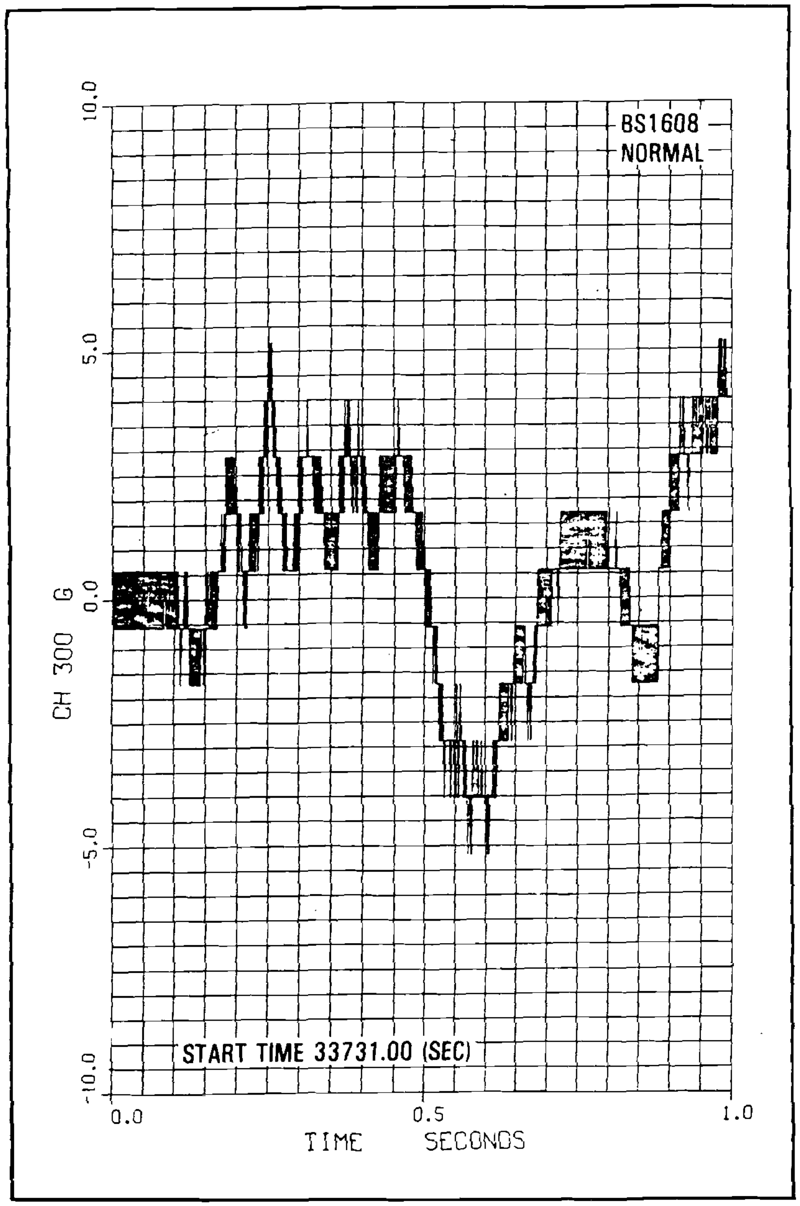

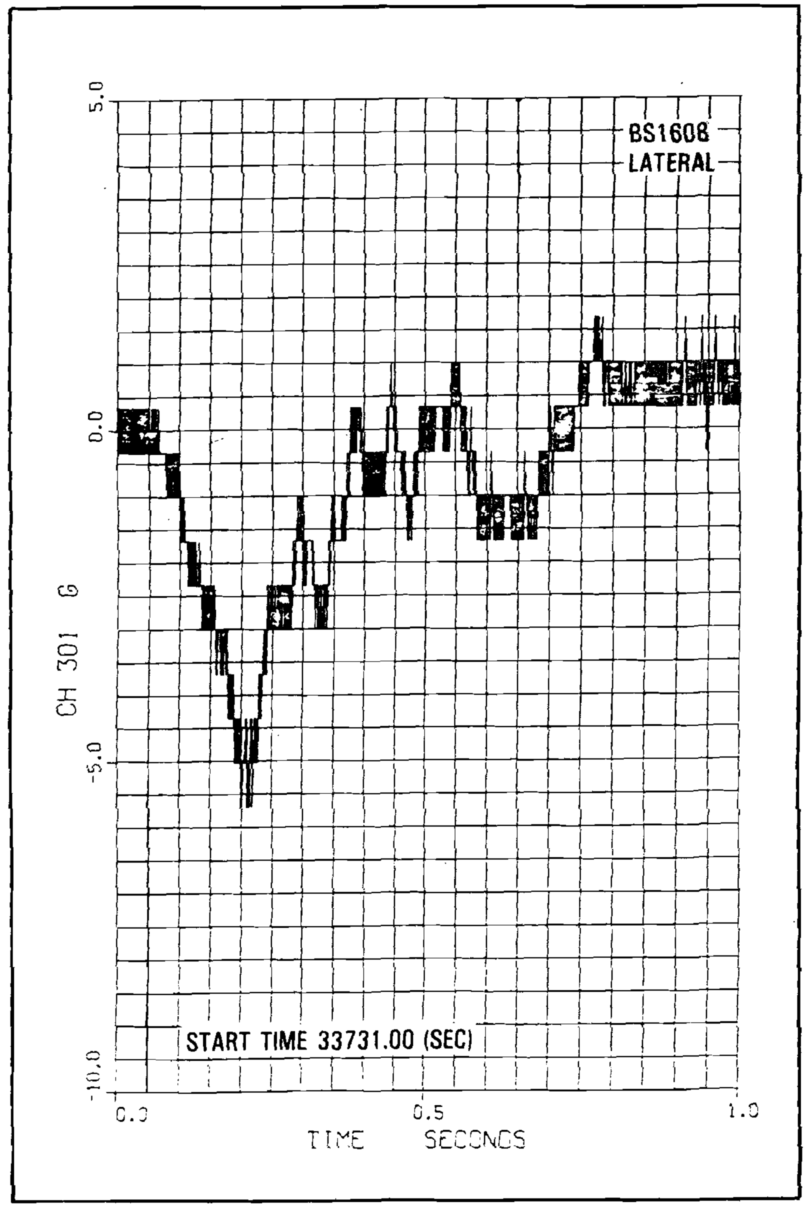

FIGURE A-18. CID TEST DATA, BS1608

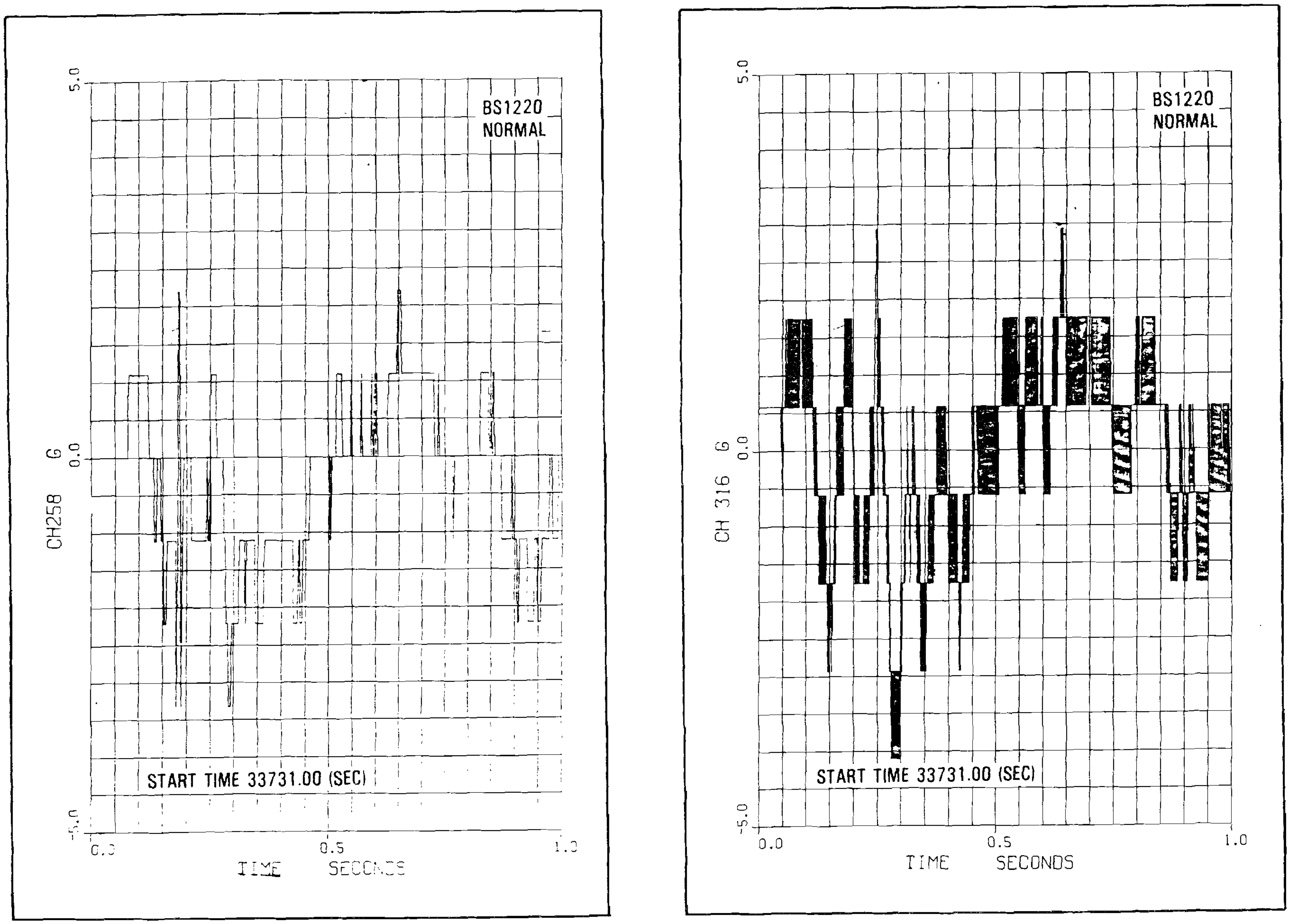

FIGURE A-19. CID TEST DATA, BS1220

APPENDIX B

DISTRIBUTION LIST

Civil Aviation Authority (5)
Aviation House
129 Kingsway
London WC2B 6NN England

Embassy of Australia (1)
Civil Air Attache
1601 Mass. Ave. NW
Washington, DC 20036

Scientific & Tech. Info FAC (1)
ATTN: NASA Rep.
P.O. Box 8757 BWI Airport
Baltimore, MD 21240

Northwestern University (1)
Trisnet Repository
Transportation Center Library
Evanston, ILL 60201

DOT-FAA AEU-500 (5)
American Embassy
APO New York, NY 09667

University of California (1)
Service Dept Institute of
Transportation Standard Lib
412 McLaughlin Hall
Berkely, CA 94720

British Embassy (1)
Civil Air Attache ATS
3100 Mass Ave. NW
Washington, DC 20008

Director DuCentre Exp DE LA (1)
Navigation Aerineene
9141 Orly, France

ANE-40 (2)
ASW-52C4 (2)
APM-13 Nigro (2)
AEA-66.1 (3)
ADL-32 North (1)
AES-3 (1)
ANM-60 (2)

ACT-624 (2)
AAL-62 (2)
M-493.2 Bldg. 10A (5)
APM-1 (1)
APA-300 (1)
AGL-60 (2)

ASW-53B (2)
AAC-44.4 (2)
ACE-66 (2)
ADL-1 (1)
ALG-300 (1)
ACT-8 (1)

FAA, Chief, Civil Aviation Assistance Group (1)
Madrid, Spain
c/o American Embassy
APO-New York 09285-0001

Al Astorga (1)
Federal Aviation
Administration (CAAG)
American Embassy, Box 38
APO-New York 09285-0001

Dick Tobiason (1)
ATA of America
1709 New York Avenue, NW
Washington, DC 20006

Burton Chesterfield, DMA-603 (1)
DOT Transportation Safety Inst.
6500 South McArthur Blvd.
Oklahoma City, OK 73125

FAA Anchorage ACO
701 C Street, Box 14
Anchorage, Alaska 99513

FAA Atlanta ACO
1075 Inner Loop Road
College Park, Georgia 30337

FAA Boston ACO
12 New England Executive PArk
Burlington, Mass. 01803

FAA Brussels ACO
% American Embassy, APO,
New York, NY 09667

FAA Chicago ACO
2300 E. Devon, Room.232
Des Plains, Illinois 6008

FAA Denver
10455 East 25th Ave., Suite 307
Aurora, Colorado 98168

Frank Taylor
3542 Church Road
Ellicott City, MD 21043

FAA Fort Worth ACO
P.O. Box 1689
Fort Worth, TX 76101

FAA Long Beach ACO
4344 Donald Douglas Drive
Long Beach, CA 90808

FAA Los Angeles ACO
P.O. Box 92007, Worldway Postal Center
Hawthorne, CA 90009

FAA New York ACO
181 So. Frankline Ave., Room 202
Valley Stream, NY 11581

FAA Seattle ACO
17900 Pacific Highway South, C-68966
Seattle, Washington 98168

FAA Wichita ACO
Mid Continent Airport, Room 100 FAA Bldg.
1891 Airport Road
Wichita, KA 67209

Government Activities

FAA, Washington, DC 20591
(Attn: Harold W. Becker, ASF-300;
Thomas McSweeny, AWS-100) (2)

FAA, 4344 Donald Douglas Drive,
Long Beach, CA 90808
(Attn: Stephen Soltis, ANW-102N) (1)

FAA, Central Region Headquarters,
601 East 12th Street, Federal Building,
Kansas City, Missouri, 64106
(Attn: Earsa Tunkesley, ACE-100) (1)

FAA, Southwest Region Headquarters,
4400 Blue Mound Road,
P.O. Box 1689
Fort Worth, Texas 76101
(Attn:: John Shapley, ASW-110) (1)

FAA, Northwest Mountain Region
Headquarters,
17900 Pacific Highway South, C-68966,
Seattle, Washington 98168
(Attn: Steven Wallace, ANW-110) (1)

FAA, Mike Monroney Aeronautical Center,
P.O. Box 25082,
Oaklonoma City, OK 73125
(Attn: Richard Chandler; AAM-119) (1)

NASA, Langley Research Center,
Hampton, VA 23365
(Attn: Emilio Alfaro-Bou, MA-495;
Huey Cardin, MS-495) (2)

U.S. Army Aviation Applies Technology
Directorate, USAARTA, (AVSCOM),
Fort Eustis, VA 23604
(Attn: Roy Burrows, Code SAVRT-TY-ASV) (2)

U.S. Navy Naval Air Development Center,
Warminister, PA 18974
(Attn: Leon Domzalski, Code 60322) (1)

NTSB, 800 Independence Ave. S.E.,
Washington, DC 20594
(Attn: John C. Clark, TE 60) (1)

Non-Government Activities

Beech Aircraft Corp.,
P.O. Box 85,
Wichita, KS 67201
(Attn: Dayton L. Hartley;
James E. Terry; William Schultz) (3)

Bell Helicopter Co.,
P.O. Box 482,
Fort Worth, TX 76101
(Attn: James Cronkite, Dept. 81,
MS 11; Roy G. Fox) (2)

Boeing Airplane Co.,
P.O. Box 3707,
Seattle, WA 98124
(Attn: Edward Widmayer, MC-9W-22) (1)

Boeing Co., Vertol Division,
P.O. Box 16858,
Philadelphia, PA 91942
(Attn: Denise Vassilakos, MS P30-27) (1)

Cessna Aircraft Co.,
P.O. Box 7704,
Wichita, KS 67277
(Attn: John Berwick; Robert Held;
Richard Soloski) (3)

Fairchild Aircraft Corp.,
P.O. Box 3246,
San Antonio, TX 78284
(Attn: Walt Dwyer) (1)

General Dynamics/Convair,
P.O. Box 80847,
San Diego, CA 92138
(Attn: L. Mastay, MA 80-6030) (1)

Grumman Aerospace Corp.,
So. Oyster Bay Road,, Bethpage,
L.I., NY. 11714
(Attn: Robert Winter, A08-35;
Allan B. Difko, A08-35) (2)

Gulfstream Aerospace Corp.,
P.O. Box 2206,
Savannah, GA 31402
(Attn: George Westphal) (1)

Non-Government Activities (Continued)

Gulfstream Aerospace Corp.,
P.O. Box 22500,
Oklhoma City, OK 73123
(Attn: Richard Southard) (1)

Lockheed-California Co.,
Burbank, CA 91503
(Attn: Gil Wittlin, D 76-12,
B 63G, PLT A-1) (1)

McDonnell Douglas Corp.,
3855 Lakewood Drive,
Long Beach, CA 90846
(Attn: J. Webster;
John L. Galligher) (2)

McDonnell Douglas Helicopter,
4645 S. Ash Ave.,
Tempe, AZ 85182
(Attn: Lyndon Landborne;
J.K. Sen) (2)

Piper Aircraft Corp.,
2925 Piper Drive,
Vero Beach, FL 32960
(Attn: Marion Dees) (1)

Sikorsky Aircraft,
North Maint Street,
Stratford, CT 06601
(Attn: Brain Cornell, MS 5207A;
Pramonik Mukunda, MS 5207A) (2)

☆U.S. GOVERNMENT PRINTING OFFICE: 1987-704-075/40210